1-1-2016

Phase Boundary Propagation in Mass Spring Chains and Long Molecules

Qingze Zhao
University of Pennsylvania, qingze@seas.upenn.edu

Phase Boundary Propagation in Mass Spring Chains and Long Molecules

Abstract
Martensitic phase transitions in crystalline solids have been studied and utilized for many technological applications, including biomedical devices. These transitions typically proceed by the nucleation and propagation of interfaces, or phase boundaries. Over the last few decades, a continuum theory of phase transitions has emerged under the framework of thermoelasticity to study the propagation of these phase boundaries. It is now well-established that classical mechanical and thermodynamic principles are not sufficient to describe their motion within a continuum theory, and a kinetic relation must be supplied to complete the constitutive description. A few theoretical techniques that have been used to infer kinetic relations are phase-field models and viscosity-capillarity based methods, within both of which a phase boundary is sharp, but smeared over a short length. Here we use a different technique to infer a kinetic relation. We discrete a one-dimensional continuum into a chain of masses and springs with multi-well energy landscapes and numerically solve impact and Riemann problems in such systems. In our simulations we see propagating phase boundaries that satisfy all the jump conditions of continuum theories. By changing the boundary and initial conditions on the chains we can explore all possible phase boundary velocities and infer kinetic relations that when fed to the continuum theory give excellent agreement with our discrete mass-spring simulations. A physical system that shares many features with the mass-spring systems analyzed in this thesis is DNA in single molecule extension-rotation experiments. DNA is typically modeled as a one-dimensional continuum immersed in a heat bath. It is also known from fluorescence experiments that some of these transitions proceed by the motion of phase boundaries, just as in crystalline solids. Hence, we use a continuum theory to study these phase boundaries in DNA across which both the stretch and twist can jump. We show that experimental observations from many different labs on various DNA structural transitions can be quantitatively explained within our model.

Degree Type
Dissertation

Degree Name
Doctor of Philosophy (PhD)

Graduate Group
Mechanical Engineering & Applied Mechanics

First Advisor
Prashant Purohit

Keywords
Biomechanics, Mass spring chain, numerical simulation, Phase transition

Subject Categories
Engineering Mechanics

PHASE BOUNDARY PROPAGATION IN MASS SPRING CHAINS AND LONG MOLECULES

Qingze Zhao

A DISSERTATION

in

Mechanical Engineering and Applied Mechanics

Presented to the Faculties of the University of Pennsylvania
in
Partial Fulfillment of the Requirements for the
Degree of Doctor of Philosophy
2016

Prashant K. Purohit,
Associate Professor of Mechanical Engineering and Applied Mechanics
Supervisor of Dissertation

Prashant K. Purohit,
Associate Professor of Mechanical Engineering and Applied Mechanics
Graduate Group Chairperson

Dissertation Committee:
Professor John L. Bassani,
Mechanical Engineering and Applied Mechanics
Professor Celia Reina,
Mechanical Engineering and Applied Mechanics

Acknowledgments

I would like to thank my advisor, Dr. Prashant K. Purohit. I am grateful for his support and guidance during my PhD studies. His passion and dedication to science and research have made these five years a very rewarding experience.

I would like to express my gratitude to the members of my dissertation committee, Dr. John L. Bassani and Dr. Celia Reina, for their advice and instruction. I have taken several classes from them and have learnt a lot from their knowledge and experience.

My grateful thanks also to the members of the Mechanics of Materials Group. We have learnt a lot from each other during our time together.

I want to thank my parents for what they have given to me. I want to thank my grandma for her caring and love during my early life. I want to thank my former wife Yumeng, for her selfless support and company during my PhD studies. I want to thank my son Nemo, for the joy and happiness he has given to me. They are the ones who I love and the reason I keep going.

ABSTRACT

PHASE BOUNDARY PROPAGATION IN MASS SPRING CHAINS AND LONG MOLECULES

Qingze Zhao

Prashant K. Purohit

Martensitic phase transitions in crystalline solids have been studied and utilized for many technological applications, including biomedical devices. These transitions typically proceed by the nucleation and propagation of interfaces, or phase boundaries. Over the last few decades, a continuum theory of phase transitions has emerged under the framework of thermoelasticity to study the propagation of these phase boundaries. It is now well-established that classical mechanical and thermodynamic principles are not sufficient to describe their motion within a continuum theory, and a kinetic relation must be supplied to complete the constitutive description. A few theoretical techniques that have been used to infer kinetic relations are phase-field models and viscosity-capillarity based methods, within both of which a phase boundary is sharp, but smeared over a short length. Here we use a different technique to infer a kinetic relation. We discrete a one-dimensional continuum into a chain of masses and springs with multi-well energy landscapes and numerically solve impact and Riemann problems in such systems. In our simulations we see propagating phase boundaries that satisfy all the jump conditions of continuum theories. By changing the boundary and initial conditions on the chains we can explore all possible phase boundary velocities and infer kinetic relations that when fed to the continuum theory give excellent agreement with our discrete mass-spring simulations. A physical system that shares many

features with the mass-spring systems analyzed in this thesis is DNA in single molecule extension-rotation experiments. DNA is typically modeled as a one-dimensional continuum immersed in a heat bath. It is also known from fluorescence experiments that some of these transitions proceed by the motion of phase boundaries, just as in crystalline solids. Hence, we use a continuum theory to study these phase boundaries in DNA across which both the stretch and twist can jump. We show that experimental observations from many different labs on various DNA structural transitions can be quantitatively explained within our model.

Contents

List of Tables

List of Figures

Chapter 1

Introduction

1.1 Background

The work in this thesis is partially inspired by phase transitions in crystalline materials and the shape memory effect. Crystalline materials can exist in different solid phases with various crystal structure. Under certain physical conditions, one phase is usually preferred over the other phases. This property lays the foundation of phase transition theory in crystalline materials. Shape memory alloys, like NiTi and CuAlNi [15, 38, 84] are typical examples of such crystalline materials, as are martensitic steels [19, 20], which are by far the most significant technologically. However, in the last two decades NiTi has been increasingly in medical devices, such as, stents. More recently, NiTi wires have been used in medical robots due to their super-elastic behavior [92]. The book by Bhattacharya [19] gives a very good summary and explanations of shape memory alloys, their detailed lattice structure, phase transitions between these micro-structures, and so on. Figure 1.1 shows illustrations of optical micro-structures of an NiTi sample subjected to the deformation.

At a stress free state, if such a multi-phase crystalline material is slowly cooled from a

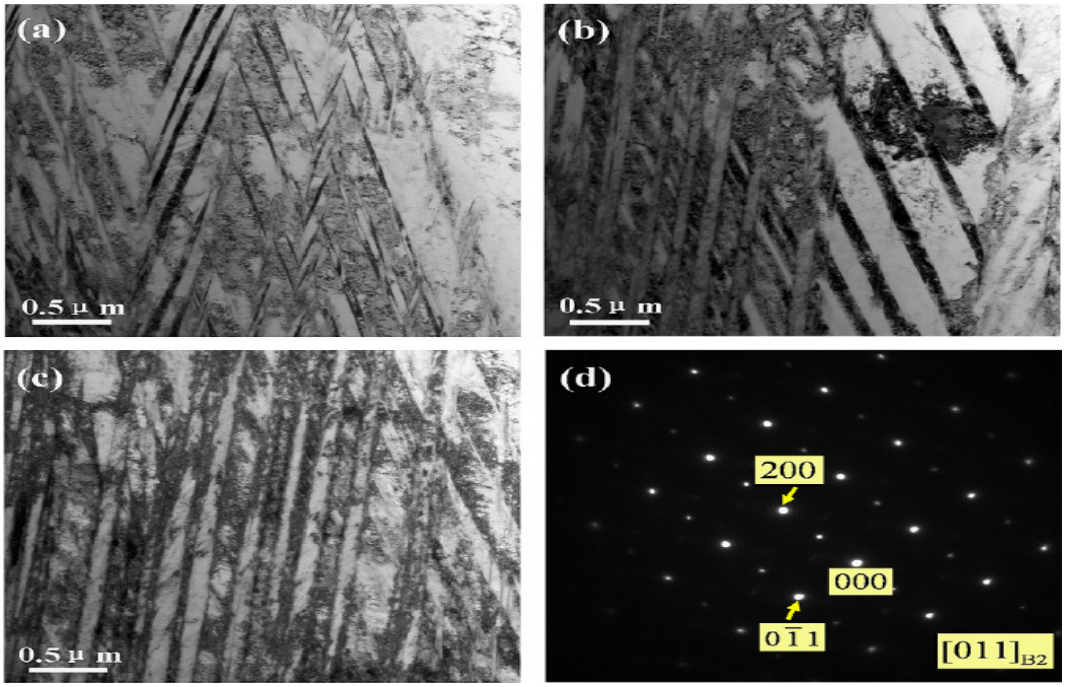

Figure 1.1: Illustration of micro-structures of the NiTi sample subjected to the deformation. (a), (b) and (c) Transmission electron microscopy bright field images showing the martensite-like plates formed in two directions; (d) SAEDP(Selected Area Electron Diffraction Pattern) of (b) showing B2 austenite. This figure is from [97].

very high temperature, then the material begins a phase transition from a 'high temperature phase' to a 'low temperature phase'. This process does not happen instantly, rather it's a relatively slow process where part of the material goes to the 'low temperature phase' first, and there is an interface separating different phases of material. Figure 1.2 gives a graphic illustration of this process. As the temperature keeps decreasing, this interface, or phase boundary, propagates into the 'high temperature phase' region. Eventually, the whole region becomes 'low temperature phase'. The propagation of such phase boundaries is our main interest in this thesis.

Over the last several decades a continuum theory of phase transitions under the framework of thermoelasticity has emerged from the study of crystalline solids [7]. It has been recognized that continuum mechanical principles of the balance of mass, momentum and

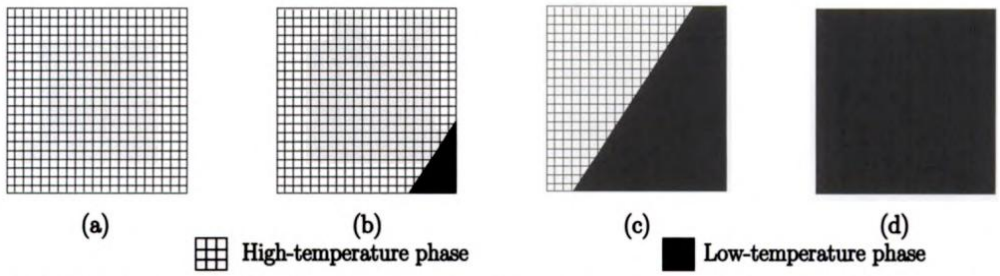

Figure 1.2: Schematic depiction of a stress-free single crystal of a two-phase material at a sequence of progressively decreasing temperatures. This figure is from [19].

energy are not sufficient to determine the evolution of phase boundaries in continua and additional constitutive relations have to be provided [1, 2, 6]. This additional information comes in the form of a *kinetic relation* and it relates thermodynamic driving force and phase boundary velocity. The notion of thermodynamic driving force was first introduced by Eshelby (1956) as 'force on a defect' and was later adapted for phase transitions by Abeyaratne and Knowles (1990). One of the main objectives of this work is to obtain kinetic relations for phase boundaries in 1-D continua with the help of numerical simulation.

A kinetic relation that comes up quite often is the Arrhenius law which is based on thermal activation. This law assumes that jumps from a given state to another are limited by the free energy barrier that the system has to overcome. A common expression for kinetics based on the Arrhenius law is

$$V = R(\exp(-\frac{b^+}{rk\theta}) - \exp(-\frac{b^-}{rk\theta})) \tag{1.1}$$

where V is the phase boundary velocity, θ is temperature, b^+ and b^- are the two energy barriers, k is the Boltzmann constant and r is a scaling factor. The Arrhenius law is applicable when inertial effects are not significant and thermal activation is dominant in a

phase transition. It was employed in early studies of phase boundary motion in crystalline solids. For example, in [37] the Arrhenius law used to describe dislocation glide motion was utilized to predict the mobility of martensitic phase boundaries in β-CuAlNi alloy. Thus, this in this case phase boundary motion is driven by a thermally activated process. In [60], the Arrhenius law is employed to understand phase transformations in other metals and alloys, as well. In [67], it has been shown that Arrhenius kinetics describes the motion of phase boundaries in DNA. This is consistent with the idea that the mechanics of the DNA molecule in tension, torsion and bending is characterized by the absence of inertia and dominance of thermal fluctuations.

The discussion above is also why an interesting application of the continuum theory of phase transitions in 1-D continua that we explore in this thesis is not in crystalline solids, but in long one-dimensional molecules, such as DNA. DNA can store bending, twisting and stretching energy and is known to behave as an elastic rod at small length scales [51, 53, 87]. It is also known that it can undergo several structural transitions in response to changes in temperature and loads just as many crystalline solids do [22, 50]. For this reason a second objective of this thesis is to apply the 1-D continuum theory of phase transitions to DNA.

1.2 Mass-spring chains

Our main tools for numerical analysis are mass-spring chains as shown in figure 1.3. Chains of masses and springs have been used as models to understand the mechanical and thermal behaviour of crystalline solids for a long time [36, 41]. For instance, the dispersion relation for phonons (normal modes) in a one-dimensional chain with linear springs is a calculation that appears in all standard text books in solid state physics [36]. The specific heat of a

solid can be computed starting from the density of these normal modes in frequency space as was done by Debye (and Einstein) in the early 1900s. In this thesis, we are interested in non-linear chains in which the potential of the springs has multiple wells and the constitutive relations are piecewise linear. This kind of calculation can be traced back to Krumhansl and Schreiffer in the 1970s [42]. When the potentials characterizing the springs have multiple wells then the dynamics of mass-spring chains has been shown to be similar to that of one-dimensional bars capable of phase transitions [7, 8, 13, 18, 27, 29, 30, 42, 54, 73, 82, 85, 89]. This insight has been utilized to extract kinetic relations for moving phase boundaries by comparing solutions of impact and Riemann problems in continuum bars to those in the mass-spring chains [65, 85]. The extracted kinetic relation has a simple analytical form that has been recently shown to have a universal near sonic limit [89]. More recently, mass-spring chains have also provided insights into the mechanics of biological macromolecules [17, 18], and this work is, at least partly, motivated by them. We give a short account of the recent work in mass-spring chains in the following.

Puglisi and Truskinovsky [62] are among the first to consider a model where a material has several crystallographic phases with non (quasi)-convex energy. They studied a 1-D chain with a finite number of bi-stable elastic elements and their springs have two convex wells separated by a spinodal region. They obtained a quantitative description of the possible quasi-static evolution paths. Balk, Cherkaev and Slepyan [13, 14] have considered dynamical processes in materials with non-monotonic constitutive relation. They introduced a model of a chain of masses joined by springs with a non-monotone strain-stress relation and conducted numerical experiments to find the dynamics of that chain under different excitations. They concluded that the dynamics leads either to a vibrating steady state or

to a hysteresis instead of a unique stress-strain dependence. They observed 'waves of phase transition' in their numerical calculations. These waves were associated with oscillations that did not die off even long after the passage of the wave-front. Later authors working with mass-spring chains with non-convex energies have made similar observations [57, 58]. We will show in this thesis that these oscillations contain information about dissipation due to phase boundary propagation which has its origin in the *kinetic law* that is central to the continuum theory.

The kinetics and dissipation at propagating phase boundaries in mass-spring chains has also been studied by Agrawal and Dayal using very different techniques[10]. These authors use a phase-field model that does not require explicit numerical tracking of the interface (or phase boundary) and allows for better study of interface kinetics and nucleation by studying the hysteresis. Benichou, Cohen and Givli [18] reexamined the bi-stable chain by introducing the concept of an ideal bistable element. They showed that any bi-stable material can be conceptually modeled as series of ideal bistable elements connected with elastic springs. They have studied the consequences of the discrete nature of these structures, especially on finite size effects, non-trivial stability, and so on. They have also studied biological systems (like the muscle protein titin) with their bistable mass-spring model. Recently, Nadkarni, Dairio and Kochmann [54] have investigated the dynamics of a bistable chain in which there is a dashpot at every lattice site in addition to the mass and non-linear springs. They have shown that this produces three different regimes of wave propagation in which one is very much like the propagation of a solitary wave [93]. In particular, they reveal that the velocity of this wave is determined by balancing the energy dissipated in each dash pot with the energy released due to each spring jumping from one phase to the other. Their results

highlighted opportunities in the design of mechanical meta-materials with negative-stiffness elements and shed light on the study of the dynamics of nonlinear small scale instabilities in solids and structures.

Notably, none of the studies mentioned above goes beyond extensional degrees of freedom at the masses in the chains. Only a few study Langevin dynamics of these chains to model the effects of heat baths [31]. These are the novel elements that we bring into the study of mass-spring chains through this thesis.

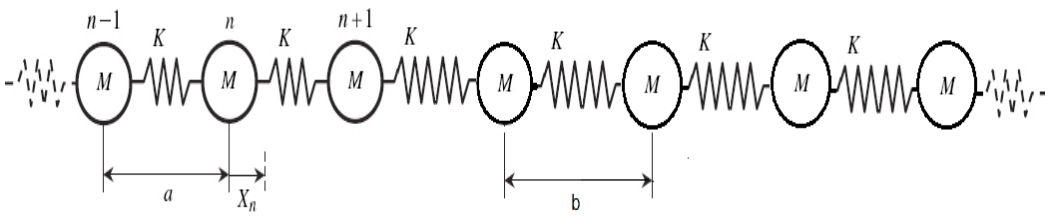

Figure 1.3: Mass spring chain. The energy landscape of the springs is assumed to have multiple wells corresponding to lattice spacings a and b. X_n is the displacement of nth mass.

1.3 Overview of this Thesis

This thesis is organized as follows.

Chapter 2 studies kinetic relations for phase boundaries in a bistable chain of masses and springs. We pay special attention to the effect of thermal fluctuation on the dynamics of the system. We integrate Langevin's equations of motion for the chain of masses and springs to account for the presence of a heat bath at a fixed temperature. We find that the xt-plane looks similar to the purely mechanical numerical experiments at low temperatures, but at high temperatures there is an increased incidence of random nucleation events. Using results from both impact and Riemann problems, we show that the kinetic relation is a function

of the bath temperature.

Chapter 3 studies kinetic relations for phase boundaries in a bistable chain with twist stretch coupling. We set up a numerical model in which each mass has a translational and rotational degree of freedom and study the dynamics of phase boundaries across which both the twist and stretch can jump. We find a kinetic relation from simulations of impact problems and use it to solve Riemann problems analytically. However, for some combinations of parameters characterizing the energy landscape of our springs we find propagating phase boundaries for which the rate of dissipation, as calculated using isothermal expressions for the driving force, is negative. This suggests that we cannot neglect the energy stored in the oscillations of the masses in the interpretation of the dynamics of mass-spring chains. We also find a range of driving forces for which the phase boundaries remain static. At the end of the chapter we use our chain to shed some light on experiments involving yarns that couple twist and stretch to perform useful work in response to various stimuli.

Chapter 4 studies the dynamics of phase boundary motion in a mass and spring chain with twist-stretch coupling and thermal effects. In this setting, we have a chain where each mass has a translational and rotational degree of freedom and the chain is immersed in a thermal bath. The governing equation for both translational and rotational degrees of freedom is Langevin's equation. We have found that when bath temperature is high enough, the unphysical negative dissipation of chapter 3 goes away. Also just like chapter 2, we find that the kinetic relation depends on the temperature of the heat bath.

Chapter 5 studies 1D continua with twist-stretch coupling and its application in DNA mechanics. Our goal in this chapter is to model experiments of the type shown in figure 1.4. In this set up it is possible to apply both tensile forces and twisting moments on the

DNA while tracking its end-to-end distance and the number of turns of the bead. Large forces and moments cause phase transitions in DNA that have been extensively documented [11, 76]; some of these phase transitions have been shown to proceed by the motion of one or two phase boundaries in the DNA [12, 22]. We describe a continuum framework to study the propagation of phase boundaries across which the stretch and twisting curvature are discontinuous. We derive an expression for the driving force and assume a kinetic relation for the mobility of these phase boundaries as a function of this driving force. We also develop a finite difference method to integrate the equations of motion for our DNA including the phase boundary. We use it to study the B-DNA to L-DNA transition and the B-DNA to Z-DNA transition at equilibrium and away from it.

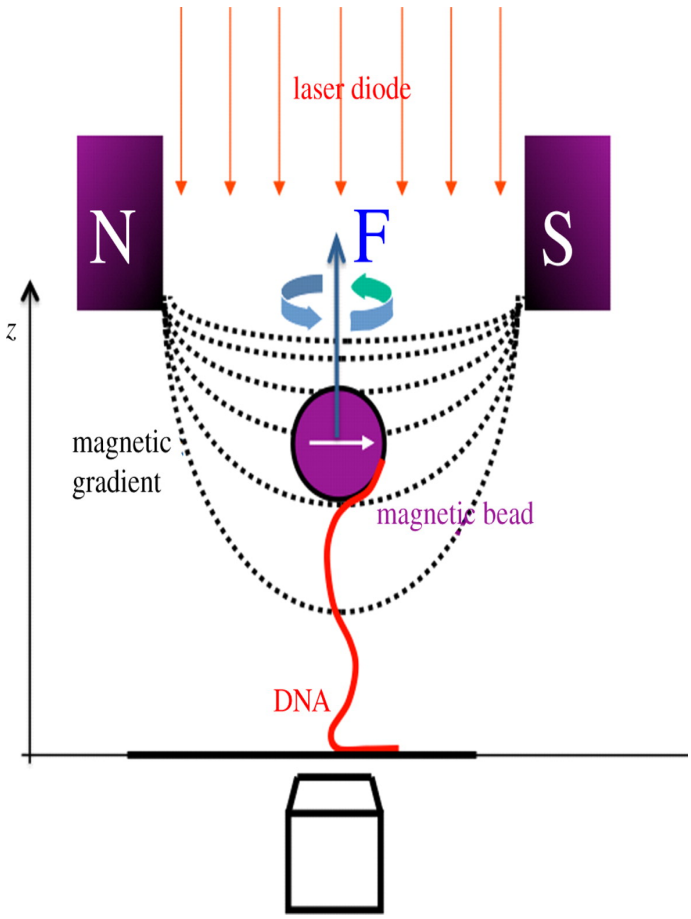

Figure 1.4: DNA held in an optical trap. It is possible to apply forces and torques on the DNA and track the number of turns of the bead as well as the extension of the DNA. DNA undergoes several structural transitions in response to tensile and torsional stresses. Figure from "On the topology of chromatin fibres".

Chapter 2

Extracting a kinetic relation from the dynamics of a bistable chain

The use of mass-spring chains as simple lattice models for solids has been prevalent for a long time. For instance, the dispersion relation for phonons (normal modes) in a one-dimensional chain with linear springs is a calculation that appears in all standard text books in solid-state physics [36]. The specific heat of a solid can be computed starting from the density of these normal modes in frequency space as was done by Debye (and Einstein) in the early 1900s. If the masses in the chain are not all identical but are of two different types then the dispersion relation has two branches – the acoustic and the optical branches. The concept of a 'band-gap' arises from these ideas and has been extensively used in semi-conductor physics for many decades [36].

An early effort to use a non-linear chain to study phase transitions in solids was that of Krumhansl and Schreiffer in the 1970s [43]. In a beautiful paper they showed that thermal oscillations (just like phonons) and moving domain walls or phase boundaries can result from a non-convex potential. Balk et al. [13, 14] performed numerical experiments on a chain with piecewise linear elements and found analytical solutions describing the frequency, kinetic energy and speed of the waves of phase transition. They found that a part of the energy stays in the form of high frequency oscillations that become 'invisible' in

the continuum limit. This results in an energy cascade toward smaller scales and can lead to significant dissipation. The loss of information in the continuum limit also causes initial-boundary value problems with propagating phase boundaries to be ill-posed unless a *kinetic relation* describing the motion of the phase boundary is supplied. Accounting for the energy fluxes carried by the lattice waves in the discrete model Truskinovsky and Vainchtein [85] obtained kinetic relations for chains with a special type of springs characterized by double-well potentials with no 'spinodal' region. Kinetic relations were also derived for other non-linear chains by Ngan and Truskinovski [58]. These authors numerically solved Riemann problems for discrete lattices with one and two phase boundaries and compared their results with analytical solutions based on the kinetic relations extracted from the traveling wave solutions [57, 88]. An explicit kinetic relation was obtained by Purohit [63] in a chain with double-well springs with a spinodal region and second nearest neighbor interactions. This type of kinetic relation was recovered in an elegant analytical calculation by Vainchtein [88] in a recent paper and has also been shown as a universal near sonic limit [86]. Tan and co-workers [82, 83] have explored the hysteresis of 1-D mass-spring chains with double well potentials by applying a cyclic load to the chains. They perform molecular dynamic calculations with thermostat. The hysteresis they observe contains some information about the kinetic relation for the moving phase boundaries, but an explicit kinetic relation is not recovered because there can be multiple phase boundaries and nucleation events in these calculations. Our goal in this paper is not only to extract an explicit kinetic relation by solving impact problems on mass-spring chains but also to show that this kinetic relation can be used to solve a continuum Riemann problem whose solution closely matches its discrete analogue.

None of the studies described thus far tried to understand the motion of a single phase boundary in a chain of masses and springs immersed in a thermal bath where there is constant bombardment of each mass by surrounding water molecules. The studies of Tan and co-workers address this issue but they do not comment on the effect of the bath temperature on the kinetic relation. Efendiev and Truskinovsky studied the thermalization of a chain with bi-stable springs (with no spinodal region) and showed that the numerical calculations recover the equilibrium stress-strain relations obtained by computation of the partition function [85]. Thermalized mass spring chains with non-linear energies have been studied before by Fermi, Pasta and Ulam [61], but the goal in this classic work was to determine if the masses thermalized due to the exchange of energy between various normal modes of the system which would be coupled if the springs connecting the masses were non-linear. They did not account for the presence of the heat bath. Our goal in this paper is to determine the effect of bath temperature on the kinetic relation of a single phase boundary. Our work is motivated in part by experiments on single molecules capable of displacive phase transitions, such as, coiled-coil proteins and DNA, that have been extensively studied using single molecule techniques for the last two decades [68, 72, 77, 90]. It has long been known that the phase transitions in these molecules as well as regular crystalline solids are dependent on temperature and stress (or force) [7, 36, 47, 71, 94, 95].

The paper is laid out as follows: First, we confine ourselves to a purely mechanical chain for which we integrate Newton's second law. We recover the kinetic relation obtained by Purohit [63] by solving impact problems and we solve Riemann problems analytically with this kinetic relation. The results correspond very well with our numerical simulation of Riemann problems, indicating that the kinetic relation which relates driving force and phase

boundary motion is an inherent property of the nonlinear chain. Finally, we also explore the dynamics of the chain with thermal fluctuations and try to understand the effect of the bath temperature on the movement of the phase boundary.

2.1 Short review of continuum theory

2.1.1 Tri-linear material

Consider a bar in one dimension which occupies the interval $(0, L)$ in the reference configuration. The material of the bar is capable of phase transitions. In other words, its energy has two wells so that the stress-strain relation is of the up-down-up type. We will consider double well potentials that are constructed from the piecewise quadratic functions so that the stress-strain relation is tri-linear [65]. If x is the reference coordinate and $y(x,t)$ is the position of particle x in the deformed configuration at time t then the displacement field is denoted as $u(x,t) = y - x$ and the strain field is denoted as $\epsilon(x,t) = \frac{\partial u}{\partial x}$. The stress strain relation is given as

$$T(\epsilon) = \begin{cases} E\epsilon & \epsilon \leq \epsilon_M \\ -E(\epsilon + 1 - \epsilon_o) & \epsilon_M \leq x \leq \epsilon_m \\ E(\epsilon - \gamma_T) & \epsilon \geq \epsilon_m \end{cases} \tag{2.1}$$

Here T is stress and E plays the part of Young's modulus. γ_T is the transformation strain of the tri-linear material and ϵ_0, ϵ_M and ϵ_m are material constants. The corresponding stored energy function is a double well potential. Figure 2.1(c) gives a representation of the stress strain relation, while figure 2.1(b) shows a typical energy landscape. Following Abeyaratne and Knowles [7], we refer to the first rising part of the stress strain curve as the low-strain phase and the second rising part as the high-strain phase.

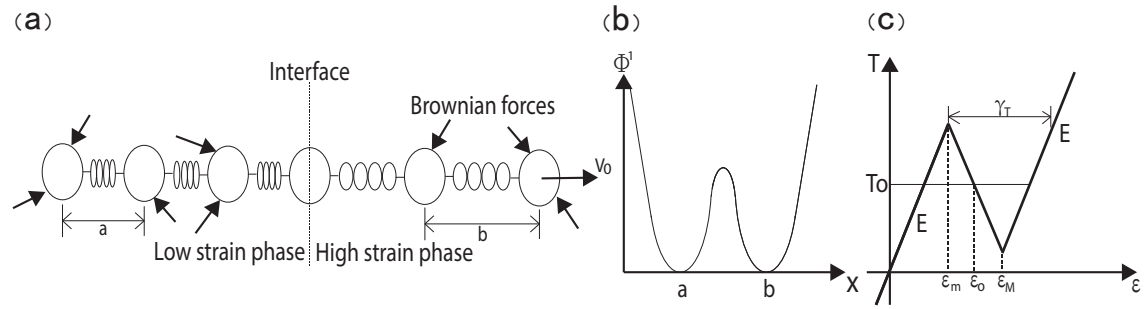

Figure 2.1: 1-D mass spring chains with tri-linear force-stretch relations. We fix the left end and pull the right end at a constant velocity v_0. We call this an impact problem. (a) Moving interfaces with either side in different phases are possible. Towards the end of the paper we assume that the chain is immersed in a heat bath that exerts random (or Brownian) forces on each mass. (b) The energy landscape of a typical spring has two wells separated by a spinodal region. The height of the wells is not necessarily the same. (c) The force-stretch relation is assumed to be tri-linear with the spring constant in the two stable regions being the same.

For a bar made of the tri-linear material described above, two kinds of discontinuities may exist. They are shock waves (or sonic waves) which originate from vibration within one phase, and phase boundaries which originate from the transition between the two different phases [7]. For shock waves, the material ahead and behind the discontinuity fall in the same region of stress strain relations. By applying $T(\epsilon)$ both in low or high strain phase to (A.1) and (A.3) we get

$$\rho \dot{s}^2 = \frac{E(\epsilon^+ - \epsilon^-)}{\epsilon^+ - \epsilon^-}, \qquad \text{so that} \quad \dot{s}^2 = \frac{E}{\rho} = c^2. \tag{2.2}$$

Here we assume that there exists a discontinuity at reference location $x = s(t)$ and denote $x \geq s(t)$ as the + side, $x \leq s(t)$ as the - side. For any quantity $f(x,t)$ we denote $f(x_+,t) - f(x_-,t)$ by $[|f|]$ and $\frac{f(x_+,t)+f(x-,t)}{2}$ by $\langle f \rangle$. ρ here represents material density. Eqn. 2.2 means that a discontinuity with both sides in the same phase of the tri-linear material can only travel with one speed. This speed c, is the sonic wave speed of the bar. As the low

strain phase and high strain phase share the same Young's modulus and mass density is constant, we will only have one sonic wave speed. For a phase boundary we assume that the material ahead and behind the discontinuity are in different phases so the stresses are $T^+ = E(\epsilon^+ - \gamma_T)$ for the material on the right hand side of the discontinuity and $T^- = E\epsilon^-$ for the material on the left. Applying this to $(A.1)$ and $(A.3)$ gives

$$[|\epsilon|] = \frac{\gamma_T}{1 - \dot{s}^2/c^2}. \tag{2.3}$$

A phase boundary can have a non-zero driving force accross it (see appendix). Here, by driving force, we mean the jump in Gibbs free energy per unit reference length across the phase boundary. For the constitutive law given in eqn. 2.1 driving force is given as

$$f_{driving} = \frac{E\gamma_T}{2}(2\epsilon_0 - \epsilon^+ - \epsilon^-), \tag{2.4}$$

where ϵ^+ and ϵ^- are the strains immediately ahead and behind a phase boundary respectively. It has been demonstrated that the driving force across a sonic wave is zero. We will use the results summarized above when we solve Riemann and Goursat-Riemann problems as described below.

2.1.2 Riemann problem and Goursat-Reimann problems

In a Riemann problem we focus on the evolution of an infinite bar made of trilinear material given in the previous section. We place a discontinuity at $x = 0$ at $t = 0$, so that the initial

conditions are:

$$\epsilon(x,0) = \epsilon_L, \quad v(x,0) = v_L \quad \text{for} \quad x \leq 0 \tag{2.5}$$

$$\epsilon(x,0) = \epsilon_H, \quad v(x,0) = v_H \quad \text{for} \quad x \geq 0 \tag{2.6}$$

where v_L and v_H are constants. There are no boundary conditions since the domain is $-\infty < x < \infty$. The goal is to watch the motion of the discontinuity as time evolves.

In a Goursat-Riemann problem or impact problem the domain is semi-infinite $-\infty < x \leq 0$. The initial conditions are: $\epsilon(x,0) = \epsilon_L$, $v(x,0) = v_L$ for $x \leq 0$. The boundary condition at $x = 0$ is given as

$$v(0,t) = v_0, \qquad t > 0. \tag{2.7}$$

Once again, the goal is to watch the evolution of the bar in response to this boundary condition. Various problems of these types have been solved with the discontinuities being phase boundaries or shocks. It has been demonstrated that when the discontinuity is a shock then the evolution of the bar can be completely described by the balance laws of mass, momentum and energy. If the discontinuity is a phase boundary the balance laws of mass, momentum and energy are not sufficient to determine the evolution of the phase boundary [65]. For a tri-linear bar with a phase boundary at $x = 0$ at $t = 0$ there exists a one parameter family of solutions for the Riemann problem. We can think of this parameter as the phase boundary velocity. In order to get a unique solution to the Riemann problem with a phase boundary we need a *kinetic relation* which relates the driving force f with the phase boundary velocity $\dot{s}$. Similarly, in the Goursat-Riemann problem we need a kinetic relation as well as a *nucleation criterion* in order to get a unique solution. In the next section

we show how a kinetic relation can be obtained for the corresponding discrete problem by performing an 'atomistic' calculation with a chain of masses and springs.

2.2 Chain of masses and springs

We study the chain of masses as an atomic-level proxy for the 1D bar with each mass having only one degree of freedom. Thus we have N masses connected by springs as shown in figure 2.1(a). The potential energy of the springs is a double well (piecewise quadratic) and the force elongation relation of each spring is tri-linear. We have used:

$$f(x_i) = \begin{cases} 4(x_i - 1) & x_i \leq 1.25 \\ -4(x_i - 1.5) & 1.25 \leq x_i \leq 1.75 \\ 4(x_i - 2) & x_i \geq 1.75 \end{cases} \tag{2.8}$$

where $x_i = u_{i+1} - u_i$ is the stretch of the ith spring. We only consider the interaction of nearest neighbors. The total potential energy of the system is given as $\phi = \sum_1^{N-1} \phi^1(x_i)$ where $\phi^1(x_i)$ is the inter atomic double well potential. In the purely mechanical setting, the dynamics of the chain is governed by a system of ordinary differential equations (ODEs). For simplicity we assume $m_i = m$. The system of ODEs becomes:

$$m\ddot{u}_i = -\frac{\partial \phi}{\partial u_i}. \tag{2.9}$$

These ODEs must be integrated subject to some initial conditions $u_i = u_i^0$ and $\dot{u}_i = \dot{u}_i^0$ for all i, where u_i^0 and $\dot{u}_i^0$ are given functions. The equations are integrated numerically using

a Leap-frog algorithm with time step Δt as:

$$\dot{u_i}(t + \frac{\Delta t}{2}) = \dot{u_i}(t - \frac{\Delta t}{2}) + \ddot{u_i}(t)\Delta t, \tag{2.10}$$

$$u_i(t + \Delta t) = 2u_i(t) - u_i(t - \Delta t) + \ddot{u_i}(t)\Delta t^2, \tag{2.11}$$

$$\dot{u_i}(t) = \frac{\dot{u_i}(t - \frac{\Delta t}{2}) + \dot{u_i}(t + \frac{\Delta t}{2})}{2}. \tag{2.12}$$

We choose a time step Δt that is much smaller than a/c to ensure that our numerical calculation is stable. Recall that a is the 'interatomic' spacing and c is the sonic wave speed.

2.2.1 Impact problem

For the impact problems, ideally the domain is semi-infinite. In our calculations, we approximate the problem as a mass spring system with N masses and $N - 1$ springs connecting them. We fix the left end of the chain ($i = 1$) and prescribe a constant applied velocity at the right end ($i = N$). Hence, $u_1 = 0$ and $u_N = v_0 t + u_N^0$ for all $t > 0$. Initially, all springs are in the low strain phase at $x_i = 1$ for all i. We integrate (2.9) for the system up to the point that the sonic wave which originated at $i = N$ hits the left end ($i = 1$). We find that below a critical applied velocity there is only a sonic wave passing through the chain from right to left. The sonic wave travels at a constant speed c. If we pull the chain with rate higher than the critical value, a phase transition nucleates at $i = N$ and the phase boundary propagates inwards towards $i = 1$ as shown in figure 2.2. The phase boundary moves from the right to the left at a constant speed $\dot{s}$ that is smaller than the sonic wave speed. The speed of the phase boundary depends on the applied velocity v_0 as shown in figure 2.3. From the figure we see that as applied velocity becomes larger and larger, the

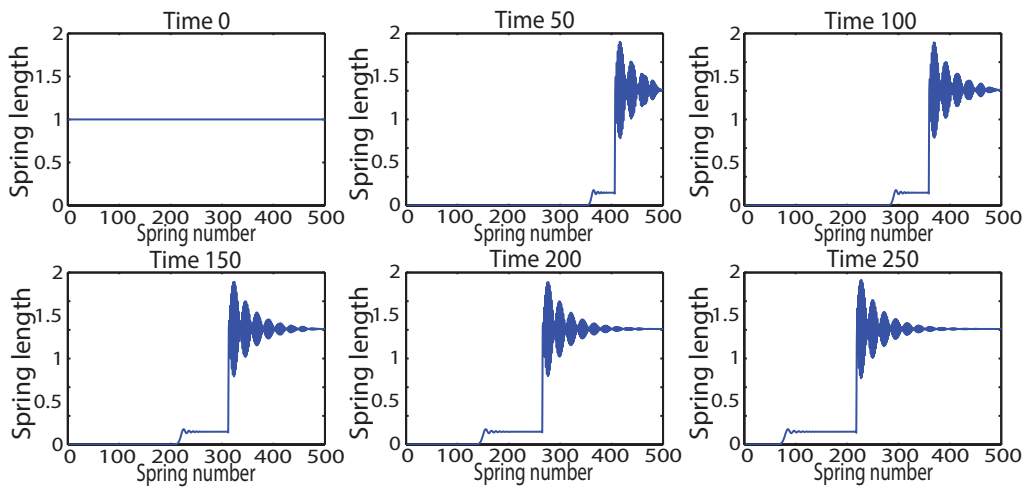

Figure 2.2: Time snap-shots of the chain for an impact problem with applied velocity, v_0, higher than a critical value. A sonic wave and phase boundary are seen propagating to the left from the right. The sonic wave speed c is independent of the applied velocity v_0 but the speed of the phase boundary is not. If the applied velocity is below the critical value then we only see the sonic wave and no phase boundary.

ratio $\dot{s}/c$ tends to 1. This is expected because information cannot travel faster than the sonic wave speed in a material. For each $\dot{s}$, we have also calculated the driving force using (2.4). The relation of $f_{driving}$ versus $\dot{s}$ appears in figure 2.3 as an inset. The data for $f_{driving}$ as a function of $\dot{s}/c$ can be fit with an expression of the form given in [63, 88]. The result is:

$$\frac{f_{driving}}{E\gamma_T} = \frac{3}{2}(1 + \frac{\gamma_T}{1 - \dot{s}^2/c^2}) \tag{2.13}$$

where γ_T is the transformation strain, $\dot{s}$ is phase boundary velocity and E is Young's modulus. Thus, we have arrived at a kinetic relation from our 'atomistic' simulations which relied solely on integrating Newton's second law for a discrete version of the Goursat-Riemann problem.

In the next section we show that this kinetic relation can be used to solve Riemann problems analytically for a continuum bar and that the resulting phase boundary velocities agree quite well with the discrete version of the same problems. We have also explored the

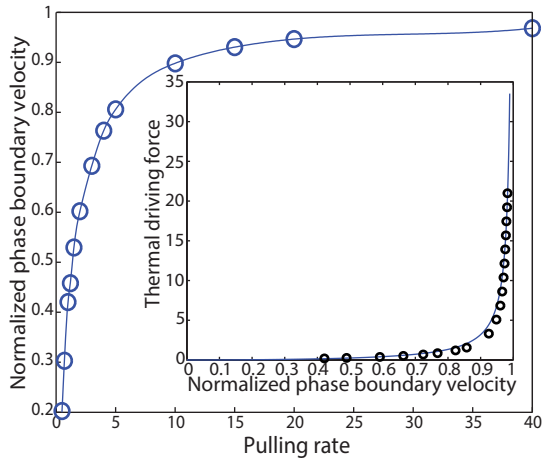

Figure 2.3: Phase boundary velocity $\dot{s}$ increases as a function of applied velocity v_0. The solid line is a fit to the data. The y-axis is $\dot{s}/c$ and the x-axis is v_0. $\dot{s}$ asymptotes at the sonic wave speed c, as expected. The inset shows the kinetic relation emerging from these calculations.

dynamical response of the chain with different potentials for the springs. So far, the force-stretch relation of the springs corresponds to $\epsilon_0 = 1.5$. We have calculated the evolution of the system with $\epsilon_0 = 1.35$ and $\epsilon_0 = 1.85$ and few values in between. The result is shown in figure 2.4. For the same applied velocity v_0 we generally see that lower ϵ_0 results in higher $\dot{s}$. However, the kinetic relation is quite similar no matter what ϵ_0 we use (see figure 2.5). The differences are apparent only when applied velocity is low. Lastly, we have performed compression experiments on our chain starting with all springs at the bottom of the well corresponding to the high strain phase and $\epsilon_0 = 1.5$. The resulting kinetic relation is the same as (2.13).

2.2.2 Solving a Riemann problem involving a single phase boundary

Riemann problems in bars with a single phase boundary have been treated earlier [7, 65]. In the analytical solution with the infinite domain $-\infty < x < \infty$ there are two shock waves originating from $x = 0$ and moving outwards towards $-\infty$ and ∞. However, we cannot

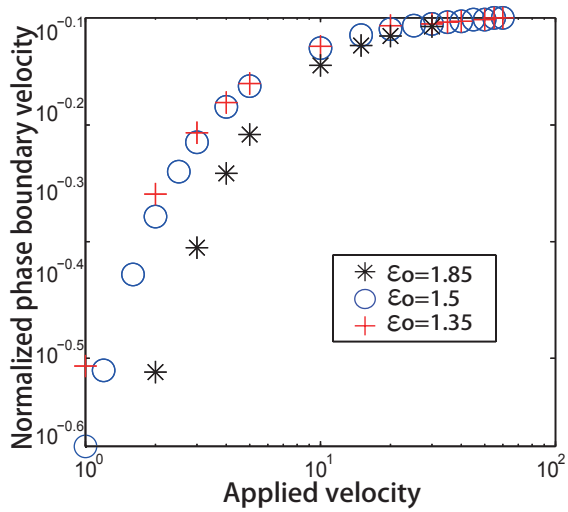

Figure 2.4: Loglog plot of normalized phase boundary velocity $\dot{s}/c$ as a function of applied velocity v_0 for different values of ϵ_0. The differences between various values of ϵ_0 are apparent only for small values of $\dot{s}/c$.

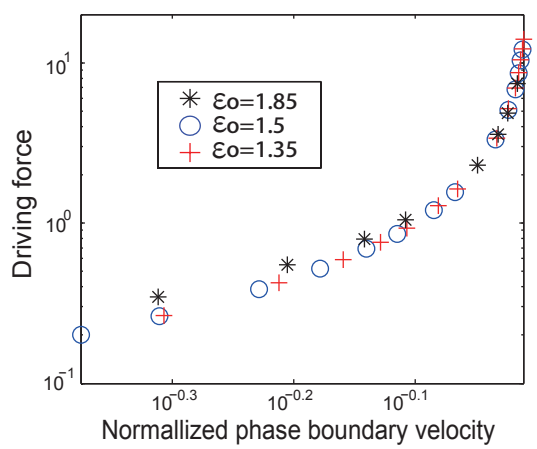

Figure 2.5: Loglog plot of driving force as a function of normalized phase boundary velocity for different values of ϵ_0. Over the range $1.35 \leq \epsilon_0 \leq 1.85$, we do not see much change in the kinetic relation.

simulate an infinite mass spring system. We have used $N+1$ masses and N springs with an initial phase boundary in the middle of the chain between mass number $\frac{N}{2}$ and $\frac{N}{2}+1$. The equation of motion for the masses is (2.9) and the two boundaries are left free (zero force). The force stretch relation for the springs is unchanged. Since our mass-spring system has a finite number of masses and has two boundaries there are two additional sonic waves which originate from the two ends. We integrate the dynamics of the mass spring system up to the point when the two sonic waves originating at the center of the chain and those coming from the ends meet each other.

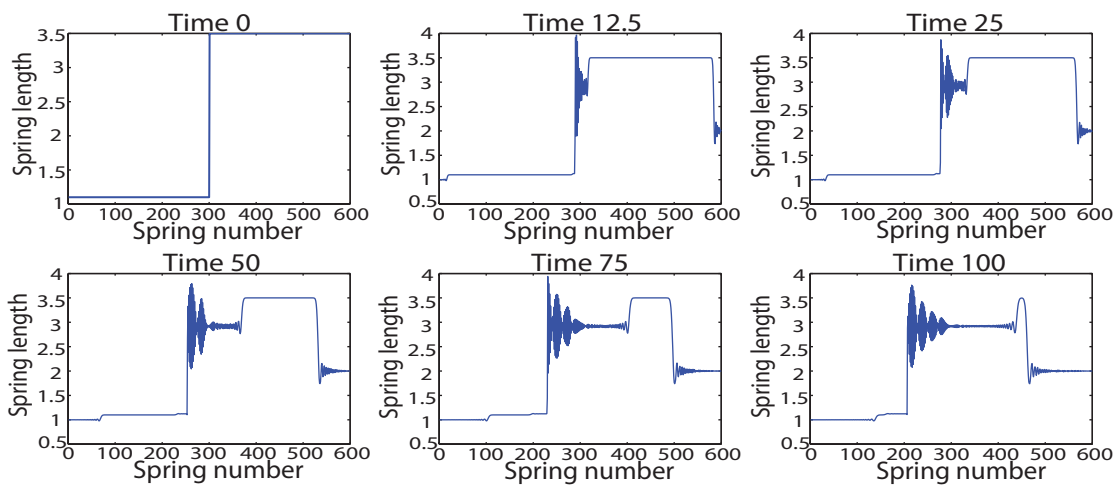

Figure 2.6: Time snap-shots of the chain whose initial conditions correspond to a Riemann problem with a single phase boundary. Two sonic waves move from the center towards the left and right ends. Two other sonic waves move from the left and right ends towards the center. The phase boundary also moves. We integrate only upto the time when the sonic waves coming from the ends meet those coming from the center.

The evolution of the system is shown in fig. 2.6. We see that there is a phase boundary moving from the middle of the chain to the left end in addition to the four sonic waves described above. If we focus on the middle part of the chain between the two sonic waves moving outward then the $x-t$ plane looks exactly like that expected from the continuum theory of bars as shown in fig. 2.7(a). We can determine the phase boundary velocity directly

from this numerical calculation. Next, we will solve the corresponding analytical problem for a bar and compare the result for the phase boundary velocity with that obtained from the discrete calculation.

The strain and velocity fields in the Riemann problem in the continuum theory of bars are piecewise constant in x and t as shown in fig. 2.7(a). The resulting equations from the jump conditions (A.1) and (A.3) are summarized below.

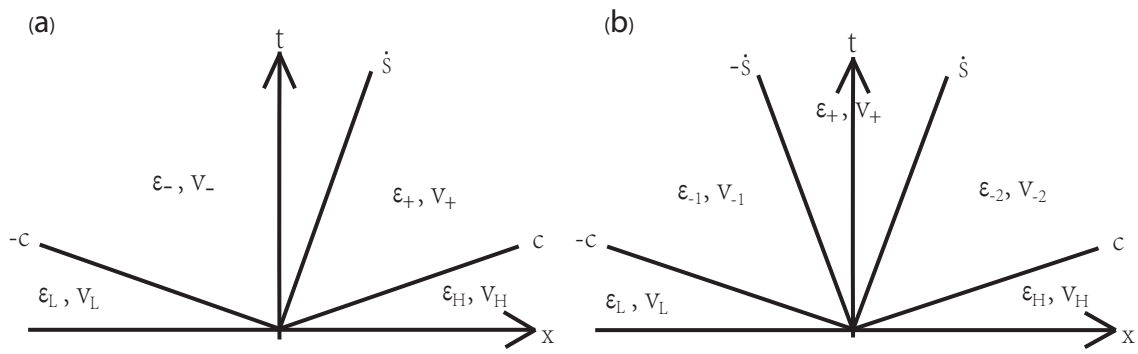

Figure 2.7: x-t plane representation of continuum Riemann problem with one phase boundary (left) and two phase boundaries (right). The strain and velocity fields are piece-wise constant, separated by propagating discontinuities.

$$-c(\epsilon_L - \epsilon_-) + v_L - v_- = 0, \tag{2.14}$$

$$c(\epsilon_H - \epsilon_+) + v_H - v_+ = 0, \tag{2.15}$$

$$\rho\dot{s}(v_+ - v_-) + E(\epsilon_+ - \gamma_T - \epsilon_-) = 0, \tag{2.16}$$

$$\dot{s}(\epsilon_+ - \epsilon_-) + v_+ - v_- = 0. \tag{2.17}$$

As ϵ_L,ϵ_H,v_L,v_H are known from the initial conditions, we have five unknowns ϵ_-,ϵ_+,v_-,v_+ and $\dot{s}$, but only four equations. The fifth equation is the kinetic relation (2.13) obtained in

ϵ_L	ϵ_H	v_L	v_H	Analytical $\dot{s}$	Numerical $\dot{s}$	Error
-0.2	1.6	0.05	0.1	-0.3984	-0.352	0.0464
-0.2	1.6	0.25	0.5	-0.4789	-0.425	0.0539
-0.2	1.6	0.05	0.75	-0.6183	-0.59	0.0283
0.1	2.5	0.1	1	-0.9211	-0.935	-0.0139
0.1	2.5	0.1	1.5	-0.9657	-0.985	-0.0193
0.1	2.5	0.1	2	-1.0028	-1.025	-0.0222
0.1	2.5	0.1	2.5	-1.0343	-1.055	-0.0207
0.1	2.5	0.1	4.5	-1.1231	-1.15	-0.0269
0.1	2.5	0.1	6	-1.1665	-1.185	-0.0185
0.1	2.5	0.1	7.5	-1.1986	-1.215	-0.0164

Table 2.1: Comparison of numerical results with analytical solution of Riemann problems. The numerical results are from our mass-spring chains with the same potentials as in the impact problems. The analytical results use the kinetic relation obtained from the impact problem on the chain. The agreement between the phase boundary velocities obtained from the numerical integration for the chain and those from the analogous continuum analytic solution is quite good.

the previous section.

$$\frac{f_{driving}}{E\gamma_T} = \frac{3}{2}(1 + \frac{\gamma_T}{1 - \frac{\dot{s}^2}{c^2}}) = -\frac{2}{E\gamma_T}(\epsilon_+ + \epsilon_- - 2). \tag{2.18}$$

We can therefore solve for all the unknowns analytically. The result of the analytical calculation and the numerical simulation of the Riemann problem are given in table 2.1. We see that the phase boundary velocity calculated by the analytic method is very close to the result we get by numerical integration of Newton's law for the chain. The error is relatively large for the case when phase boundary velocity is small (around 0.4). We believe that this relatively large error has its origins in the difficulty in obtaining the correct phase boundary velocity due to its 'jerky' motion.

2.2.3 Solving a Riemann problem involving multiple phase boundaries

As shown in earlier work, it is possible to get two phase boundaries in a Riemann problem for appropriate initial conditions [7]. We demonstrate that our kinetic relation can correctly

predict the phase boundary velocities in this type of problems too. In this example the initial condition is: $\epsilon_L = 1.15, \epsilon_H = 0.75, v_L = -2, v_H = 5$. The system evolution is shown in fig. 2.8. The corresponding $x - t$ plane representation is shown in fig. 2.7(b).

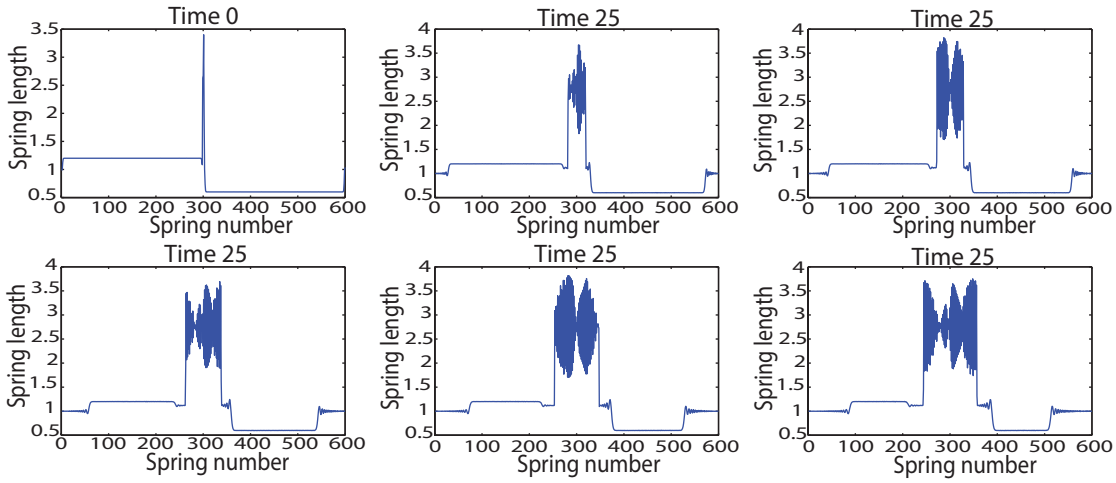

Figure 2.8: Time snap-shots of a chain with initial conditions corresponding to a Riemann problem where nucleation of two phase boundaries is expected. The two phase boundaries travel to the left and right at the same speed. This is in agreement with the solution of the corresponding continuum Riemann problem.

We can write the equations resulting from the jump conditions for the continuum version of this Riemann problem. There are eight unknowns: ϵ_{-1}, ϵ_{-2}, v_{-1}, v_{-2}, ϵ_+, v_+, $\dot{s_1}$, $\dot{s_2}$. With the kinetic relation we have eight equations in total – two from the two sonic waves

and six from the two phase boundaries. They are

$$
\begin{aligned}
-c(\epsilon_L - \epsilon_{-1}) + v_L - v_{-1} &= 0, && (2.19)\\
-\dot{s_1}(\epsilon_{-1} - \epsilon_+) + v_{-1} - v_+ &= 0, && (2.20)\\
-\dot{s_1}(v{-}1 - v_+) + E(\epsilon_{-1} - \gamma_T - \epsilon_+) &= 0, && (2.21)\\
\dot{s_2}(\epsilon_+ - \epsilon_{-2}) + v_+ - v_{-2} &= 0, && (2.22)\\
\dot{s_2}(v{+} - v_{-2}) + E(\epsilon_+ - \gamma_T - \epsilon_{-2}) &= 0, && (2.23)\\
c(\epsilon_{-2} - \epsilon_R) + v_{-2} - v_R &= 0, && (2.24)\\
f_1 = \frac{E\gamma_T}{2}(2\epsilon_0 - \epsilon_{-1} - \epsilon_+) &= \frac{3}{2}E\gamma_T(1 + \frac{\gamma_T}{1 - \frac{\dot{s_1}^2}{c^2}}), && (2.25)\\
f_2 = \frac{E\gamma_T}{2}(2\epsilon_0 - \epsilon_{-2} - \epsilon_+) &= \frac{3}{2}E\gamma_T(1 + \frac{\gamma_T}{1 - \frac{\dot{s_2}^2}{c^2}}). && (2.26)
\end{aligned}
$$

By solving these equations, we get

$$
\begin{aligned}
\epsilon_+ - \epsilon_{-1} &= \frac{\gamma_T}{1 - \dot{s_1}^2/c^2}, && (2.27)\\
\epsilon_+ + \epsilon_{-1} &= \epsilon_0 - \frac{3}{2}(1 + \epsilon_+ - \epsilon_{-1}), && (2.28)\\
\epsilon_+ - \epsilon_{-2} &= \frac{\gamma_T}{1 - \dot{s_2}^2/c^2}, && (2.29)\\
\epsilon_+ + \epsilon_{-2} &= \epsilon_0 - \frac{3}{2}(1 + \epsilon_+ - \epsilon_{-2}). && (2.30)
\end{aligned}
$$

Therefore, we have $\dot{s_1}^2 = \dot{s_2}^2$. The analytically calculated result for $\dot{s}_1$ and $\dot{s}_2$ is 1.5303, compared with numerical result $\dot{s}_1 = 1.4533$, $\dot{s}_2 = 1.48$. The error is around 4%.

2.2.4 Temperature rise behind phase boundary

We have observed high kinetic energies of the masses right behind phase boundaries in our

numerical calculation for both impact problems and Riemann problems (see section 2.3.2. If we use the average kinetic energy in the oscillations as a surrogate for the temperature and compute it as the time averaged value of $\frac{m}{2}(v - \langle v \rangle)^2$ then it is possible to make some connections with earlier work. Abeyatane and Knowles [7] discuss the jump in temperature across a phase boundary for Mie-Gruneisen type thermoelastic material. Analytical expressions are obtained for jump in temperature as a function of applied velocity, phase boundary velocity, latent heat of transformation and other material properties. As for our model, we have not used Mie-Gruneisen type material, but we still present our results for the 'temperature' jump here (as interpreted above).

We find that the jump in temperature across the phase boundary in our impact problem is only a function of phase boundary velocity. This has been shown theoretically for a Mie-Gruneisen type material [7]. The situation for the Riemann problem is similar. The result from our calculation for the temperature jump $[|\theta|]$ as a function of phase boundary velocity is shown in fig. 2.9. We fit the data with an expression of the type

$$[|\theta|] = A + \frac{B + D\frac{\dot{s}}{c}}{1 - \frac{\dot{s}^2}{c^2}}, \tag{2.31}$$

where A, B and D are constants.

2.3 Langevin dynamics on the mass-spring chain

So far we have summarized our observations from purely mechanical simulations on the chain. We compared the results from the discrete mass-spring chain with the isothermal versions of the continuum Riemann and Goursat-Riemann problems. However, if we think of the kinetic energy stored in the oscillations around the steady state velocity as a surrogate

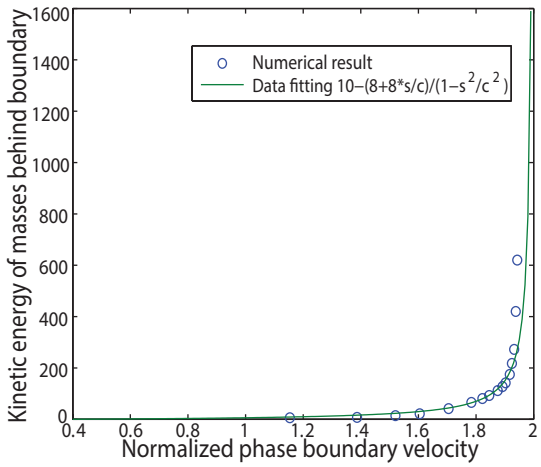

Figure 2.9: Temperature jump across the phase boundary. Here, by temperature we mean the time averaged kinetic energy stored in the oscillations of the masses. We find that the jump in temperature is a function of the phase boundary velocity only.

for the temperature then we notice a jump in the temperature across the phase boundary. This motivates us to consider a more rigorous setting where we can set the temperature of the chain by immersing it in a heat bath which supplies random impulses to the masses. This can be done by integrating Langevin's equations of motion for the masses in our chain. Our goal is to prescribe initial and boundary conditions on the chain just like we did for the Riemann and Goursat-Riemann problems discussed above and deduce a kinetic relation. We point out that such an exercise could be a model for pulling a DNA or protein molecule in an atomic force microscope (AFM). Experiments of this type are usually done with the AFM pulling the molecule at constant velocity. The long slender molecule can be viewed as a one-dimensional bar which undergoes a phase transition (abrupt structural change) at some critical tension. The macro-molecule is in a fluid, typically some buffer, so it is being constantly bombarded by the fluid molecules.

We discrete the bar into a chain of masses and springs as we did before for our numerical

calculation and the equation of motion for each mass becomes Langevin's equation:

$$\frac{du_i}{dt} = v_i, \tag{2.32}$$

$$\frac{dv_i}{dt} = -\nu v_i - \frac{\partial \phi}{\partial u_i} + F_i(t), \tag{2.33}$$

where u_i and v_i are displacement and velocity of mass i, ν is viscosity, $\frac{\partial \phi}{\partial u_i}$ is the force due to the springs, and $F_i(t)$ is the random impulse exerted on the mass from the heat bath. The random impulses on each mass are assumed to be white noise:

$$\langle F_i(t) \rangle_e = 0, \quad \langle F_i(t) F_i(t') \rangle_e = 2\nu k_B T \delta(t - t'), \quad \text{for all } i, \tag{2.34}$$

where $\langle \cdot \rangle_e$ denotes an ensemble average.

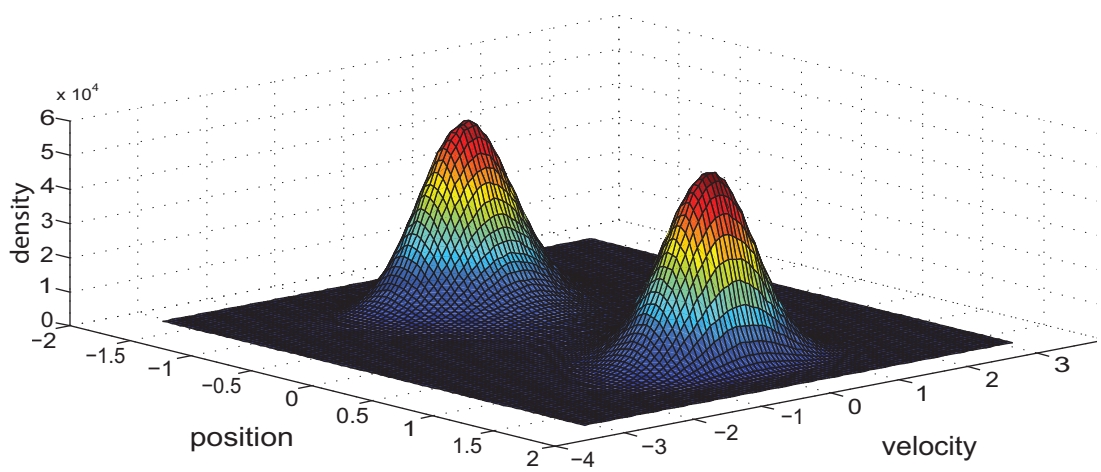

Figure 2.10: Joint probability density of velocity and position of a mass attached to a bistable spring. The velocity distribution is Gaussian, but there are two peaks in position distribution corresponding to the bottom of two energy wells.

We integrated these equations using a symplectic integrator with time step τ [52, 91].

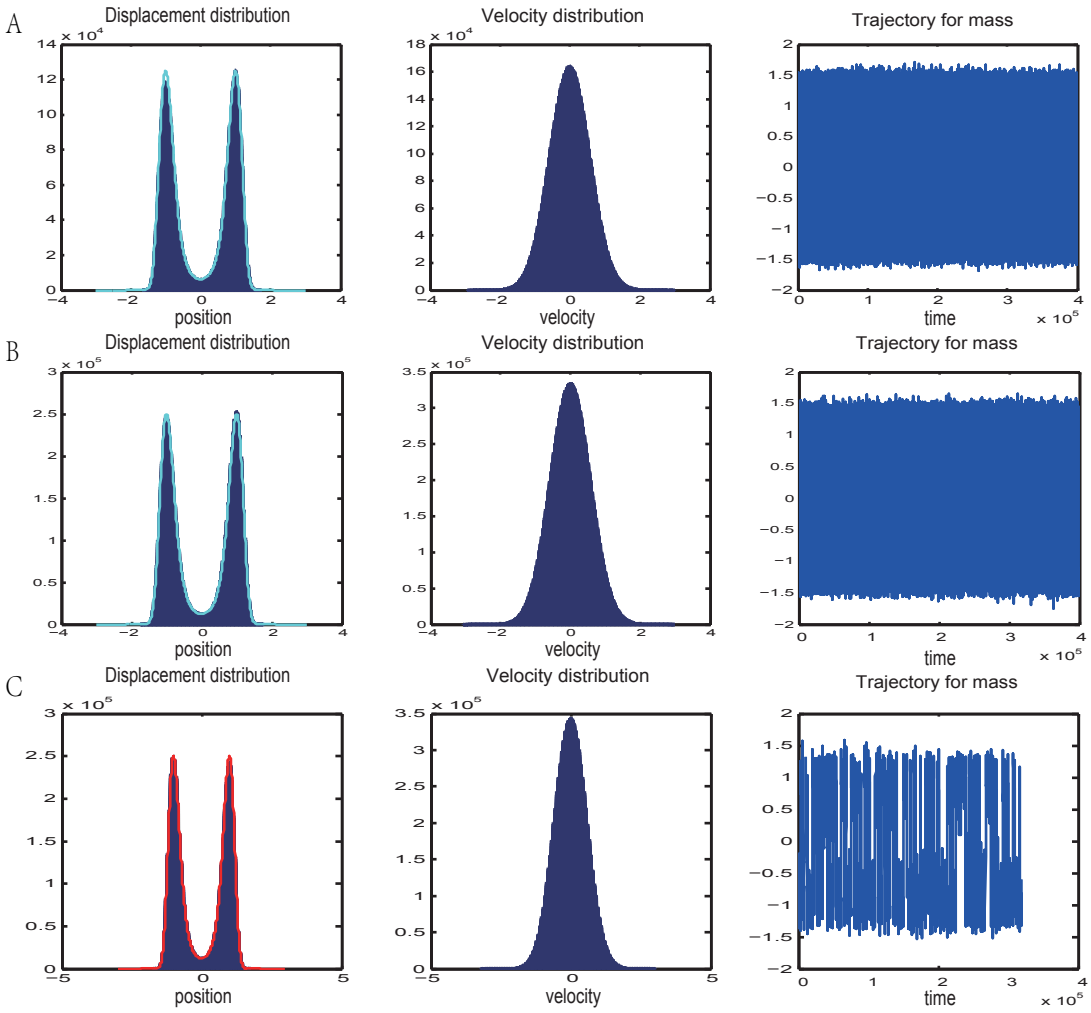

Figure 2.11: Distribution of mass position for one mass one spring system governed by Langevin's equation with different viscosity. The lines in the displacement distributions are from equation (40). (A) ν=1 (B) ν=0.01 (C) ν=0.0001.

The numerical scheme is as follows:

$$v_{1,k} = v_{II}(\frac{\tau}{2}; v_k), \tag{2.35}$$

$$u_{1,k} = u_k + \frac{\tau}{2} v_{1,k}, \tag{2.36}$$

$$v_{2,k} = v_{1,k} + \tau f(x_{1,k+1} - x_{1,k}) + \tau^{1/2} \sigma \xi_k, \tag{2.37}$$

$$v_{k+1} = v_{II}(\frac{\tau}{2}; v_{2,k}), \tag{2.38}$$

$$u_{k+1} = u_{1,k} + \frac{\tau}{2} v_{2,k}, \tag{2.39}$$

where k=0,1,....M-1, $v_{II}(t, v) = v^{-\nu t}$, $\sigma = \sqrt{2\nu k_B T}$. Using this scheme we calculated the joint probability density function for velocity and position of a mass attached to a non-linear spring. The spring is attached to the wall at one end and its potential energy is a double well. We exert no external forces on the mass and let it evolve starting from arbitrary initial conditions. The invariant density for this system is

$$\rho(v, u) = \frac{2}{Z} e^{-\beta H(v,u)}, \tag{2.40}$$

where H is the Hamiltonian of the system given as $H(v, u) = \frac{1}{2}v^2 + \phi(u)$, Z is partition function and $\beta = \frac{1}{k_B T}$ is inverse temperature. We show in fig. 2.10 and fig. 2.11 that our Langevin dynamics simulation recovers this distribution for different values of the viscosity. The time step τ depends on viscosity and spring constants. It is known that for a system of one degree of freedom, the numerical error of the calculation decreases linearly with decreasing time step [44]. We found that a time step τ that is four orders of magnitude smaller than the inverse of the natural frequency at the bottom of the energy wells gives the correct joint probability density. We verified our calculation with smaller time step to

ensure that it does not affect the final result.

2.3.1 Goursat-Riemann problems with random impulses

We now simulate the impact problem on the chain of masses and springs with Langevin's equation of motion. Just as in the purely mechanical setting we start with all springs in the low-strain phase at steady state. We prescribe a constant applied pulling rate at the right end of the chain while keeping the left end fixed and watch the evolution of the system. Note that we are constantly injecting energy into the system, so this is a non-equilibrium process. For this reason the temperature at various locations on the chain changes with time and is not necessarily the same as the bath temperature.

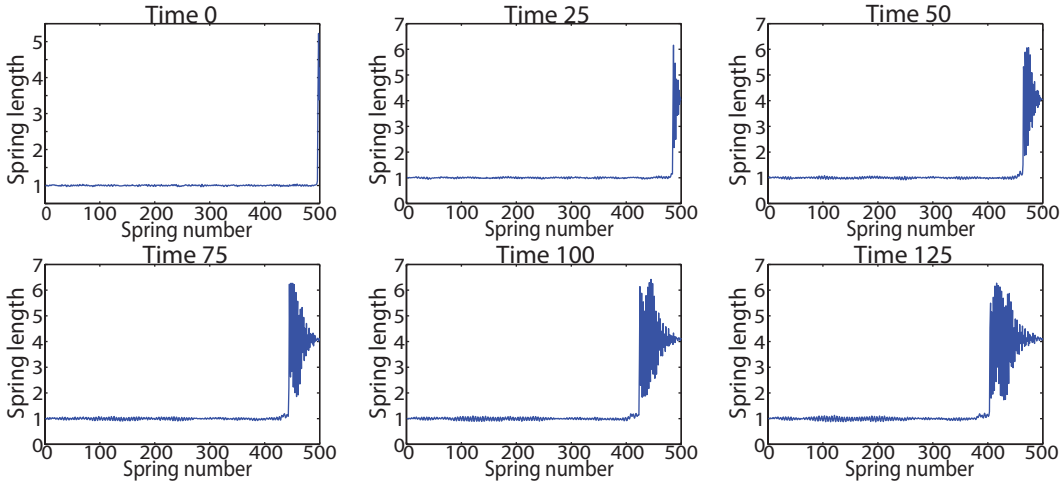

Figure 2.12: Time snap-shots of the chain for an impact problem at low bath temperature. The sonic wave is obscured but the phase boundary is clearly visible. The dynamics is similar to the purely mechanical setting.

When we set bath temperature to be relatively low, the evolution of the system is similar to our purely mechanical simulations as shown in fig. 2.12. The sonic wave is obscured due to the thermal fluctuations but the phase boundary is clearly visible and it moves at a constant speed. We have examined the effects of varying the bath temperature. If we

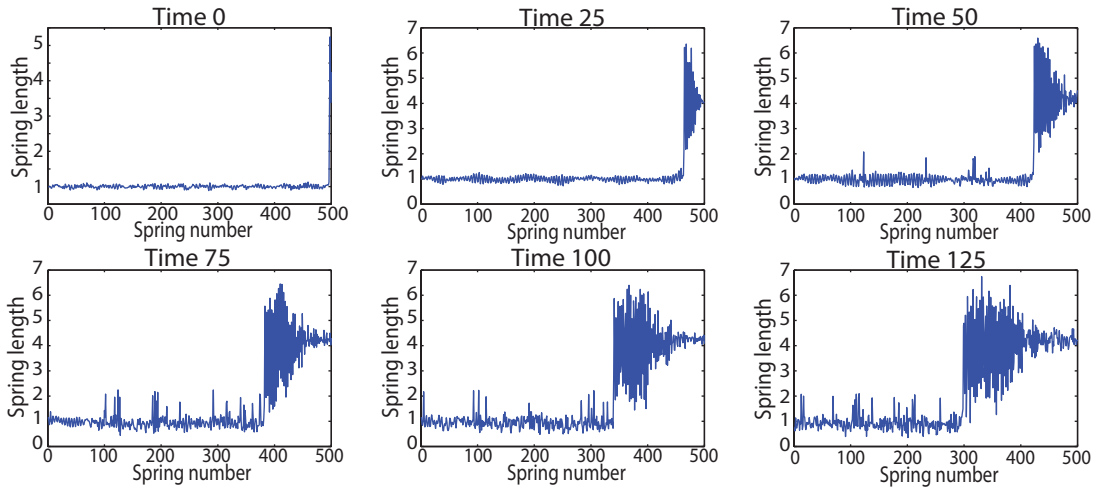

Figure 2.13: Time snap-shots of the chain for an impact problem at higher bath temperature. The dynamics is similar to the purely mechanical setting but random nucleation events are observed.

set bath temperature to be larger, which means the random kicks are larger, we observe phase transitions at random locations even before the phase boundary has arrived as shown in fig. 2.13. Thus, as temperature increases the number of random nucleation events will increase.

2.3.2 Equipartition

To verify whether our calculation has observed equipartition, we have plotted the kinetic energy of a specific mass as a function of time as shown in fig. 2.14. Temperature, which is proportional to the velocity variance from the mean is calculated as $\frac{1}{2}m(v - \langle v \rangle)^2$ where $\langle v \rangle$ is numerically determined using window averaging. We have verified that at times when phase boundary is not nearby, $\frac{1}{2}m(v - \langle v \rangle)^2 = k_B T$ for three masses positioned differently in the chain and T here represent temperature. This shows that equipartition is realized.

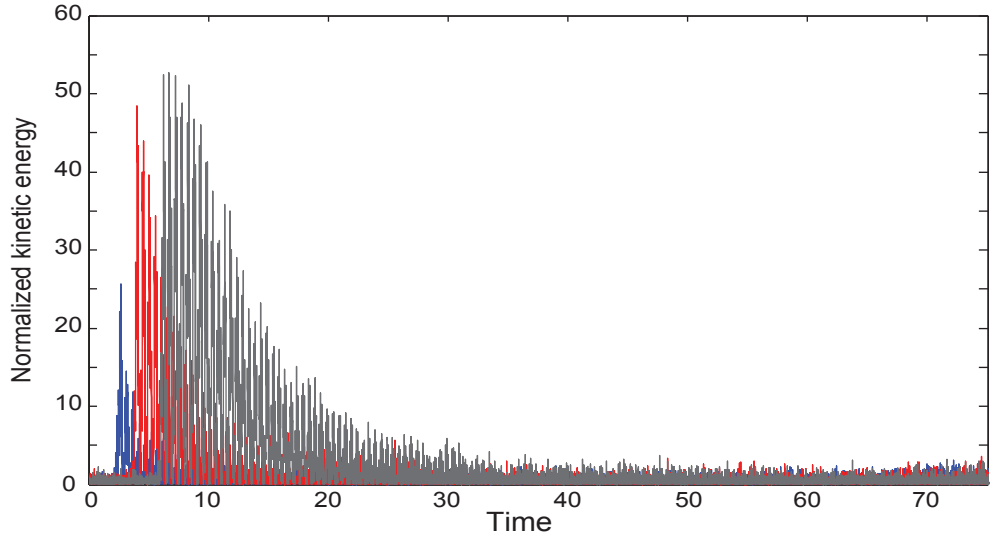

Figure 2.14: Kinetic energy of 3 different masses calculated as $\frac{1}{2}m(v - \langle v \rangle)^2$ as a function of time. On the y-axis we normalize this kinetic energy against $k_B T$ where k_B is the Boltzmann constant and T is bath temperature. Notice that when a phase boundary is not nearby the normalized average kinetic energy is 1. The temperature increases suddenly when a phase boundary passes a mass and comes down gradually to the bath temperature after some time.

2.3.3 Results from Langevin dynamics calculations on the chain

We have done calculations with different applied velocities at fixed bath temperature. For each case we calculate driving force and phase boundary velocity as we did in purely mechanical simulations. We can only get results when phase boundary velocity is above a certain value because thermal fluctuations cause jerky motion of the low velocity phase boundaries. This problem is circumvented by solving Riemann problems. In a Riemann problem there is no input of energy into the system at the boundaries, so we do not encounter the same issues as we did for the impact problem. We also remark that the kinetic energy of the masses immediately behind the phase boundary is much higher than those far away from it. This suggests that the local temperature in the bar is higher behind the phase boundary. This has been observed in experiments and has been used as a way of

tracking the phase boundary in metallic specimens [66].

After solving many such problems we get kinetic relations for fixed bath temperature. Results for two different bath temperatures are given in fig. 2.15. Data from the Riemann and impact problems are plotted together and they agree with each other. This confirms that the kinetic relation is a material property and it depends on temperature. The effect of temperature is apparent only for low phase boundary velocities. We observe that for the same driving force higher temperatures result in faster phase boundary velocities.

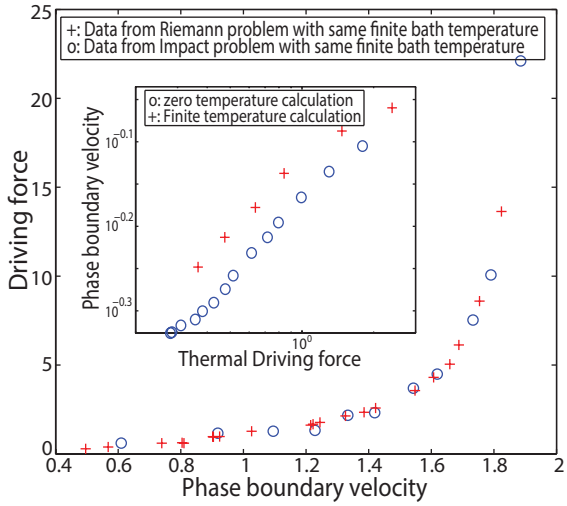

Figure 2.15: Effect of bath temperature on the kinetic relation. The data for the kinetic relations at the same finite bath temperature with two methods calculated fall on the same curve, which indicates that the kinetic relation is an inherent property of phase changing material. The inset shows that the effect of temperature is more apparent at low phase boundary velocities for different bath temperatures.

2.3.4 Force extension relation

In order to confirm that higher temperatures result in faster phase boundary velocities we plotted the force at the end (which is being pulled) of the chain as a function of time in fig. 2.16. The force increases linearly, reaches a plateau and then increases again. The plateau begins when a phase boundary is nucleated at the end being pulled and it ends

when the phase boundary has reached the other end of the chain. In order to plot the curves in fig. 2.16 we have performed an ensemble average of 10 realizations with exactly the same initial and boundary conditions. As the temperature increases the plateau ends at an earlier time point, suggesting that the phase boundary travels faster.

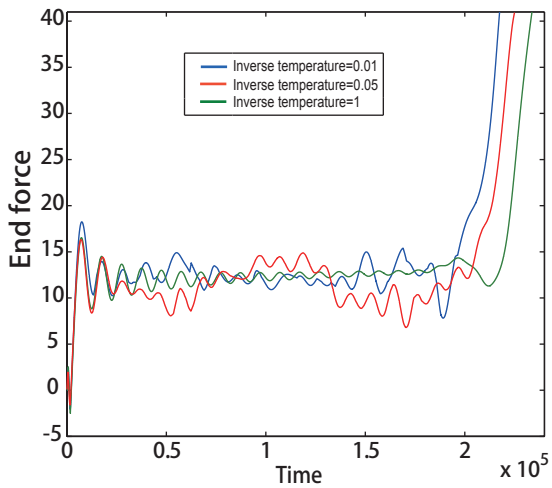

Figure 2.16: Force at the right end of the chain which is being pulled at a constant velocity $v_0 = 5$. Each color corresponds to a different temperature,the plateau ends earlier for higher temperatures. This confirms that the phase boundary travels faster as the temperature increases.

2.4 Conclusions

In this chapter we have shown how to obtain kinetic relations for moving phase boundaries in mass-spring chains. We demonstrated that the kinetic relations can be used to solve continuum Riemann problems to give results that are consistent with the mass-spring chain. We demonstrated that the kinetic relation is a function of the bath temperature. A future effort will focus on how to extend these ideas to two-dimensional lattices of masses and springs capable of phase change. We will also explore a wider temperature range to understand how the transition changes from a phase-boundary propagation dominated process

to a nucleation dominated process.

Chapter 3

(Adiabatic) phase boundaries in a bistable chain with twist and stretch

Chains of masses and springs (see figure 4.1) have been used as models to understand the mechanical and thermal behaviours of crystalline solids for a long time [36, 41]. In most of these studies the potentials characterizing the springs have one well. When the potentials characterizing the springs have multiple wells then the dynamics of mass-spring chains has been shown to be similar to that of one-dimensional bars capable of phase transitions [7, 8, 10, 13, 18, 27, 29, 42, 54, 73, 82, 85, 89]. This insight has been utilized to extract kinetic relations for moving phase boundaries by comparing solutions of impact and Riemann problems in continuum bars to those in the bistable chains [65, 85]. The extracted kinetic relation has a simple analytical form that has been recently shown to be a universal near sonic limit [89]. More recently, mass-spring chains have also provided insights into the mechanics of biological macromolecules [17, 18]. The present work is also motivated by biological examples. However, we will go beyond mass-spring chains in which each mass has just a translational degree of freedom – each of our masses will translate and rotate about the line connecting them. The continuum analogue of this mass-spring chain is a rod that can stretch and twist (but not bend). Our goal is to study the dynamics of phase boundaries in such a rod.

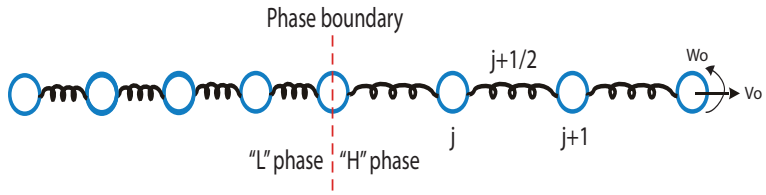

Figure 3.1: Mass-spring chain in which each mass has an extensional and rotational degree of freedom. The masses are labeled j, $j+1$, etc., and the spring connecting these two masses is labeled $j+\frac{1}{2}$. A phase boundary separates regions of the chain in which springs are in different phases. Springs in the 'H' phase correspond to the top right well in the contour plot in figure 3.2 and the 'L' phase correspond to the bottom left well in the contour plot . We specify extensional velocity v_0 and rotational velocity w_0 on the masses at the boundary. We can also specify force and moment boundary conditions.

We are inspired by three different biological examples in which twist-stretch phase transitions occur. The first is the dynamics of a primitive motile system regulated by binding of calcium ions in the horseshoe crab sperm [81]. In these organisms a bundle of actin filaments that stores both twisting and stretching energy undergoes a phase transition when calcium binds to the actin filaments. The phase transition is localized and propagates along the length of the bundle releasing energy and causing large conformational changes that result in actuation. Similar phase transitions also occur in DNA which is a rod-like helical polymer capable of stretching, twisting and bending deformations. Bending deformations (caused by external loads or by thermal bombardment) are beyond the scope of this paper but they can be neglected when the tensions are large enough that the DNA is mostly straight and aligned with the direction of the applied tension. Phase transitions can be caused in straight DNA by changing the temperature, applying large forces and twisting moments, or by changing the concentration of ions in the solution [96]. Often, phase transitions in DNA are localized and propagate by the motion of a phase boundary [90]. Our third example also concerns helical filaments forming the tail sheath of a T4 bacteriophage [32]. These filaments undergo a phase transition as soon as the tail binds to a host bacterium causing

the radius of the helix to increase and the pitch to decrease, so that the cylinder formed by several of these helices arranged side-by-side inflates (radially) and compresses (axially) to transfer the viral DNA into the host cell. All these examples involve filaments whose lengths are microns or smaller and they are usually surrounded by a viscous fluid, so that inertia forces are negligible. We have studied the propagation of phase boundaries in such rods earlier [67, 100]. Recently, however, macroscopic yarns (called 'artificial muscles') have been fabricated to perform actuation in which inertia forces cannot be neglected [48]. These filaments are made by twisting and braiding carbon nanotube yarn; they are activated by heat, binding of small molecules, and even light. They can perform useful extensional and rotational work over thousands of cycles. The common features in all of these examples are (a) filaments in which twist and stretch are coupled, and (b) phase transitions driven by ions, forces or heat. The key constitutive information that is needed to study these phase transitions (in dynamic or quasi-static problems) is a kinetic relation. Finding a kinetic relation for twist-stretch phase boundaries is the primary objective of this work.

The paper is laid out as follows. First, we give a short account of the balance laws and constitutive relations for rods capable of phase transitions in twist and stretch. Second, we describe an analogous mass-spring chain and integrate its dynamics with a leapfrog algorithm. We have simulated both impact and Riemann problems to study the motion of a phase boundary. Third, we extract a kinetic relation from our mass-spring simulations and show that we can correctly solve continuum problems with it. Even though this kinetic relation is useful it must be interpreted with care without neglecting the energy stored in the oscillations of the masses and springs which may represent a local temperature. Lastly, we apply our ideas to some recently developed artificial muscles mentioned above.

3.1 Thermomechanics of 1-D chain

3.1.1 Balance Laws

Let us begin by considering phase boundaries propagating in a one-dimensional continuum in the interval $0 \leq x \leq L$. Here x is the reference coordinate along the continuum of length L. The specific realization of the continuum we have in our minds is a rod with circular cross-section. At each reference point we have two variables – the deformed position $z(x,t)$ of the rod cross-section located at x at time t, and $\alpha(x,t)$ the angle through which that cross-section has rotated at time t. We require that $z(x,t)$ and $\alpha(x,t)$ be continuous at all x and t so that the rod does not break. We do not allow bending deformations of the rod. The stretch of the rod is $\lambda(x,t) = \frac{\partial z}{\partial x}$ and the twist is $\kappa(x,t) = \frac{\partial \alpha}{\partial x}$. These quantities are allowed to jump at a finite number of points in our continuum. If one such jump is located at $x = s(t)$ then let us denote $x > s(t)$ as the + side, $x < s(t)$ as the - side. For any quantity $y(x,t)$ we denote $y(x_+,t) - y(x_-,t)$ by $[|y|]$ and $\frac{y(x_+,t)+y(x-,t)}{2}$ by $\langle y \rangle$. From continuity of the deformed material we have $[|z|] = 0$ and $[|\alpha|] = 0$. Differentiating these two equations with respect to time we get the kinematic jump conditions

$$\dot{s}[|\lambda|] + [|\dot{z}|] = 0, \tag{3.1}$$

$$\dot{s}[|\kappa|] + [|\dot{\alpha}|] = 0. \tag{3.2}$$

The equation for balance of linear momentum for a portion of the rod in the interval (x_1, x_2) in the absence of body forces is

$$\frac{d}{dt}\int_{x_1}^{x_2} \rho \dot{z}\, dx = T|_{x_1}^{x_2}, \tag{3.3}$$

where $\rho(x,t)$ is the mass per unit length and and $T(x,t)$ is the tension in the rod[65–67]. If we localize this equation to a discontinuity $s(t)$ (with $x_1 \leq s(t) \leq x_2$) then we get the linear momentum jump condition

$$[|T|] + \dot{s}[|\rho v|] = 0, \tag{3.4}$$

with $v(x,t) = \dot{z}$. If we localize this away from discontinuity we get

$$\rho \ddot{z} = \frac{\partial T}{\partial x}. \tag{3.5}$$

The equation for the balance of angular momentum for a portion of the rod in the interval (x_1, x_2) in the absence of body moments is

$$\frac{d}{dt} \int_{x_1}^{x_2} \rho r_g^2 \dot{\alpha} dx = M|_{x_1}^{x_2}, \tag{3.6}$$

where r_g is the radius of gyration of the cross-section and $M(x,t)$ is the torque in the rod. If we localize this equation to a discontinuity $s(t)$ (with $x_1 \leq s(t) \leq x_2$) then we have

$$[|M|] + \dot{s}[|\rho r_g^2 w|] = 0, \tag{3.7}$$

where $w(x,t) = \dot{\alpha}$. If we localize this equation away from the discontinuity at $x = s(t)$ then we get

$$\rho r_g^2 \ddot{\alpha} = \frac{\partial M}{\partial x}. \tag{3.8}$$

Starting from the balance laws given above one can derive an expression for the thermodynamic driving force across a discontinuity. This exercise has been carried out in detail in

[64] for the more general case when the 1D continuum can stretch, bend and twist. The expression for the driving force is

$$f_{driving} = [|W|] - \langle T \rangle [|\lambda|] - \langle M \rangle [|\kappa|], \tag{3.9}$$

where $W(\lambda, \kappa)$ is the Helmholtz free energy per unit length of our continuum.

3.1.2 Constitutive law

We will now choose a specific form for $W(\lambda, \kappa)$. We imagine that $W(\lambda, \kappa)$ has two wells located at different points on the $\lambda - \kappa$ plane. The phase corresponding to low values of λ and κ is denoted as $j = L$ and the Helmholtz free energy per unit length in this phase is $W_L(\lambda, \kappa)$. Similarly, the phase corresponding to large values of λ and κ is denoted as $j = H$ with free energy density $W_H(\lambda, \kappa)$. We assume $W(\lambda, \kappa)$ is a quadratic form in both these phases. Hence,

$$W_j(\lambda, \kappa) = \frac{S_j}{2}(\lambda - \lambda_j^0)^2 + g_j(\lambda - \lambda_j^0)(\kappa - \kappa_j^0) + \frac{C_j}{2}(\kappa - \kappa_j^0)^2, \tag{3.10}$$

where j denotes a phase, S_j is the stretching modulus of phase j, C_j is the twisting modulus and g_j is the twist-stretch coupling modulus. The constants λ_j^0 and κ_j^0 have to do with the intrinsic stretch and twist of phase j with respect to some reference state. We choose the reference state as the bottom of the well in phase L, so that $\lambda_L^0 = 1$ and $\kappa_L^0 = 0$. To simplify matters we choose $S_L = S_H = S$, $g_L = g_H = g$ and $C_L = C_H = C$. For the high strain phase we choose $\lambda_H^0 = 2$ and $\kappa_H^0 = 1$. This type of Helmholtz free energy density is illustrated in figure 3.2. The two phases are separated by a line on the $\lambda - \kappa$ plane. The

equation of the line is:

$$A\lambda + B\kappa + D = 0, \tag{3.11}$$

where

$$A = S(\lambda_H^0 - \lambda_L^0) + g(\kappa_H^0 - \kappa_L^0), \tag{3.12}$$

$$B = g(\lambda_H^0 - \lambda_L^0) + C(\kappa_H^0 - \kappa_L^0), \tag{3.13}$$

$$D = \frac{S}{2}((\lambda_L^0)^2 - (\lambda_H^0)^2) + \frac{C}{2}((\kappa_L^0)^2 - (\kappa_H^0)^2) + g(\lambda_L^0\kappa_L^0 - \lambda_H^0\kappa_H^0). \tag{3.14}$$

Here we denote $A\lambda + B\kappa + D \geq 0$ as the 'H' phase and $A\lambda + B\kappa + D \leq 0$ as the 'L' phase. The force and moment constitutive relations can be immediately computed by

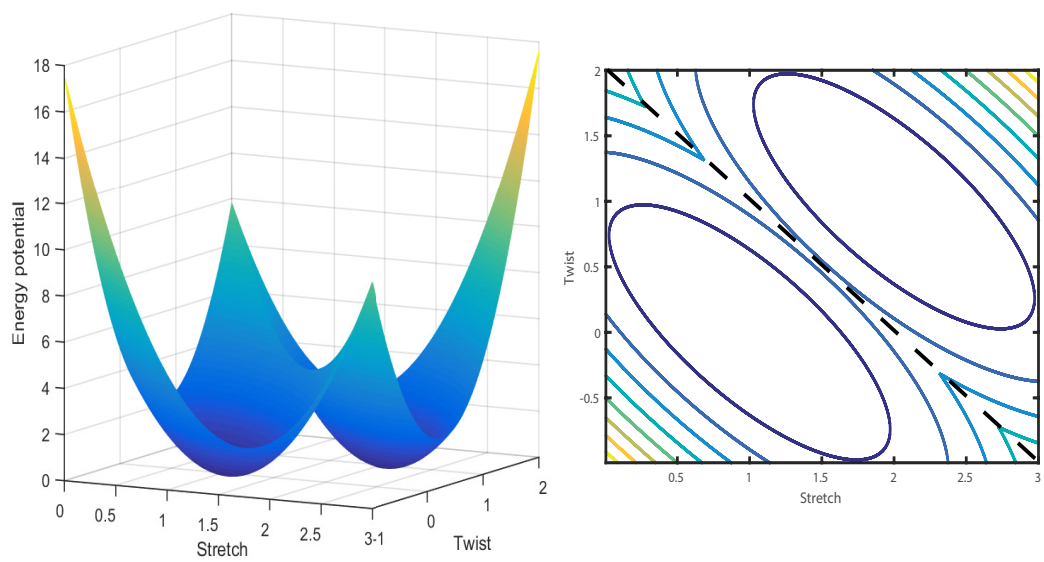

Figure 3.2: Energy landscape of the rod. (a) Helmholtz free energy per unit length plotted as a function of stretch λ and twist curvature κ. It has two wells. (b) The location of the two wells shown on a contour plot in the λ–κ plane. The dashed line which separates the two phases is described by the equation $A\lambda + B\kappa + D = 0$.

differentiating the $W(\lambda, \kappa)$. These are

$$T(\lambda, \kappa) = \begin{cases} S(\lambda - \lambda_L^0) + g(\kappa - \kappa_L^0), & \text{for the 'L' phase,} \\ \\ S(\lambda - \lambda_H^0) + g(\kappa - \kappa_H^0), & \text{for the 'H' phase,} \end{cases} \tag{3.15}$$

and

$$M(\lambda, \kappa) = \begin{cases} g(\lambda - \lambda_L^0) + C(\kappa - \kappa_L^0), & \text{for the 'L' phase,} \\ \\ g(\lambda - \lambda_H^0) + C(\kappa - \kappa_H^0), & \text{for the 'H' phase.} \end{cases} \tag{3.16}$$

3.1.3 Sonic waves

For this kind of material three kinds of discontinuities are possible – two kinds of 'sonic waves' with both sides of the discontinuity in the same phase, and a phase boundary with the two sides in different phases. Let us first consider a sonic wave type of discontinuity whose speed in the reference configuration is denoted by c. At such a discontinuity the jump conditions give

$$\begin{aligned} c(\lambda_+ - \lambda_-) + v_+ - v_- &= 0, \\ c(\kappa_+ - \kappa_-) + w_+ - w_- &= 0, \\ c\rho(v_+ - v_-) + S(\lambda_+ - \lambda_-) + g(\kappa_+ - \kappa_-) &= 0, \\ c\rho r_g^2(w_+ - w_-) + g(\lambda_+ - \lambda_-) + C(\kappa_+ - \kappa_-) &= 0. \end{aligned}$$

We eliminate $v_+ - v_-$ between the first and third equations, and $w_+ - w_-$ between the second and fourth equations to get

$$\begin{aligned} -c^2\rho(\lambda_+ - \lambda_-) + S(\lambda_+ - \lambda_-) + g(\kappa_+ - \kappa_-) = 0, \\ -c^2\rho r_g^2(\kappa_+ - \kappa_-) + g(\lambda_+ - \lambda_-) + C(\kappa_+ - \kappa_-) = 0. \end{aligned} \tag{3.17}$$

This system of equations can have a non-trivial solution for $\lambda_+ - \lambda_-$ and $\kappa_+ - \kappa_-$ only if

$$\frac{S - \rho c^2}{g} = \frac{g}{C - \rho r_g^2 c^2}, \quad \text{or,} \quad \rho^2 r_g^2 c^4 - \rho(S r_g^2 + C)c^2 + SC - g^2 = 0. \tag{3.18}$$

This is a quadratic equation for c^2 of which there are two solutions:

$$\begin{aligned} c_1 &= \sqrt{\frac{\rho r_g^2 S + \rho C + \sqrt{(\rho r_g^2 S - \rho C)^2 + 4\rho^2 g^2 r_g^2}}{2\rho^2 r_g^2}}, \\ c_2 &= \sqrt{\frac{\rho r_g^2 S + \rho C - \sqrt{(\rho r_g^2 S - \rho C)^2 + 4\rho^2 g^2 r_g^2}}{2\rho^2 r_g^2}}. \end{aligned} \tag{3.19}$$

We have chosen $c_1 > c_2$. Note that c_1 would be the bar wave speed $\sqrt{S/\rho}$ and c_2 would be the torsional wave speed $\sqrt{C/\rho r_g^2}$ if the twist-stretch coupling modulus $g = 0$.

3.1.4 Continuum impact problem with no phase boundary

We will now use the jump conditions given above to solve an impact problem. Consider a semi-infinite domain, $-\infty < x \leq 0$. At $t = 0$, $\lambda(x, 0) = \lambda_L$, $\kappa(x, 0) = \kappa_L$, $v(x, 0) = v_L$ and $w(x, 0) = w_L$ for all $x < 0$. We apply the boundary conditions $v(0, t) = v_o$ and $w(0, t) = w_o$ for all $t > 0$. This problem has a piece-wise constant solution with two propagating discontinuities as shown in the x-t plane depicted in figure 4.2. These discontinuities travel at speeds c_1 and c_2 if v_o and w_o are so small that no phase change occurs.

In the regions of the x-t plane between discontinuities the quantities $\lambda(x,t)$, $\kappa(x,t)$, $v(x,t)$ and $w(x,t)$ are constant. Hence, they trivially satisfy the field equations (3.5) and (3.8). At the propagating discontinuities we have to enforce the jump conditions. These are summarized below.

$$
\begin{aligned}
c_1(\lambda_1 - \lambda_L) + v_1 - v_L &= 0, \\
c_1(\kappa_1 - \kappa_L) + w_1 - w_L &= 0, \\
c_1\rho(v_1 - v_L) + S(\lambda_1 - \lambda_L) + g(\kappa_1 - \kappa_L) &= 0, \\
c_2(\lambda_2 - \lambda_1) + v_0 - v_1 &= 0, \\
c_2(\kappa_2 - \kappa_1) + w_0 - w_1 &= 0, \\
c_2\rho(v_0 - v_1) + S(\lambda_2 - \lambda_1) + g(\kappa_2 - \kappa_1) &= 0.
\end{aligned}
\tag{3.20}
$$

These are six equations for the six unknowns λ_1, κ_1, v_1, w_1, λ_2, κ_2. Note that there are three jump conditions at each of the two discontinuities. The fourth jump condition at each discontinuity does not give us any extra information because we have already used it to get the speeds c_1 and c_2. After solving this set of equations we got the analytical result for λ_1, κ_1, v_1, w_1, λ_2, κ_2.

In the next section we will see that this type of solution can be recovered by discretizing the continuum as a mass-spring chain with an extensional and rotational degree of freedom at each mass and solving the dynamical problem numerically. We will also see propagating phase boundaries when v_o or w_o are sufficiently large.

3.2 Mass-spring chain

3.2.1 Description and time integration algorithm

We have considered the dynamics of a discrete system of masses and springs to obtain the kinetics of moving phase boundaries in bars earlier [98]. The masses interacted with their first-nearest neighbors via potentials $\phi_1(x_i)$ where $x_i = u_{i+1} - u_i$ and u_i is the displacement of the ith mass. The function $\phi_1(x)$ was a double well potential such that the equilibrium spacing between the masses at zero force could have two possible values, a and b. The potential was constructed by using piece-wise quadratic expressions, so that the force-extension relation for each spring was trilinear (with spinodal region). We now propose that mass i has a rotational degree of freedom $\theta_i(t)$ as well. We will call $x_i = u_{i+1} - u_i$ and $y_i = \theta_{i+1} - \theta_i$. Each mass interacts with its first nearest neighbor through a potential $\phi_1(x_i, y_i)$. Just like before, the potential ϕ as a function of the stretch and twist variables x_i and y_i has two wells representing two phases (but with no spinodal region). In each well we will assume that $\phi_1(x, y)$ is a quadratic form:

$$\phi_1(x,y) = \begin{cases} \frac{B_1}{2}(x-a_1)^2 + B_2(x-a_1)(y-b_1) + \frac{B_3}{2}(y-b_1)^2, & \text{in phase L,} \\ \frac{B_1}{2}(x-a_2)^2 + B_2(x-a_2)(y-b_2) + \frac{B_3}{2}(y-b_2)^2, & \text{in phase H,} \end{cases} \tag{3.21}$$

where the well corresponding to phase L is located at (a_1, b_1) on the $x_i - y_i$ plane (for all i) and the well corresponding to phase H is located at (a_2, b_2). The constant B_1 is related to the stretch modulus S, B_2 to the twist-stretch coupling modulus g, and B_3 to the twisting modulus C as follows. Assume that the reference length for a unit in mass spring chain is Δ, then $S = \Delta B_1$, $g = \Delta B_2$, $C = \Delta B_3$ and $\lambda_L^0 = a_1/\Delta$, $\lambda_H^0 = a_2/\Delta$, $\kappa_L^0 = b_1/\Delta$, $\kappa_H^0 = b_2/\Delta$. This results in linear relations between the force/torque and stretch/twist. The total energy

of the chain consisting of N masses connected by $N-1$ springs can be written as:

$$\phi(u_1, u_2, ..., u_N, \theta_1, \theta_2, ..., \theta_N) = \sum_{i=1}^{N-1} \phi_1(x_i, y_i). \tag{3.22}$$

The dynamics of the chain is governed by the following system of ordinary differential equations:

$$m_i \ddot{u}_i = \frac{\partial \phi}{\partial u_i}, \quad I_i \ddot{\theta}_i = \frac{\partial \phi}{\partial \theta_i}, \qquad i = 1, ..., N. \tag{3.23}$$

Here m_i is the ith mass and I_i is the moment of inertia of the ith mass about the straight line connecting all the masses. We assume for simplicity that $m_i = m$ and $I_i = I$ for all i. The evolution of the variables $u_i(t)$ and $\theta_i(t)$ can be calculated by solving the above system of differential equations subject to some initial conditions $u_i(0) = u_i^0, \dot{u}_i(0) = v_i^0, \theta_i(0) = \theta_i^0, \dot{\theta}_i(0) = w_i^0, i = 1, ..., N$ and some boundary conditions on $u_0(t), \theta_0(t)$ and $u_N(t), \theta_N(t)$. Here, u_i^0 is the ith component of a given vector u^0 with N entries, and similarly for v_i^0, θ_i^0, w_i^0.

The equations of motion of the masses for $i = 2, ..., N-1$ can be written as

$$\begin{aligned} m\ddot{u}_i &= T_{i+\frac{1}{2}} - T_{i-\frac{1}{2}}, \\ I\ddot{\theta}_i &= M_{i+\frac{1}{2}} - M_{i-\frac{1}{2}}, \end{aligned} \tag{3.24}$$

where $i + \frac{1}{2}$ and $i - \frac{1}{2}$ denote the springs attached to mass i. Here $T_{i+\frac{1}{2}}$ is the force in the spring connecting masses $i+1$ and i, etc. Without loss of generality we can take $m = 1$ and $I = 1$, then

$$\begin{aligned} \ddot{u}_i &= T(u_{i+1} - u_i, \theta_{i+1} - \theta_i) - T(u_i - u_{i-1}, \theta_i - \theta_{i-1}), \\ \ddot{\theta}_i &= M(u_{i+1} - u_i, \theta_{i+1} - \theta_i) - M(u_i - u_{i-1}, \theta_i - \theta_{i-1}). \end{aligned} \tag{3.25}$$

We use a leapfrog algorithm to integrate the system. We start from an initial condition in which we know the position and velocity (both linear and angular) of each mass, then we carry out our calculation by updating the state of each mass as follows.

$$
\begin{aligned}
T^i_{j+\frac{1}{2}} &= B_1(x^i_{j+\frac{1}{2}} - a_k) + B_2(y^i_{j+\frac{1}{2}} - b_k), \\
M^i_{j+\frac{1}{2}} &= B_2(x^i_{j+\frac{1}{2}} - a_k) + B_3(y^i_{j+\frac{1}{2}} - b_k), \\
u^{i+1}_j &= u^i_j + \Delta t v^i_j + \frac{1}{2}\Delta t^2(T^i_{j+\frac{1}{2}} - T^i_{j-\frac{1}{2}}), \\
\theta^{i+1}_j &= \theta^i_j + \Delta t w^i_j + \frac{1}{2}\Delta t^2(M^i_{j+\frac{1}{2}} - M^i_{j-\frac{1}{2}}), \\
v^{i+1}_j &= v^i_j + \frac{1}{2}\Delta t(T^i_{j+\frac{1}{2}} - T^i_{j-\frac{1}{2}} + T^{i+1}_{j+\frac{1}{2}} - T^{i+1}_{j-\frac{1}{2}}), \\
w^{i+1}_j &= w^i_j + \frac{1}{2}\Delta t(M^i_{j+\frac{1}{2}} - M^i_{j-\frac{1}{2}} + M^{i+1}_{j+\frac{1}{2}} - M^{i+1}_{j-\frac{1}{2}}).
\end{aligned}
\tag{3.26}
$$

Here the lower index denotes the mass number, the upper index denotes the time step, and $k = 1$ or 2, depending on whether the spring is in the 'L' phase of 'H' phase. We choose a time step Δt that is much smaller than a_1/c_1 to ensure that our numerical calculation is stable. Recall that a_1 is the distance between masses (or the lattice parameter in the 'L' phase) when no forces are applied on the chain.

3.2.2 Impact problem

Now, we would like to simulate an impact problem using our mass-spring chain. For impact problems, ideally the domain is semi-infinite. In our calculations, we approximate the problem as a mass-spring chain with N masses and $N-1$ springs connecting them. We take $N = 100$ and fix the left end of the chain ($j = 1$) and apply constant linear and angular velocity at the right end ($j = N$). Hence, $u^i_1 = 0, \theta^i_1 = 0$ and $u^i_N = v_0 i\Delta t + u^0_N, \theta^i_N = w_0 i\Delta t + \theta^0_N$, where i is the time-step number. Initially, all springs are in the 'L' phase. We

integrate equations 3.26 for the system up to the point that the faster sonic wave which originated at $j = N$ hits the left end ($j = 1$). We find that below some critical set of values of applied velocities v_0, w_0, there are only two sonic waves passing through the chain from right to left. The sonic waves travel at constant speeds c_1 and c_2 as given in equation 3.19 and shown in figure 4.2. The oscillatory strains and velocities behind these waves decay

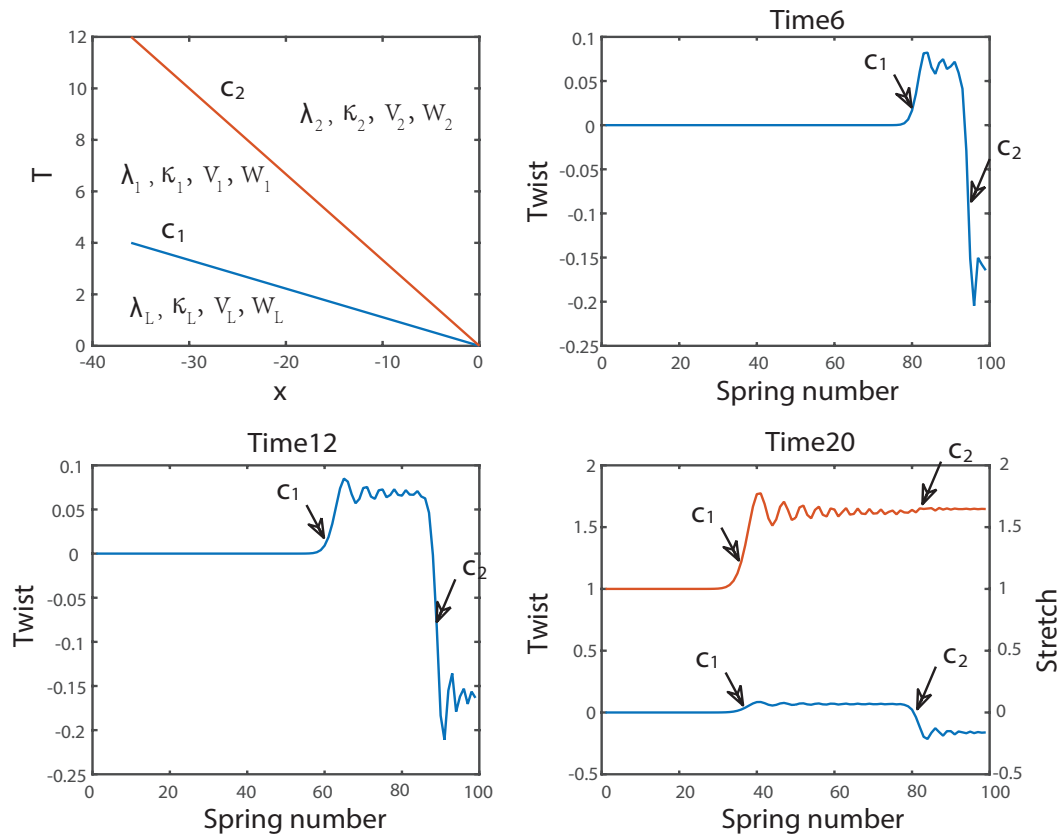

Figure 3.3: An example of an impact problem with only two sonic waves. On the top left is the x–t plane for the problem. The remaining three panels show the twist as a function of spring number at three different times. Two discontinuities with a jump in twist are clearly seen. They move at speeds c_1 and c_2. The bottom right panel also shows the stretch as a function of spring number, again revealing two waves.

to constants as expected from the analytical solution of the impact problem. If we apply higher extensional and angular velocities, a phase transition nucleates at $j = N$ and the phase boundary propagates inwards towards $j = 1$ as shown in figure 3.4 with velocity

$\dot{s}$. We initially use the material parameter set $B_1 = 10$, $B_2 = 7.6$ and $B_3 = 10$ for our numerical calculation. However, we have also used other material parameter combinations like $B_1 = 10$, $B_2 = 3$, $B_3 = 10$ and $B_1 = 100$, $B_2 = 8$, $B_3 = 10$ and have confirmed that the results are similar. We have observed in our numerical simulations that phase boundary

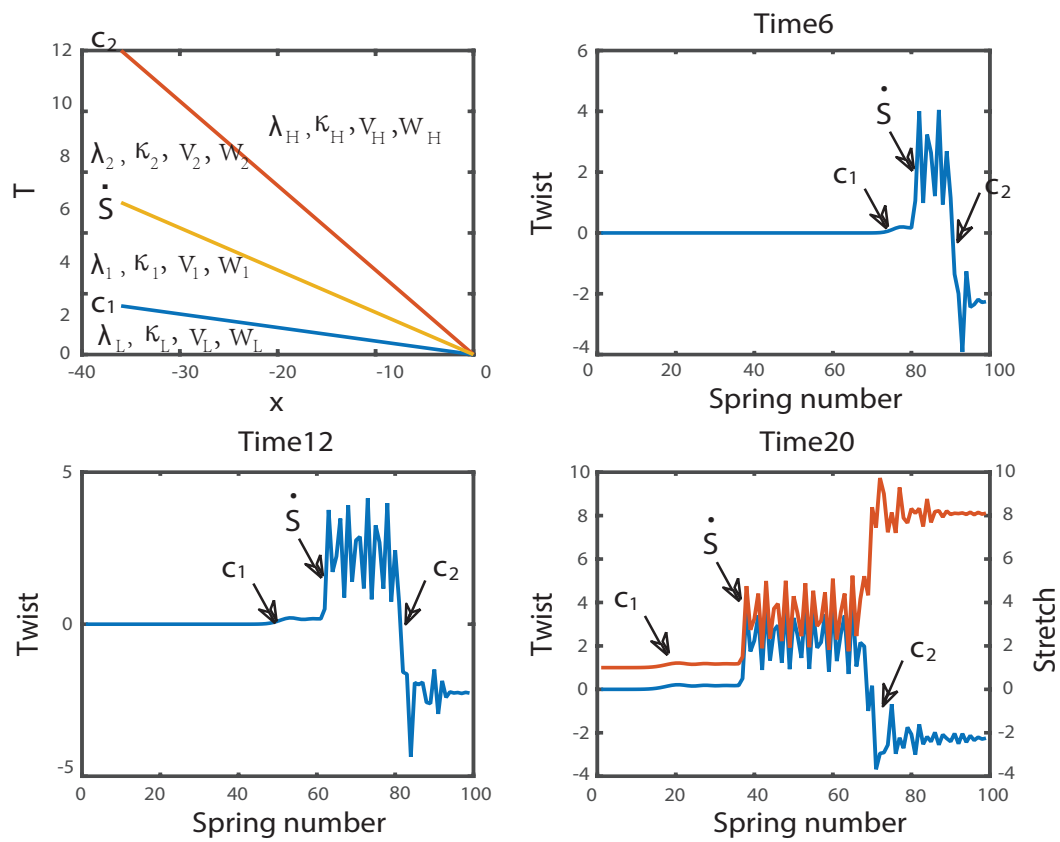

Figure 3.4: An example of an impact problem with a single phase boundary. The top left panel shows the x–t plane. Three waves are present, two sonic waves at speeds c_1 and c_2, and a phase boundary at speed $\dot{s}$ with $c_1 > \dot{s} > c_2$. The rest of the panels show snapshots of the twist in the chain as function of spring number at three different times. The bottom right panel also shows a snapshot of the stretch, again showing three discontinuities.

speed $\dot{s}$ is always smaller than c_1. We find, interestingly, that for most material parameter sets B_1, B_2, B_3, the phase boundary velocity is larger than the slower sonic wave speed c_2, no matter what boundary condition we apply. For some material parameter sets we get phase boundary speeds smaller than c_2, but surprisingly the dissipation rates for these

cases, as calculated using isothermal expressions for the driving force, are *negative*. We will consider this case later.

Now, there are instances in the literature in which subsonic and intersonic phase boundaries are discussed. For example, Abeyaratne and Knowles [3] have considered wave propagation in bilinear and trilinear materials. For the trilinear stress strain relation they have defined subsonic, intersonic and supersonic phase boundaries. By analyzing Riemann and impact problems they concluded that kinetics must be prescribed for subsonic phase boundaries to guarantee uniqueness of solutions, while for intersonic phase boundaries kinetics may not be imposed. In [7], they have gone beyond one-dimensional bars and considered solids in which the extensional wave speed can be different in different directions due to anisotropy. In this setting, a kinetic relation is not needed for supersonic phase boundaries, but it is needed for subsonic ones. Our situation is slightly different because we do not see supersonic phase boundaries with $\dot{s} > c_1$. However, we do see subsonic ($\dot{s} < c_2$) and intersonic ($c_1 > \dot{s} \geq c_2$) phase boundaries and we need kinetic relations for both.

First, we consider the situation in which $c_1 > \dot{s} > c_2$. As we can see from the $x - t$ plane in figure 3.4 and the dynamics of the chain, there are three moving discontinuities and piecewise constant strain and velocity profiles between these discontinuities. Note, however, that the strains and velocities behind the phase boundary do not decay, but oscillate around constant values. It is these constant strains and velocities behind the phase boundary that will enter the jump conditions. For the continuum impact problem with a single phase

boundary we can now write down the jump conditions:

$$
\begin{aligned}
c_1(\lambda_1 - \lambda_L) + v_1 - v_L &= 0, \\
c_1(\kappa_1 - \kappa_L) + w_1 - w_L &= 0, \\
c_1(v_1 - v_L) + S(\lambda_1 - \lambda_L) + g(\kappa_1 - \kappa_L) &= 0, \\
c_2(\lambda_H - \lambda_2) + v_H - v_2 &= 0, \\
c_2(\kappa_H - \kappa_2) + w_H - w_2 &= 0, \\
c_2(v_H - v_2) + S(\lambda_H - \lambda_2) + g(\kappa_H - \kappa_2) &= 0, \\
\dot{s}(\lambda_2 - \lambda_1) + v_2 - v_1 &= 0, \\
\dot{s}(\kappa_2 - \kappa_1) + w_2 - w_1 &= 0, \\
\dot{s}(v_2 - v_1) + S(\lambda_2 - \lambda_1) + g(\kappa_2 - \kappa_1) &= 0, \\
\dot{s}(w_2 - w_1) + g(\lambda_2 - \lambda_1 - \lambda_H^0 + \lambda_L^0) + C(\kappa_2 - \kappa_1 - \kappa_H^0 + \kappa_L^0) &= 0.
\end{aligned}
\tag{3.27}
$$

We have ten equations for the eleven unknowns $\lambda_1, \kappa_1, v_1, w_1, \lambda_2, \kappa_2, v_2, w_2, \lambda_H, \kappa_H, \dot{s}$. These jump conditions are not sufficient to describe the motion of the phase boundary or the dynamics of the system. We need a kinetic relation which relates phase boundary velocity and driving force to close the analysis. We will extract this kinetic relation from the simulations of our mass-spring system.

3.2.3 Kinetic relation

We have carried out a series of computations for impact problems with different material sets B_1, B_2, B_3. For each set we have applied several extensional and rotational velocities (or boundary conditions) and in each case we have obtained quantities like λ_1, κ_1, v_1, w_1, λ_2, κ_2, v_2, w_2, λ_H, κ_H, $\dot{s}$ by post-processing the numerical result. We then compute the

driving force as defined in equation 3.9 and normalized phase boundary velocity $\dot{s}/c_1$. For each material set we plot the driving force versus phase boundary velocity to find a relation between them. If we normalize the driving force suitably then all the curves of driving force versus phase boundary velocity can be described by the equation 4.24 which is the kinetic relation we wanted. The normalizing factor for the driving force depends on the material parameter set.

$$\frac{(\frac{c_2}{c_1})^2 - (1-(\frac{c_2}{c_1})^2) f_{threshold} - (\frac{\dot{s}}{c_1})^2}{1-(\frac{\dot{s}}{c_1})^2} = f_{normalized} = \frac{[|W|] - \langle T\rangle[|\lambda|] - \langle M\rangle[|\kappa|]}{\frac{2}{l_0}\sqrt{SC+g^2}}. \quad (3.28)$$

In this kinetic relation, $\frac{2}{l_0}\sqrt{SC+g^2}$ is the normalizing factor for the driving force, $f_{threshold}$ is the threshold value of driving force when the phase transition just begins to happen and $l_0 = \frac{\lambda_H^0 - \lambda_L^0}{\kappa_H^0 - \kappa_L^0}$. This kinetic relation has the familiar form

$$f_{driving} = q_1 + \frac{q_2}{1-\frac{\dot{s}^2}{c_1^2}}, \quad (3.29)$$

where q_1 and q_2 are constants that depend on the chosen material parameters. It can be rearranged in the following manner

$$\frac{1}{1-(\frac{\dot{s}}{c_1})^2} = \frac{1 - \frac{l_0}{2\sqrt{SC+g^2}}([|W|] - \langle T\rangle[|\lambda|] - \langle M\rangle[|\kappa|])}{(1+f_{threshold})(1-(\frac{c_2}{c_1})^2)}. \quad (3.30)$$

The RHS of this equation is plotted on the x-axis of figure 3.5 and $\dot{s}/c_1$ is plotted on the y-axis. We have solved the continuum impact problem analytically by using the kinetic relation equation 3.30. The result is shown in table 3.1 and figure 3.8 for two material parameter sets. We see from the table that the analytical result is consistent with the numerical result. This suggests that the kinetic relation we have extracted can be used to

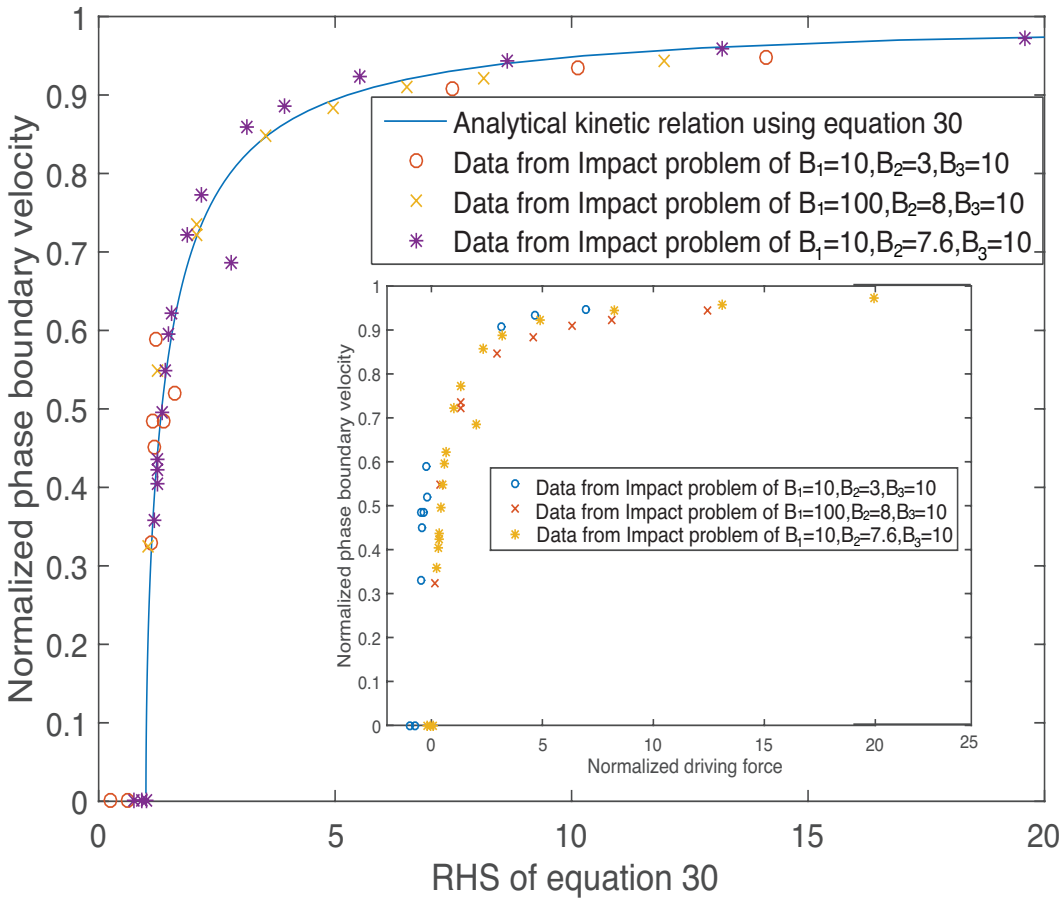

Figure 3.5: Kinetic relation using equation 3.30. The data for this plot was obtained from many simulations with different material sets for the 'springs'. Phase boundary velocity $\dot{s}$ is normalized against c_1 and plotted on the y-axis. Driving force $f_{driving}$ is normalized according to equation 3.30 and plotted on the x-axis. Note that for driving forces below a threshold the phase boundary velocity is zero. The inset of the figure is the original data of normalized phase boundary velocity vs. the normalized driving force (as in equation 4.24). Note that some of the blue circles result in $\dot{s} f_{driving} < 0$.

solve other types of problems.

3.2.4 Analytical and numerical solutions of Riemann problem

Riemann problems in bars with a single phase boundary have been treated earlier [7, 65]. It is well understood that for the type of constitutive relations we use in this work the solutions of these problems are piecewise constant in the x-t plane. The domain for a

v_0	4.5	8	10	16	20	30	50
w_0	1	1	0	0	0	0	0
Analytical $\dot{s}$	-1.7	-2.205	-2.505	-3.0512	-3.2528	-3.5361	-4.1642
Numerical $\dot{s}$	-1.75	-2.35	-2.55	-3.1	-3.3	-3.55	-4.15
Analytical λ_1	0.1679	0.2546	0.2639	0.3628	0.4394	0.6643	0.8636
Numerical λ_1	0.1537	0.1783	0.161	0.1785	0.1862	0.1987	0.1974
Analytical λ_2	1.2473	1.741	1.818	2.4859	2.9469	4.1181	6.4593
Numerical λ_2	1.1545	1.76	1.86	2.479	2.972	4.048	6.461
Analytical λ_H	2.7247	4.754	5.0454	7.6498	9.4018	13.8005	22.5999
Numerical λ_H	2.685	4.758	5.058	7.652	9.432	13.81	22.65
Analytical κ_1	0.1679	0.2546	0.2639	0.3628	0.4394	0.6643	0.8636
Numerical κ_1	0.1537	0.1783	0.161	0.1785	0.1862	0.1987	0.1974
Analytical κ_2	1.2473	1.741	1.818	2.4859	2.9469	4.1181	6.4593
Numerical κ_2	1.1545	1.76	1.857	2.479	3.018	4.03	6.461
Analytical κ_H	-0.195	-1.295	-1.4095	-2.6781	-3.508	-5.5643	-9.6789
Numerical κ_H	-0.2256	-1.312	-1.416	-2.695	-3.542	-5.595	-9.691

Table 3.1: Comparison of numerical results with analytical solution of impact problems for $B_1 = 10$, $B_2 = 7.6$, $B_3 = 10$. The analytical results use the kinetic relation 3.30. The agreement between quantities like phase boundary velocity obtained from numerical integration and continuum analytic solution is quite good, especially for large v_0.

Riemann problem is $-\infty < x < \infty$. However, since we cannot simulate an infinite mass-spring chain we have used $N+1$ masses and N springs with an initial phase boundary in the middle of the chain at mass number $\frac{N}{2}$ where $N = 1000$. The equations of motion for the masses is equation 4.10 and the two boundaries are left free (zero force and moment). At $t = 0$ we prescribe initial conditions such that all springs on the left half are in the 'L' phase, while those on the right are in the 'H' phase. Since our mass-spring system has a finite number of masses and has two boundaries there could be four additional sonic waves which originate from the two ends. We integrate the dynamics of the mass spring system up to the point when the sonic waves originating at the center of the chain and those coming from the ends meet each other. Again, we start our calculation with the material set $B_1 = 10$, $B_2 = 7.6$, $B_3 = 10$, but the features we observe are similar even if we use other parameter sets. When we let this system evolve we notice three different scenarios.

In the first scenario the phase boundary in the middle propagates along the chain. An example of the evolution of such a system is shown in figure 3.7. We see that there is a phase boundary moving from the middle of the chain to the left in addition to the sonic waves described above. If we focus on the middle part of the chain between the four sonic waves moving outward, then the x-t plane looks exactly like what is expected from the continuum theory as shown in figure 3.6.

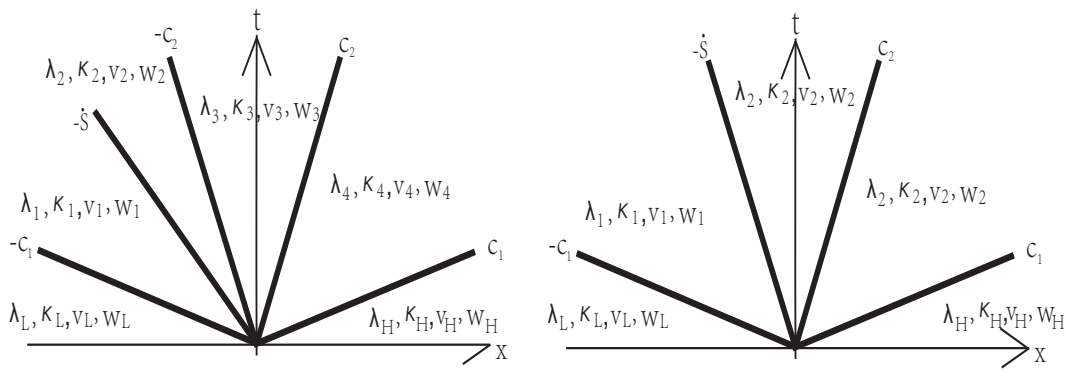

Figure 3.6: (a) x–t plane of a Riemann problem with a single phase boundary with $c_1 > \dot{s} > c_2$. (b) x–t plane of a Riemann problem in which $\dot{s} = -c_2$.

From our simulations we find that the phase boundary speed is smaller than the larger sonic wave speed c_1, as expected. For most material parameter sets the phase boundary speed is larger than the slower sonic wave c_2 no matter what initial condition we set. However, for some material parameter sets (for example, $B_1 = 10$, $B_2 = 3$, $B_3 = 10$), the phase boundary speed can be smaller than c_2. In these cases the dissipation rate $f_{driving}\dot{s}$ is negative, which is physically not possible. Cases with $\dot{s} < c_2$ were observed in the impact problem with the same set of material parameters also. We will explain this later.

By post-processing the data from our numerical calculations we can obtain λ_1, κ_1, v_1, w_1, λ_2, κ_2, v_2, w_2, λ_3, κ_3, v_3, w_3, λ_4, κ_4, v_4, w_4, λ_4, κ_4, v_4, w_4, $\dot{s}$ (see figure 3.6). We compare these numerical results with those of the solution of the continuum Riemann

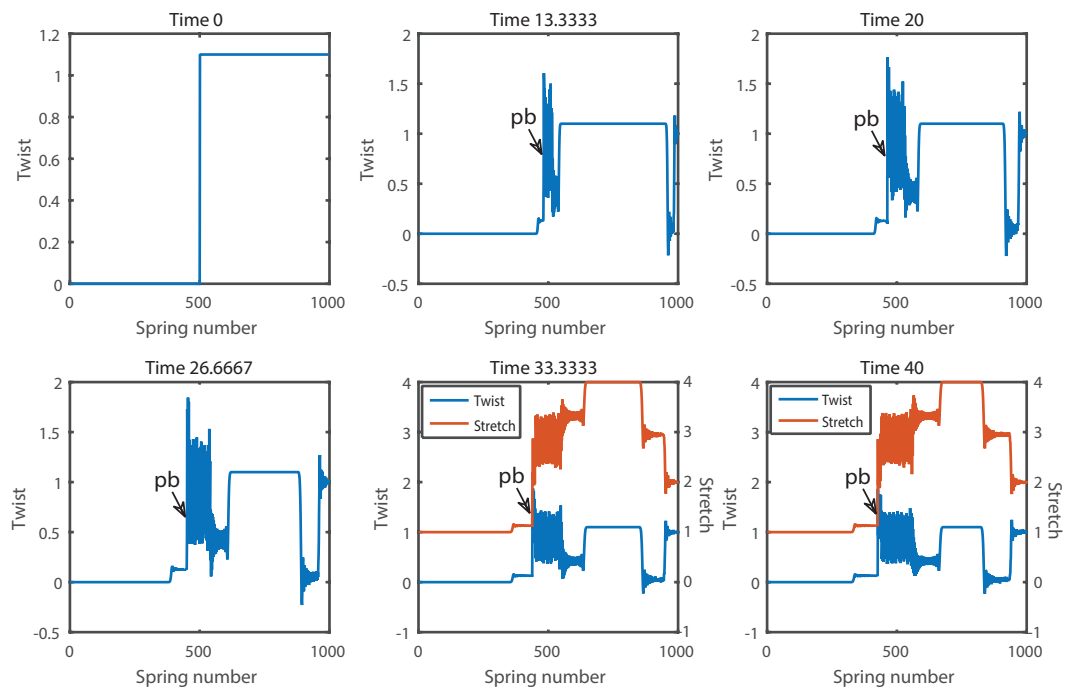

Figure 3.7: An example of an Riemann problem with a single phase boundary. Five waves are present, two sonic waves at speeds c_1 and c_2 propagating in opposite directions from the middle, and a phase boundary at speed $\dot{s}$ with $c_1 > \dot{s} > c_2$. There are also two sonic waves moving towards the left from the right boundary. In general there should also be two sonic waves moving rightwards from the left end, but we do not see them above because of the choice of initial conditions. The panels show snapshots of the twist in the chain as function of spring number at six different times. Two bottom panels also show snapshots of the stretch.

problem that can be solved analytically using the kinetic relation 3.30. We assume that the initial conditions are at $t = 0$, $\lambda = \lambda_L, v = v_L, \kappa = \kappa_L, w = w_L$ for $x < 0$ and $\lambda = \lambda_H, v = v_H, \kappa = \kappa_H, w = w_H$ for $x > 0$. For $t > 0$ this Riemann problem has piece-wise constant solution depicted in the x-t plane figure 3.6. There are a total of seventeen unknowns $\lambda_1, \kappa_1, v_1, w_1, \lambda_2, \kappa_2, v_2, w_2,\ \lambda_3, \kappa_3, v_3, w_3, \lambda_4, \kappa_4, v_4, w_4, \lambda_4, \kappa_4, v_4, w_4, \dot{s}$. We enforce the jump conditions at each discontinuity and get sixteen equations as follows. The kinetic relation equation (3.30) provides the seventeenth equation.

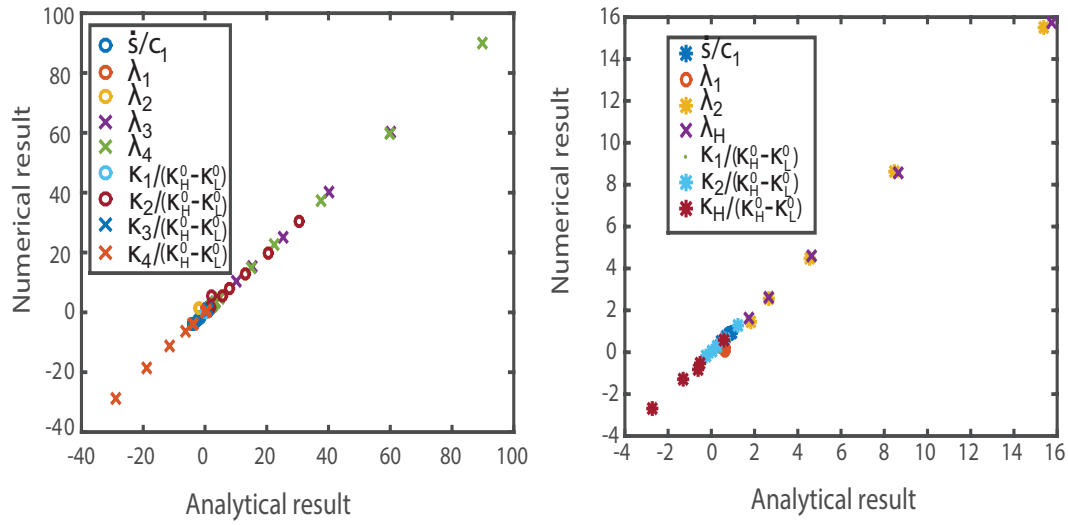

Figure 3.8: (a) Scatter plot showing comparison of numerical results with analytical solution of Riemann problems for $B_1 = 10, B_2 = 7.6, B_3 = 10$. The analytical results use the kinetic relation obtained from impact problems on the chain to solve the set of equations 3.2.4. The agreement between the phase boundary velocities and other quantities obtained from the numerical integration of the equations of motion of the chain and those from the analogous continuum analytic solution is quite good. (b) Scatter plot showing comparison of numerical results with analytical solution of impact problems for $B_1 = 100, B_2 = 8, B_3 = 10$. The analytical results use the kinetic relation 3.30.

$$\text{Across } \dot{s} \begin{cases} \dot{s}(\lambda_2 - \lambda_1) + v_2 - v_1 = 0, \\ \dot{s}(\kappa_2 - \kappa_1) + w_2 - w_1 = 0, \\ \dot{s}(v_2 - v_1) + S(\lambda_2 - \lambda_1 - \lambda_H^0 + \lambda_L^0) + g(\kappa_2 - \kappa_1 - \kappa_H^0 + \kappa_L^0) = 0, \\ \dot{s}(w_2 - w_1) + g(\lambda_2 - \lambda_1 - \lambda_H^0 + \lambda_L^0) + C(\kappa_2 - \kappa_1 - \kappa_H^0 + \kappa_L^0) = 0, \end{cases}$$

$$\text{Across } -c_2 \begin{cases} -c_2(\lambda_3 - \lambda_2) + v_3 - v_2 = 0, \\ -c_2(\kappa_3 - \kappa_2) + w_3 - w_2 = 0, \\ -c_2(v_3 - v_2) + S(\lambda_3 - \lambda_2) + g(\kappa_3 - \kappa_2) = 0, \end{cases}$$

$$
\text{Across } c_2 \begin{cases} c_2(\lambda_4 - \lambda_3) + v_4 - v_3 = 0, \\ c_2(\kappa_4 - \kappa_3) + w_4 - w_3 = 0, \\ c_2(v_4 - v_3) + S(\lambda_4 - \lambda_3) + g(\kappa_4 - \kappa_3) = 0, \end{cases}
$$

$$
\text{Across } c_1 \begin{cases} c_1(\lambda_H - \lambda_4) + v_H - v_4 = 0, \\ c_1(\kappa_H - \kappa_4) + w_H - w_4 = 0, \\ c_1(v_H - v_4) + S(\lambda_H - \lambda_4) + g(\kappa_H - \kappa_4) = 0. \end{cases}
$$

These equations can be solved analytically using Maple or similar programs. We compare the results from this exercise with those of the numerical solution in the scatter plot figure 3.11 for several different initial conditions. We plot non-dimensional quantities like λ_1, v_1/c_1, etc., obtained from the numerical calculations on the y-axis and those from the analytical solutions of equations 3.2.4 on the x-axis. We see that points in this scatter plot make a line with slope 1 which indicates good agreement between the mass-spring chain and the analytical solution. This suggests that the kinetic relation equation (3.30) is indeed a useful constitutive law.

The first scenario described above validates our kinetic relation. But, there are two more scenarios in which a kinetic relation is not needed for the solution of the Riemann problem with a single phase boundary. In the second scenario, the phase boundary in the middle remains static (a contact discontinuity), but four sonic waves with speeds $\pm c_1$ and $\pm c_2$ propagate towards the left and right. An example of the evolution of the system is given in figure 3.9. In this case the continuum Riemann problem can be solved analytically

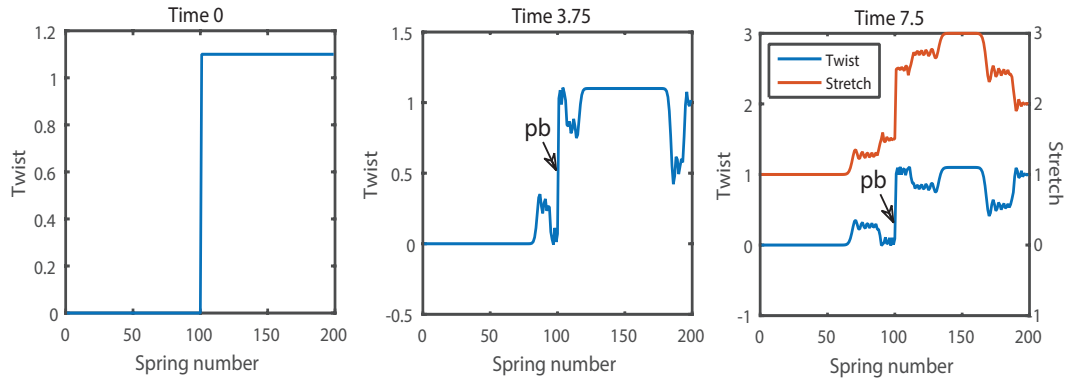

Figure 3.9: An example of an Riemann problem with a static phase boundary. Four waves are present, two sonic waves at speeds c_1 and c_2 propagating in opposite directions from the middle while the phase boundary at the middle remains static. Two sonic waves also move inwards from the right boundary. The panels show snapshots of the twist in the chain as function of spring number at three different times. The right panel also shows a snapshot of the stretch.

using the jump conditions alone. There are sixteen unknowns and sixteen equations to solve for them. Each sonic wave contributes three equations and the contact discontinuity contributes four. The equations are similar to equation 3.2.4 except that we don't need a kinetic relation since $\dot{s} = 0$. Once again, the scatter plot in figure 3.11 compares quantities from the numerical simulation of the mass-spring chain and the analytical solution. A slope of 1 indicates excellent agreement.

In the third scenario the phase boundary propagates at the speed c_2 and becomes indistinguishable from one of the sonic waves. Thus, the impact problem with a phase boundary in this pathological case has only two discontinuities instead of three, and the Riemann problem has four discontinuities instead of five. An example of the evolution of such a system is shown in figure 3.10. Note that we have four waves on the $x - t$ plane with speeds $-c_1$, $-\dot{s} = -c_2$, c_2 and c_1. There are twelve unknowns and twelve equations (three jump conditions at each discontinuity) to solve for them. We have found, again, that analytical and numerical solutions for this case agree quite well.

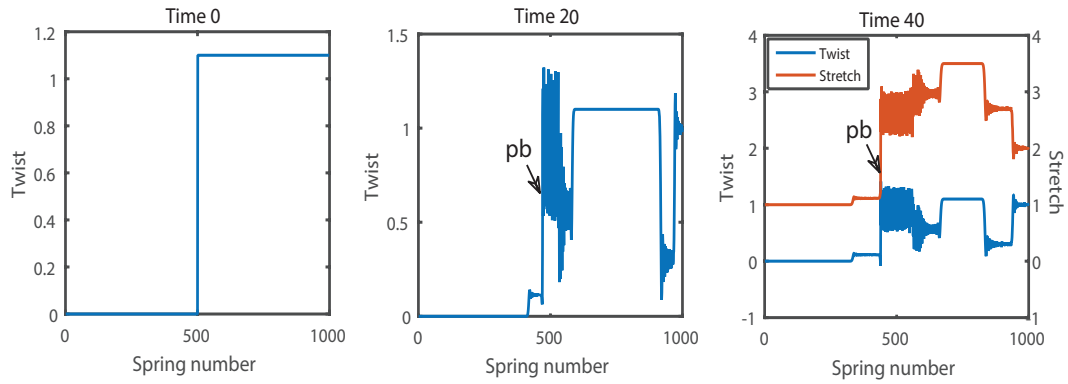

Figure 3.10: An example of a Riemann problem in which phase boundary merges with a c_2 sonic wave. Four waves are present, three sonic waves at speeds c_1 and c_2 propagating in opposite directions from the middle, and a phase boundary traveling at speed c_2. The panels show snapshots of the twist in the chain as function of spring number at three different times. The right panel also shows a snapshot of the stretch.

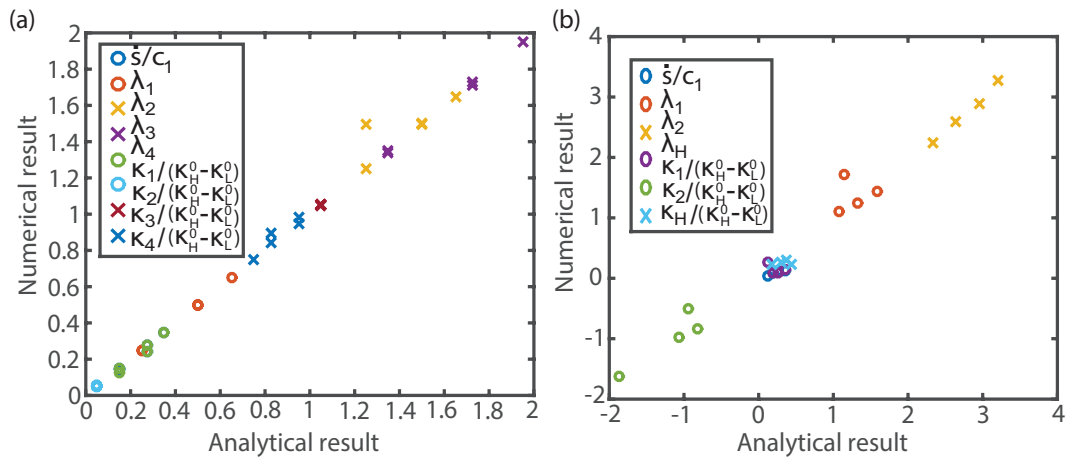

Figure 3.11: (a) Comparison of results of Riemann problem with static phase boundary from numerical integration and analytical solution using jump conditions. We have used $B_1 = 10, B_2 = 7.6, B_3 = 10$ and $B_1 = 10, B_2 = 3, B_3 = 10$. (b) Comparison of numerical results with analytical solution of impact problems for $B_1 = 10$, $B_2 = 3$, $B_3 = 10$ when $\dot{s} < c_2$. The analytical results are obtained from the jump conditions using phase boundary velocity from the numerical calculation.

So far in our analysis we have described cases in which phase boundary velocities $\dot{s} > c_2$. However, when we choose a material parameter set $B_1 = 10$, $B_2 = 3$, $B_3 = 10$, we find situations in which phase boundary speed is smaller than c_2. An example of such dynamics is given in figure 3.13. Once again, after post-processing we have verified that the piecewise

constant stretches, velocities, angular velocities and twisting curvatures satisfy all the jump conditions. Indeed, the driving force $f_{driving}$ computed using the parameters extracted from our calculations satisfies equation 3.30. However, we find that in these cases with $\dot{s} < c_2$, the dissipation rate is negative, $\dot{s} f_{driving} < 0$. Starting from eqn. (4.24) we see that negative dissipation rates occur whenever

$$\dot{s}/c_1 < \sqrt{(1 - f_{threshold})(c_2/c_1)^2 - f_{threshold}}. \tag{3.31}$$

On the $\dot{s}$-c_2 plane (see figure 3.12) the region represented by the above inequality overlaps with the region corresponding to $\dot{s} < c_2$. It seems that it is easier to see negative dissipation rates when we have another 'knob to turn' that is not available in an atomic chain with only extensional degrees of freedom. That 'knob' is the wave speed c_2. We can pick c_2 and initial/boundary conditions of a Riemann/impact problem in such a way as we sit in the region corresponding to negative dissipation rates in the $\dot{s}$-c_2 plane. If this idea is correct we might expect similar phenomena in 2D lattice simulations of phase-transforming materials in which both P- and S-waves are present. However, such simulations are outside the scope of this paper.

What are the implications of a negative dissipation rate? Naively, it means that at time t the chain has more energy than what it had at $t = 0$ plus what was injected into it at the boundary. This is unphysical and cannot be true. The reason behind this anomaly is that in calculating the driving force using data from our numerical calculations we have used an isothermal expression derived from continuum theory that only uses the average values of the stretches, velocities, etc., and neglects the oscillations of the masses and springs. In fact, it has been suggested in the the literature that simulations of phase transitions

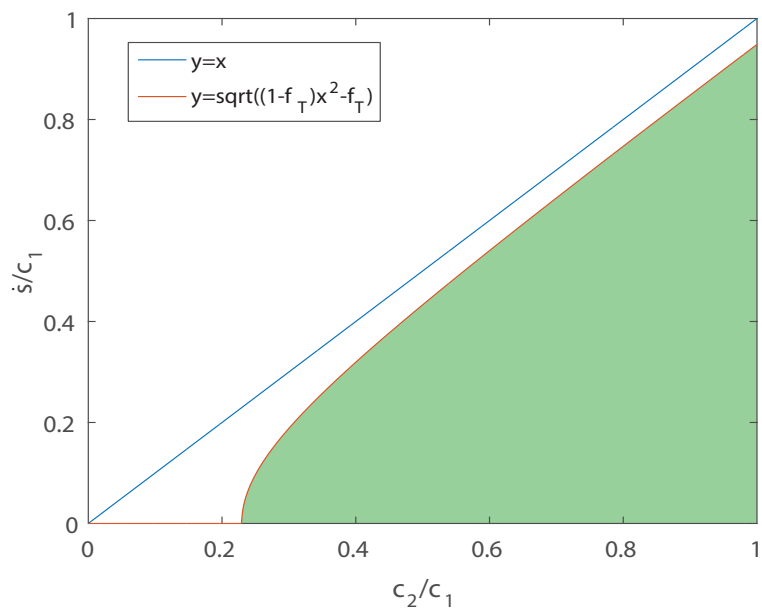

Figure 3.12: Region corresponding to negative dissipation rates in the $\dot{s}$-c_2 plane is colored green. In the legend f_T stands for $f_{threshold}$, x stands for c_2/c_1 and y stands for $\dot{s}/c_1$.

using mass-spring chains need to be done with new variables describing level of fluctuations around average stretches, velocities, etc., as well as the rate of energy fluxes into various scales and that into irreversible dissipation by elastic radiation [13, 58, 70, 75]. Dayal and Bhattacharya [30] have considered oscillations around average stretches and velocities in a peridynamic setting and found that they are of the same magnitude ahead and behind a phase boundary, leading to a zero driving force. This is not the case with oscillations in our calculations so we expect non-zero driving forces, but negative dissipation rates are still puzzling. To ensure that our results of negative dissipation rates are not spurious we performed an energy budget on our chain. We calculated the energy input over time $t = J\Delta t$ as $E_{in}(t) = \sum_{i=1}^{J} F^i_{N+\frac{1}{2}} v_0 \Delta t + \sum_{i=1}^{J} M^i_{N+\frac{1}{2}} w_0 \Delta t$, and the energy of the chain as $E_{chain}(t) = \sum_{p=1}^{N} \frac{1}{2}\dot{u}_p^2(t) + \sum_{p=1}^{N} \dot{\theta}_p^2(t) + \phi(u_1(t), u_2(t), ..., u_{N+1}(t), \theta_1(t), \theta_2(t), ...\theta_{N+1}(t))$. We have plotted the difference between input energy and the total energy of the chain $E_{in} - E_{chain}$ as a function of $t = J\Delta t$ in figure 3.14 for three different impact problems

with a single phase boundary. In all these impact problems the initial conditions were such as the potential energy of the springs and kinetic energy of the masses was zero at $t = 0$. For the top two curves (red and blue) the dissipation rate at the phase boundary is positive, while for the bottom (yellow) curve it is negative. In all cases the difference $E_{in} - E_{chain}$ is positive at all times. This is as it should be since our numerical integration scheme is imperfect and it results in some numerical dissipation. Notice from these curves that after an initial transient the difference $E_{in} - E_{chain}$ tends to a constant. In other words, the rate of energy input is equal to the rate of energy (kinetic + potential) storage in the chain after an initial transient. These observations suggest that we cannot neglect the jump in the magnitude of energy stored in the oscillations, or, loosely speaking, the jump in temperature, across a moving phase boundary.

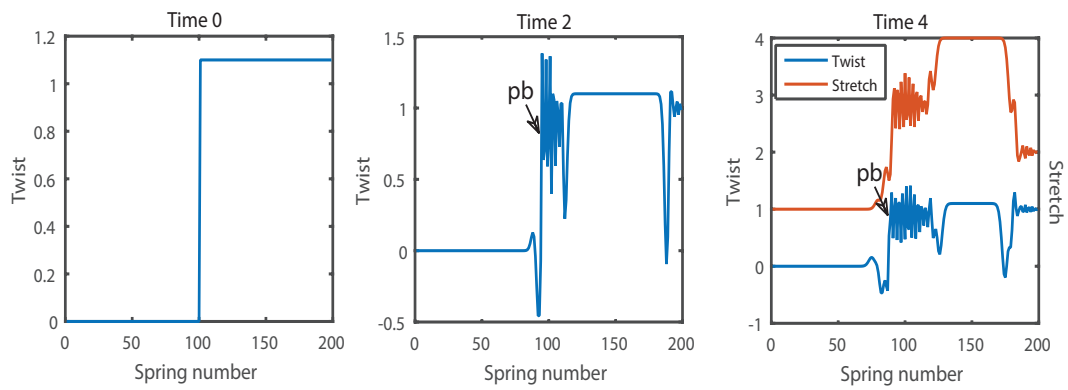

Figure 3.13: An example of an Riemann problem in which $\dot{s} < c_2$. Fives waves are present, four sonic waves at speeds c_1 and c_2 propagating in opposite directions from the middle, and the phase boundary $\dot{s} < c_2$. The panels show snapshots of the twist in the chain as function of spring number at six different times. The bottom two panels also show snapshots of the stretch.

3.2.5 Impact problem for adiabatic process

To re-examine the negative dissipation rate cases, we introduce a temperature in our analysis defined locally through

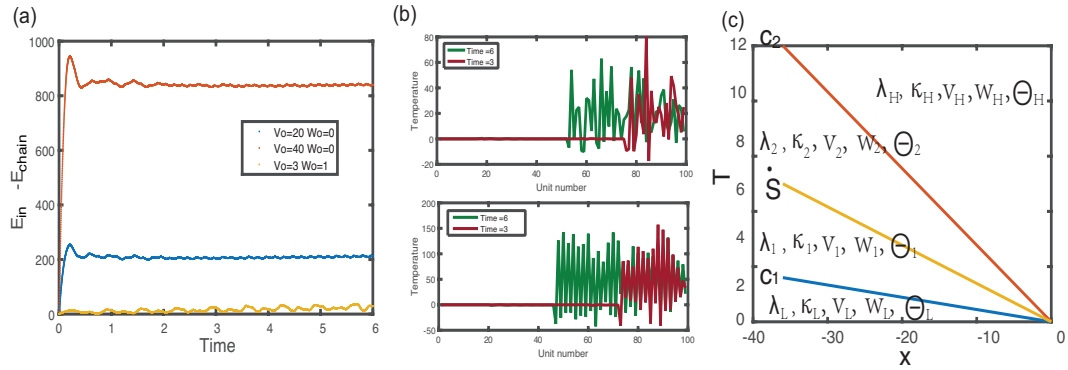

Figure 3.14: (a)Difference between input energy and PE+KE of the whole chain for three different impact problems on a chain with $B_1 = 10$, $B_2 = 3$, $B_3 = 10$. The red and blue curves involve a phase boundary in which dissipation rate is positive and the yellow curve involves a phase boundary in which dissipation rate is negative. (b) Snapshots of the local temperature Θ_j in the chain as a function of mass number j for two different boundary conditions. The top panel shows snapshots at two different times (red and green) for boundary condition $v_0 = 10$, $w_0 = 0$, and the bottom panel shows snapshots for boundary condition $v_0 = 7$, $w_0 = 0$. Note that the temperature jumps only once (across the phase boundary) even though there are three propagating discontinuities in the impact problem on the chain. (c) The new x-t plane when temperature is considered in an adiabatic impact problem on a thermoelastic bar of the Mie-Gruneisen type.

$$k\Theta_j(t) = KE_j(t) + PE_{j+\frac{1}{2}}(t) - E_j^{cont} = \frac{1}{2}m_j\dot{u}_j^2(t) + \frac{1}{2}I_j\dot{\theta}_j^2(t) + \phi_1(x_j(t), y_j(t)) - E_j^{cont}. \quad (3.32)$$

Here, $KE_j(t)$ is the kinetic energy of the jth mass (accounting for both translational and rotational contributions) at time t, $PE_{j+\frac{1}{2}}(t)$ is the potential energy of the spring between mass j and mass $j+1$ at time t and E_j^{cont} is the sum of kinetic energy at mass j and potential energy in spring $j+\frac{1}{2}$ computed using the average values of the velocities and strains that satisfy the continuum jump conditions,

$$E_j^{cont} = \frac{1}{2}m_j\langle\dot{u}_j\rangle^2 + \frac{1}{2}I_j\langle\dot{\theta}_j\rangle^2 + \phi_1(\langle x_j\rangle, \langle y_j\rangle), \quad (3.33)$$

where $\langle z \rangle$ is the temporal average of z over a time corresponding to few periods. k is proportional to a specific heat in the continuum theory and we set it equal to 1 here. So, our definition of the local temperature captures the 'thermal' portion of the energy of the masses and springs in the chain that is neglected in a purely mechanical continuum theory. We could also have defined two different temperatures [46] corresponding to rotational and extensional degrees of freedom, respectively, but we do not do so here because the temperature defined above has the property that it satisfies jump conditions expected of a Mie-Gruniesen type thermoelastic material (see the appendix for a short review of these materials). This is discussed in the following.

Since our numerical method is such as there is no leakage of energy (thermal + mechanical) from our chain we expect that the phase boundary propagation is adiabatic. To confirm if this is the case we plot the local temperature Θ_j in our chain for an impact problem as a function of mass number j in figure 3.14(b). We find that Θ does not jump across sonic waves which move at speeds c_1 and c_2, but it jumps across a phase boundary. Furthermore, Θ oscillates around a constant value behind a phase boundary. Thus, if we take a temporal average value of Θ, then our x-t plane is very similar to the x-t plane for an adiabatic impact problem of a trilinear Mie-Gruneisen thermoelastic solid in which the Gruneisen parameter is zero [7]. To make this analogy more concrete we write the jump conditions at each discontinuity in an impact problem on a bar in which both stretching and twisting are allowed and the local temperature can suffer jumps. We assume that the Gruneisen parameter is zero and that the continuum problem is adiabatic. The jump conditions are:

$$
\text{Across } -c_2 \begin{cases} -c_2(\lambda_H - \lambda_2) + v_H - v_2 = 0, \\ -c_2(\kappa_H - \kappa_2) + w_H - w_2 = 0, \\ -c_2(v_H - v_2) + S(\lambda_H - \lambda_2) + g(\kappa_H - \kappa_2) = 0, \\ \Theta_H - \Theta_2 = 0, \end{cases}
$$

$$
\text{Across } \dot{s} \begin{cases} \dot{s}(\lambda_2 - \lambda_1) + v_2 - v_1 = 0, \\ \dot{s}(\kappa_2 - \kappa_1) + w_2 - w_1 = 0, \\ \dot{s}(v_2 - v_1) + S(\lambda_2 - \lambda_1) + g(\kappa_2 - \kappa_1) = 0, \\ \dot{s}(w_2 - w_1) + g(\lambda_2 - \lambda_1 - \lambda_H^0 + \lambda_L^0) + C(\kappa_2 - \kappa_1 - \kappa_H^0 + \kappa_L^0) = 0, \\ \rho C_p(\Theta_2 - \Theta_1) = \frac{T_2+T_1}{2}(\lambda_0^H - \lambda_0^L) + \frac{M_2+M_1}{2}(\kappa_0^H - \kappa_0^L) \end{cases}
$$

The appropriate expression for the driving force across a phase boundary for such a material (with zero latent heat) is

$$
f_{driving} = -E \log(1 + \frac{[|\Theta|]}{\Theta_-}), \tag{3.34}
$$

where we treat Θ_- and E as constants. In the continuum impact problems solved in [7] Θ_- is set equal to the transformation temperature and E is related to the specific heat. We find that our numerical simulations of the mass-spring chain with $B_1 = 10$, $B_2 = 3$, $B_3 = 10$ satisfy these jump conditions if we take $\rho C_p \approx 0.07463$. We also find that $[|\Theta|] < 0$ irrespective of whether $\dot{s} < c_2$ or $\dot{s} \geq c_2$. Thus, the dissipation rate $f_{driving}\dot{s}$ computed using (3.34) is always non-negative for the phase boundaries in our chain. The kinetic relation

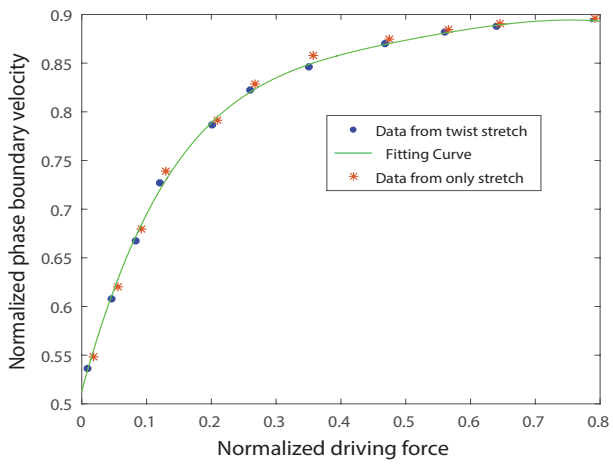

Figure 3.15: The new kinetic relation defined by 3.34 which accounts for the jump in temperature across a phase boundary. The "." data are results from calculation with twist stretch coupling and the "*" data are results from calculation with only extensional degree of freedom. We use a fitting curve $f(x) = abx^{b-1}\exp(-ax^b)$ where $a = 1.181, b = 1.139, E = 1$. $\Theta_- = 1000$ for twist stretch coupling data and $\Theta_- = 622$ with only extensional degrees of freedom.

using this new driving force is plotted in figure 3.15. While we arrived at this kinetic relation through a bistable chain having both extensional and rotational degrees of freedom, this is not necessary. This can be seen from the red curve in figure 3.15 which is the kinetic relation of a bistable chain with only extensional degrees of freedom. Remarkably, the curves are identical except for the value of the constant Θ_-.

3.3 Application to artificial muscle yarns

We now want to demonstrate a practical application where methods developed in this paper could be useful. In [48] carbon nanotube yarns are twisted, braided and then filled with wax to produce filaments that are capable of actuation. Actuation is realized by heating the filaments to cause partial melting (a phase transition) of the wax which does not flow out of the yarn due to favorable adhesive interactions with the nanotubes over very large surface areas. The mechanism behind the actuation is the change in pitch of the helical yarns due

to softening of the wax. Thus, twist and stretch are coupled in these yarns and it's a phase transition that enables its reversible operation over many cycles. Our goal here is to model one aspect of the yarn's behavior that has been deduced in the experiments of [48]. In these experiments different types of yarn are loaded with a constant tensile force. Then they are heated by an electrical current for several tens of milliseconds. This causes the yarn to stretch, so that useful work is done by the applied tension. The tensile actuation strain is measured in the experiment and plotted as a function of time as the yarn cools in figure 3 of [48]. The end of the yarn also rotates at high angular velocities due to the coupling of twist and stretch. Two types of responses are seen for the tensile actuation strain as a function of time – (a) a monotonically decaying strain, and (b) a decaying oscillatory strain. We provide a possible explanation of these two behaviors.

Consider first the monotonically decaying strain. At $t = 0$ the yarn is at temperature $\Theta = \Theta_1$ due to the electrical heating. Here, $\Theta_1 > \Theta_{air}$ where Θ_{air} is the ambient temperature. The change in length of the filament ΔL is proportional to $\Delta\Theta = \Theta - \Theta_{air}$ where $\Theta(t)$ is the current temperature of the yarn. Due to convective and radiative heat transfer to the environment one can write an equation for $\frac{d\Theta}{dt}$ at a rudimentary level [80]:

$$-\frac{d\Theta}{dt} = a(\Theta - \Theta_{air}) + b(\Theta^4 - \Theta_{air}^4), \tag{3.35}$$

where a is a constant that depends on the convective heat transfer coefficient, density, specific heat and geometry of the yarn, etc., and b is another constant that depends on a radiative heat transfer coefficient and other yarn parameters. This equation can be integrated with initial condition $\Theta(t = 0) = \Theta_1$ to get a monotonically decaying Θ. This will lead to a monotonically decaying strain ΔL as a function of t because ΔL is assumed propor-

tional to $\Delta\Theta$ in [48]. If we neglect the radiative terms then the solution of the differential equation above is simply $\Theta(t) = \Theta_{air} + (\Theta_1 - \Theta_{air})\exp(-at)$. This rudimentary analysis cannot explain the observed oscillatory decay of the strain in some other yarn samples. A possible explanation for this phenomenon combines dynamics of the yarn with the above heat transfer analysis. We model the yarn with our mass-spring chain coupling twist and stretch. Initially, all the springs are at the bottom of the low strain well and the masses are stationary. Then at $t = 0$ we suddenly apply a constant force F and constant moment $M = 0$ on mass $N+1$ while mass 1 is fixed. We plot the displacement $u_{N+1}(t) = L\epsilon(t) = \Delta L$ as a function of time in figure 3.16. Due to the sonic waves and phase boundary going back and forth in the chain the displacement oscillates. In our simulation we cannot account for the heat transfer to the environment or the change in L due to changes in temperature, but from the above analysis we know that $L(t)$ decays as a function of time, so ΔL will decay in an oscillatory fashion because $\epsilon(t)$ oscillates. We show this in figure 3.16 (b,c).

3.4 Conclusions

In this chapter we have studied the dynamics of a mass-spring chain with extensional and rotational degrees of freedom at each mass. The energy landscape of the springs has multiple wells, as would be the case for a rod capable of phase transitions. We have shown that the solutions of continuum Riemann and impact problems in rods capable of twist-stretch phase transitions are analogous to the those in the numerical solutions of our chains. In particular, we have observed discontinuities across which the twist and stretch can jump. Discontinuities of this type had been used to model impact of elasto-plastic bars and nano tubes [26, 56, 79], but we are not aware of an attempt to use them in the study of phase

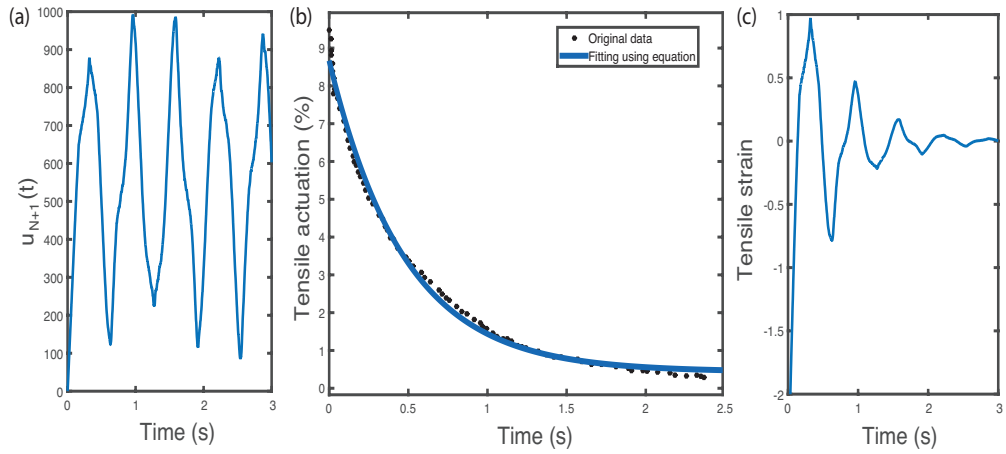

Figure 3.16: Simulation of the experiment in [48] using our mass-spring chain. We apply a constant force and moment at the end of the chain as our boundary conditions. We simulate to the point in time when the phase boundary has hit the left end and bounced back. We recover the vibration of the tensile actuation strain with our numerical result coupled with a decaying function described in equation 3.35. We have plotted the following. (a) Total length of chain from numerical simulation. (b) Experimental data in [48] for tensile actuation strain fitted using equation 3.35. (c) Oscillatory actuation strain of the chain from numerical result coupled with a decaying envelope qualitatively captures what is seen in other experiments in [48].

transitions, except [9]. Our mass-spring chain has furnished a kinetic relation for phase boundaries across which the twist and stretch can jump. This kinetic relation has a form that is familiar from earlier studies involving chains with only extensional degrees of freedom. However, for some combinations of parameters characterizing the energy landscape of the springs we find propagating phase boundaries for which the rate of dissipation, as calculated using isothermal expressions for the driving force, is negative. This is a surprising result which suggests that we cannot neglect the energy stored in the oscillations of the masses in the interpretation of the dynamics of mass-spring chains. In particular, we must incorporate temperature into the numerical solutions of these chains. We have made an attempt to do so by defining a temperature that is proportional to the energy in the vibrations of the masses and springs that a purely mechanical continuum theory neglects. A temperature defined in

this way jumps only across a phase boundary and not a sonic wave. This is exactly what happens in a Mie-Gruneisen type material with the Gruneisen parameter equal to zero. We have used this insight to extract a new kinetic relation that does not suffer from the anomaly of giving negative dissipation rates at a moving phase boundary. Does this mean that our earlier kinetic relation that was based on isothermal expressions of the driving force is useless? We do not think so for the following reason. In [98] we implemented a Langevin dynamics algorithm in which it was possible to simulate a mass-spring chain immersed in a constant temperature bath. We showed that the local temperature near a phase boundary was high but it soon decayed to the temperature of the bath due to heat transfer. We found that the kinetic relation derived using isothermal expressions was not affected much by the bath temperature, especially for large phase boundary velocities. Hence, we expect that kinetic relation summarized in equation (3.30) will be a good approximation at the near sonic limit. At the end of the paper we use our chain to shed some light on experiments involving temperature sensitive yarns that couple twist and stretch to perform useful work. We have shown that it is important to consider the dynamics of the yarn, especially reflection of sonic waves and/or phase boundaries at the ends of the yarn, in order to explain the oscillatory decay of the actuation strain due to cooling of the yarn at fixed tension. However, we must point out that there are several limitations of our model, including (a) we have not included a spinodal region in the constitutive law, (b) we have not included a heat bath, (c) we have not included bending deformations. All three are important and we plan to include them in future work.

Chapter 4

Langevin dynamics of a bistable chain with twist and stretch

Mass-spring chains have provided insights into a wide variety of phenomena in elastic solids that include wave propagation, defect motion and thermodynamic behaviour among several other topics [36, 41]. When the potentials characterizing the springs have multiple wells then the dynamics of mass-spring chains has been shown to be similar to that of one-dimensional bars capable of phase transitions [7, 8, 10, 13, 18, 27, 29, 42, 54, 73, 82, 85, 89]. This insight has been utilized to extract kinetic relations for moving phase boundaries by comparing solutions of impact and Riemann problems in continuum bars to those in the bistable chains [65, 85]. The extracted kinetic relation has a simple analytical form that has been recently shown to be a universal near sonic limit [89]. More recently, mass-spring chains have also provided insights into the mechanics of biological macromolecules [17, 18].

We built on these studies recently by adding rotational degrees of freedom to each mass in a mass-spring system to simulate a continuum rod that can twist and stretch, but not bend [99]. The potentials characterizing the springs had multiple wells so that our mass-spring system had propagating phase boundaries across which there were jumps in twist and stretch. This work was partially motivated by biological examples like [32, 81, 90, 96]. In each of these examples there is an isothermal environment because the processes occur

while the systems are immersed in a fluid which is at constant temperature. However, in [99] there was no heat bath in the simulations. This resulted in an interesting anomaly. When we calculated the driving force across the propagating phase boundaries in the mass-spring chains using isothermal expressions we found that dissipation rate was negative. We traced this unphysical result down to our assumption of isothermal conditions in the purely mechanical simulations based on integrating Newton's second law for each mass in the chain. In other words, the simulations in [99] were adiabatic rather than isothermal. Our goal in this paper is to enforce isothermal conditions by accounting for the presence of heat bath around our chain by using Langevin dynamics.

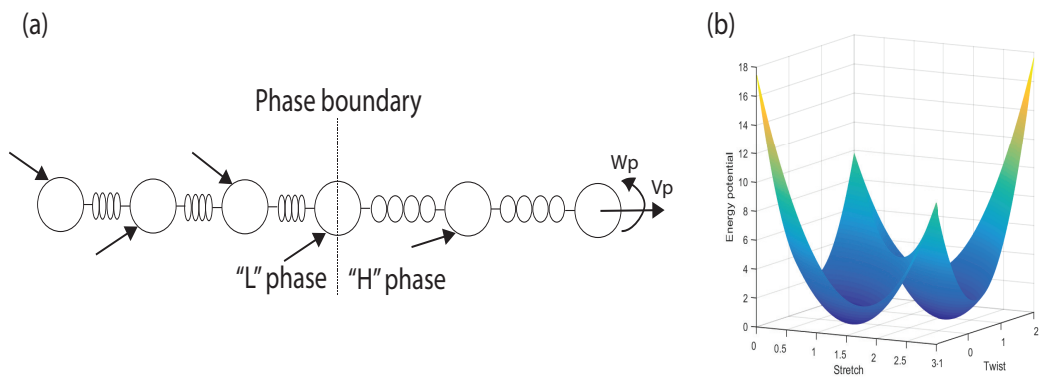

Figure 4.1: (a) Mass-spring chain in which each mass has an extensional and rotational degree of freedom. The masses are labeled j, $j+1$, etc., and the springs connecting these two masses is labeled $j+\frac{1}{2}$. A phase boundary separates regions of the chain in which springs are in different phases. Springs in the 'H' phase correspond to the top right well in the contour plot in (b) and the 'L' phase correspond to the bottom left well in the contour plot . We specify extensional velocity v_0 and rotational velocity w_0 on the masses at the boundary. We can also specify force and moment boundary conditions. (b) Energy landscape for the twist stretch coupling material with two wells.

The paper is laid out as follows. First, we give a short account of the balance laws and constitutive relations for rods capable of phase transitions in twist and stretch. Second, we describe an analogous mass-spring chain and simulate its dynamics in impact and Riemann problems with a quasi-symplectic algorithm applied to Langevin's equations of motion.

Third, we extract kinetic relations from these simulations and show that they have the same form as has been used earlier for isothermal chains with only extensional degrees of freedom. Finally, we show that the parameters entering these kinetic relations depend on bath temperature in a simple way.

4.1 Thermo-mechanics of 1D continuum with twist and stretch

4.1.1 Balance Laws

In this paper, we will consider phase transition phenomena in a one-dimensional continuum capable of storing energy in both twist and stretch. This continua is immersed in a heat bath where bath temperature is a constant. We have given a detailed treatment of the mechanics of this sort of continuum in recent work [99, 100]. For this reason we will give here only a short summary of the jump conditions that we will need to interpret our Langevin dynamics simulations of a discrete version of such a continuum. Let us begin by considering phase boundaries propagating in this continuum in the interval $0 \leq x \leq L$ where x is the reference coordinate along the continuum of length L. At each reference point we have two variables – the deformed position $z(x,t)$ of a cross-section of the continuum (imagine a rod) located at x at time t, and $\alpha(x,t)$ the angle through which that cross-section has rotated at time t. We require that $z(x,t)$ and $\alpha(x,t)$ be continuous at all x and t so that the rod does not break. We neglect the bending deformations because it's not important in our analysis. We denote $\lambda(x,t) = \frac{\partial z}{\partial x}$ as stretch and $\kappa(x,t) = \frac{\partial \alpha}{\partial x}$ as twist. The variables that are work conjugate to $z(x,t)$ and $\alpha(x,t)$ are the force $T(x,t)$ and the torque $M(x,t)$, respectively. For a discontinuity located in such a continuum at reference position $s(t)$, the following jump conditions can be derived from the continuity of deformation, balance of linear and

angular momentum and balance of energy:

$$\dot{s}[|\lambda|] + [|\dot{z}|] = 0, \tag{4.1}$$

$$\dot{s}[|\kappa|] + [|\dot{\alpha}|] = 0, \tag{4.2}$$

$$\dot{s}[|\rho\dot{z}|] + [|T|] = 0, \tag{4.3}$$

$$\dot{s}[|\rho r_g^2\dot{\alpha}|] + [|M|] = 0, \tag{4.4}$$

$$f_{driving} = [|W|] - \langle T\rangle[|\lambda|] - \langle M\rangle[|\kappa|], \tag{4.5}$$

where $W(\lambda, \kappa)$ is the Helmholtz free energy per unit length of our continuum, ρ is the mass per unit length in the reference configuration, r_g is the radius of gyration of the cross-section, $\dot{s}$ is the speed of the discontinuity in the reference configuration and $f_{driving}$ is the driving force across the discontinuity in an isothermal setting which assumes that there is no jump in temperature across the phase boundary. Note that $[|y|]$ denotes the jump $y(s_+(t), t) - y(s_-(t), t)$ at a discontinuity. We will show that these jump conditions are satisfied at discontinuities in our mass-spring chains, but we are specifically interested in the dependence of $f_{driving}$ on $\dot{s}$ and the bath temperature.

4.1.2 Constitutive relation

In order to allow for the existence of phase boundaries imagine that the stored energy function of our material has two wells located at different points on the $\lambda - \kappa$ plane, same as shown in chapter 4. The Helmholtz free energy per unit length energy is the same quadratic form as equation 3.10. The force and moment constitutive relations are thus also the same as equations 3.15 3.16. The sonic wave speed for this 1-D continua are thus equations 3.19. Readers can look up chapter 4 for the details of these derivations. While sonic waves travel at

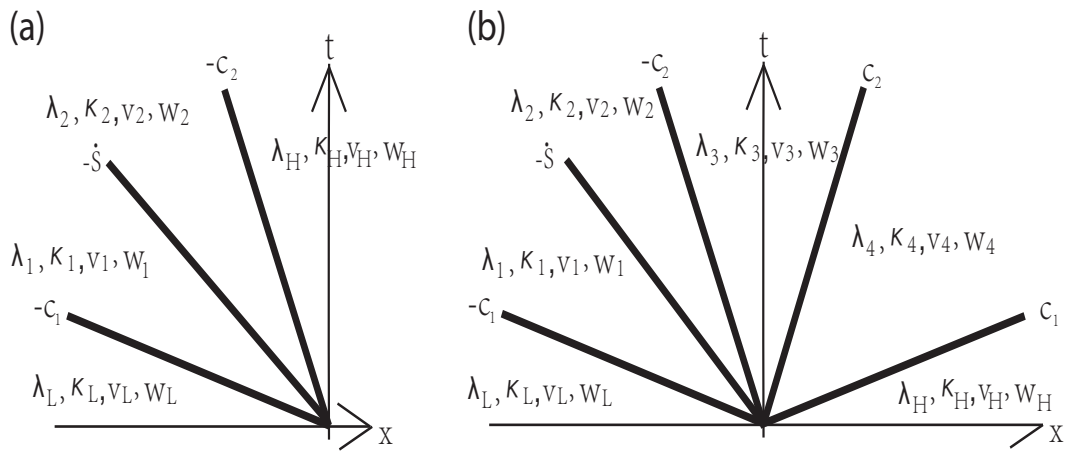

Figure 4.2: (a) X-t plane for impact problem. There are 3 waves in total, two sonic waves and one phase boundary. (b) X-t plane for Riemann problem. There are 5 waves in total, four sonic waves in different directions and one phase boundary.

these two constant speeds, the speed of a phase boundary depends on the boundary/initial conditions applied on the continuum as well as the temperature of the bath. We will show this by discretizing the continuum as a mass-spring chain with extensional and rotational degrees of freedom at each mass and solving the dynamical problem numerically using Langevin's equations.

4.2 Mass-spring chain

4.2.1 Description of the interaction potential between the masses

We have studied the dynamics of a mass spring chain with only translational degree of freedom at finite temperature in [98]. We now consider the case that each mass i has both translational and rotational degree of freedom. We denote $x_i = u_{i+1} - u_i$ and $y_i = \theta_{i+1} - \theta_i$, where u_i is the linear displacement of the ith mass and θ_i is its rotational displacement from the reference state. This is the same notation as in chapter 4 and we assume again each mass interacts with its first nearest neighbor only through a potential $\phi_1(x_i, y_i)$. This potential

is given by equation 3.21 in a quadratic form. And the well corresponding to phase L is located at (a_1, b_1) and the well corresponding to phase H is located at (a_2, b_2). The constant B_1, B_2, B_3 are related to the stretch modulus, twist-stretch coupling modulus and twisting modulus as described in [99]. This results in linear relations between the force/torque and stretch/twist. The total energy of the chain consisting of N masses connected by $N-1$ springs can be written as:

$$\phi(u_1, u_2, ..., u_N, \theta_1, \theta_2, ..., \theta_N) = \sum_{i=1}^{N-1} \phi_1(x_i, y_i). \tag{4.6}$$

4.2.2 Langevin dynamics

We now consider a setting where we can set the temperature of the chain by immersing it in a heat bath which supplies random impulses to the masses. This can be done by integrating Langevin's equations of motion for the masses in our chain. If we assume that mass and moment of inertia of each mass is unity then Langevin's equations for mass i are:

$$\frac{du_i}{dt} = v_i, \tag{4.7}$$

$$\frac{dv_i}{dt} = -\nu_1 v_i - \frac{\partial \phi}{\partial u_i} + \eta_1(t), \tag{4.8}$$

$$\frac{d\theta_i}{dt} = w_i, \tag{4.9}$$

$$\frac{dw_i}{dt} = -\nu_2 w_i - \frac{\partial \phi}{\partial \theta_i} + \eta_2(t), \tag{4.10}$$

where v_i and w_i are the linear and angular velocities of mass i, $\frac{\partial \phi}{\partial u_i}$ and $\frac{\partial \phi}{\partial \theta_i}$ are mechanical force and torque acting on mass i, and $\eta_1(t)$, $\eta_2(t)$ are the translation and rotational random impulses exerted on mass i from the heat bath. The random impulses on each mass are

assumed to be white noise so that:

$$\langle \eta_1(t) \rangle_e = 0, \quad \langle \eta_1(t)\eta_1(t') \rangle_e = 2\nu_1 k_B \Theta \delta(t-t'), \quad \text{for all } i, \tag{4.11}$$

$$\langle \eta_2(t) \rangle_e = 0, \quad \langle \eta_2(t)\eta_2(t') \rangle_e = 2\nu_2 k_B \Theta \delta(t-t'), \quad \text{for all } i, \tag{4.12}$$

where $\langle \cdot \rangle_e$ denotes an ensemble average, ν_1, ν_2 are translational and rotational drag coefficients, k_B is the Boltzmann constant and Θ is bath temperature.

4.2.3 Numerical scheme

To integrate our equations of motion based on Langevin dynamics, we employ a quasi-symplectic scheme [52] as follows:

$$v_{1,k} = g_I(\frac{\Delta t}{2}; v_k), \tag{4.13}$$

$$u_{1,k} = u_k + \frac{\Delta t}{2} v_{1,k}, \tag{4.14}$$

$$v_{2,k} = v_{1,k} + \Delta t \frac{\partial \phi}{\partial u_{1,k}} + \Delta t^{1/2} \sigma_1 \xi_k, \tag{4.15}$$

$$v_{k+1} = g_I(\frac{\Delta t}{2}; v_{2,k}), \tag{4.16}$$

$$u_{k+1} = u_{1,k} + \frac{\Delta t}{2} v_{2,k}, \tag{4.17}$$

$$w_{1,k} = g_{II}(\frac{\Delta t}{2}; w_k), \tag{4.18}$$

$$\theta_{1,k} = \theta_k + \frac{\Delta t}{2} w_{1,k}, \tag{4.19}$$

$$w_{2,k} = w_{1,k} + \Delta t \frac{\partial \phi}{\partial \theta_{1,k}} + \Delta t^{1/2} \sigma_2 \xi_k, \tag{4.20}$$

$$w_{k+1} = g_{II}(\frac{\Delta t}{2}; w_{2,k}), \tag{4.21}$$

$$\theta_{k+1} = \theta_{1,k} + \frac{\Delta t}{2} w_{2,k}, \tag{4.22}$$

where k=0,1,....M-1, $g_I(t,v) = v^{-\nu_1 t}$, $g_{II}(t,v) = w^{-\nu_2 t}$, $\sigma_1 = \sqrt{2\nu_1 k_B \Theta}$, $\sigma_2 = \sqrt{2\nu_2 k_B \Theta}$. We choose a time step Δt that is much smaller than a_1/c_1 to ensure that our numerical calculation is stable. Recall that a_1 is the distance between masses (or the lattice parameter in the 'L' phase) when no forces are applied on the chain.

4.2.4 Impact and Riemann problems

Now, we would like to simulate an impact problem using our mass-spring chain. We do this with a mass-spring chain with N masses and $N-1$ springs connecting them. We take $N = 100$ and fix the left end of the chain ($j = 1$) and apply constant linear and angular velocity at the right end ($j = N$). Hence, $u_1^i = 0, \theta_1^i = 0$ and $u_N^i = v_0 i\Delta t + u_N^0, \theta_N^i = w_0 i\Delta t + \theta_N^0$, where i is the time-step number. We have used the same material parameter set $B_1 = 10$, $B_2 = 7.6$ and $B_3 = 10$ and $B_1 = 10$, $B_2 = 3$, $B_3 = 10$ as in [99]. Initially, all springs are in the 'L' phase. We integrate equations (4.10) for the system up to the point that the faster sonic wave which originated at $j = N$ hits the left end ($j = 1$). We observe propagating phase boundaries for applied velocities v_0, w_0 larger than some critical values. We also observe sonic waves passing through the chain from right to left which travel at constant speeds c_1 and c_2 as given in equation 3.19 and shown in figure 4.3. We have verified that the jumps in strains (extensional and rotational) and velocities (linear and angular) satisfy the jump conditions at each discontinuity shown in figure 4.3.

For simulating a Riemann problem we have used $N+1$ masses and N springs with an initial phase boundary in the middle of the chain at mass number $\frac{N}{2}$ where $N = 200$. The equations of motion for the masses is again Langevin's equation 4.10 and the two boundaries are left free (zero force and moment). At $t = 0$ we prescribe initial conditions such that all springs in the left half are in the 'L' phase, while those on the right are

in the 'H' phase. Since our mass-spring system has a finite number of masses and has two boundaries there could be four additional sonic waves which originate from the two ends. We integrate the dynamics of the mass spring system up to the point when the sonic waves originating at the center of the chain and those coming from the ends meet each other. Again, we use material set $B_1 = 10$, $B_2 = 7.6$, $B_3 = 10$ and $B_1 = 10$, $B_2 = 3$, $B_3 = 10$. An example of the evolution of the system is plotted in figure 4.5. We have verified again that all jump conditions are satisfied by the average strains and velocities obtained from the Langevin dynamics calculations. The oscillatory strains and velocities behind

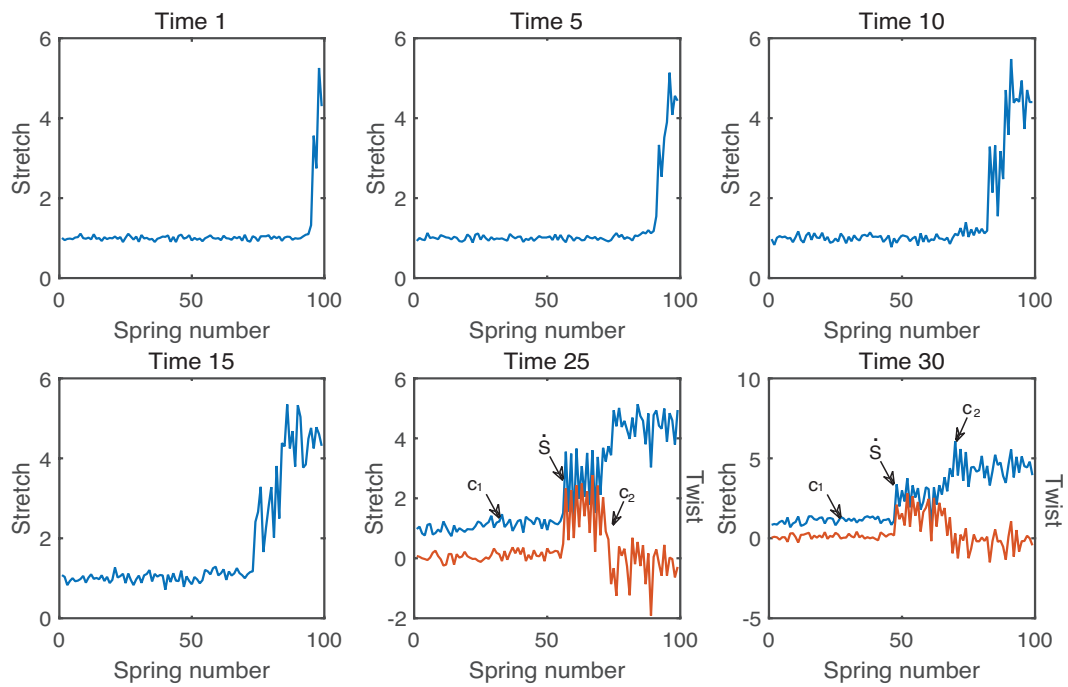

Figure 4.3: An example of an impact problem with phase boundary. The panels show the evolve of different states of the system. Three discontinuities exist in this system. The sonic wave with speed c_1 is not visible because of thermal fluctuation.

the propagating discontinuities in these simulations decay to constants (with fluctuations around the constant value) because of the presence of the heat bath and also because it is well-known from the continuum theory of phase transitions [7, 65] that the solutions to

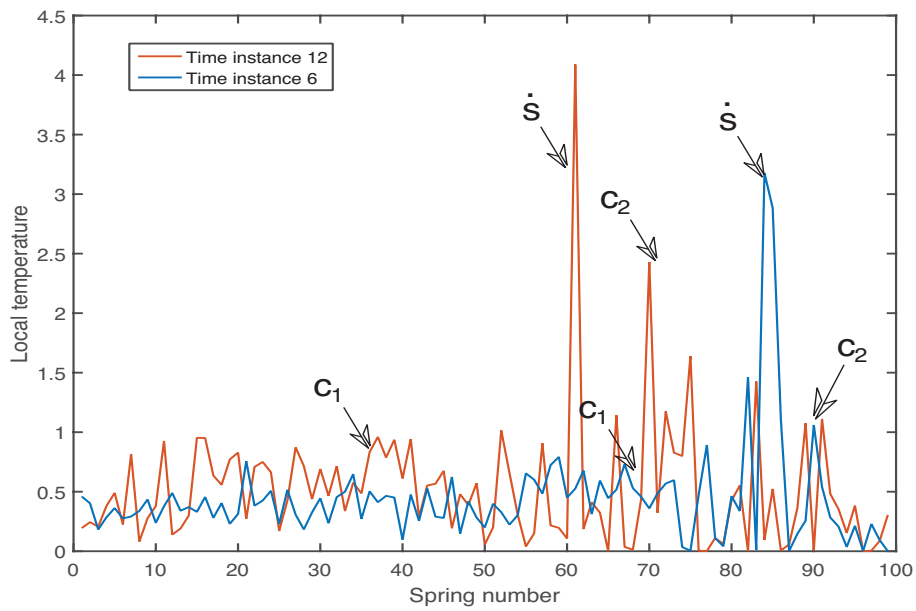

Figure 4.4: Time snapshot of local temperature of the mass spring chain at two different time instances for impact problem. Phase boundary and sonic wave positions are indicated on the graph.

these problems give piecewise constant strains and velocities in the x-t plane. This was true for the sonic waves in [99], but not for phase boundaries behind which the oscillations of the masses did not decay. In other words, some energy remained in the oscillations long after the phase boundary had passed, indicating that there was a jump in temperature across the phase boundary. In the calculations presented here the heat bath maintains the temperature of the chain at a constant value (with small fluctuations), so there is no jump in temperature across the phase boundary. We show this explicitly in figure 4.4 where snapshots of the temperature in an impacted chain are shown at two different time instants. Here local temperature is defined as the sum of translational and rotational kinetic energy:

$$\Theta \sim \langle \frac{m}{2}(v-\bar{v})^2 + \frac{I}{2}(w-\bar{w}^2)\rangle_e \tag{4.23}$$

where m and I are mass and moment of inertia, $\bar{v}$ and $\bar{w}$ are the local average translational

and rotational velocities and $\langle\rangle_e$ means ensemble average. The passage of a phase boundary can be inferred by a spike in local temperature that quickly decays to the value set by the heat bath. Hence, the energy that was earlier stored in oscillations behind the phase boundary is now dissipated into the heat bath. We have verified that the jump conditions

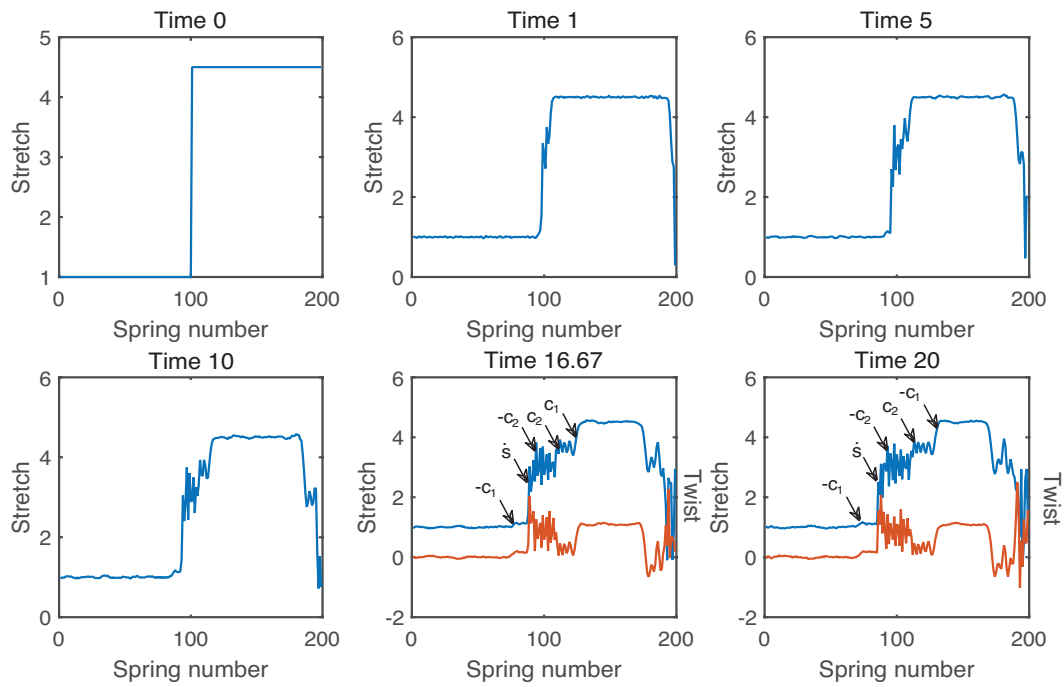

Figure 4.5: (a) x–t plane of a Riemann problem with a single phase boundary with $c_1 > \dot{s} > c_2$. (b) x–t plane of a Riemann problem in which $\dot{s} = -c_2$.

are satisfied at each discontinuity in our Langevin dynamics calculations.

4.2.5 Kinetic relation

In order to extract a kinetic relation from this type of simulations, all we need to do is record the phase boundary velocity $\dot{s}$ and the average strains ahead and behind the phase boundary as a function of applied boundary conditions and bath temperature. Then, we can compute the driving force $f_{driving}$ using eqn. (4.5). Then, a plot of $f_{driving}$ versus $\dot{s}$ is the kinetic relation we want. We have carried out a series of computations for Impact

Material set	a_1	a_2	a_3	a_4
B_1=10, B_2 = 3, B_3 = 10	0.7	-0.1	0.4	-0.3
B_1=10, B_2 = 7.6, B_3 = 10	0.75	-0.05	1.1	-0.2

Table 4.1: Table for the parameters of a_1, a_2, a_3 and a_4 in the kinetic relation 4.25.

problem and Riemann problem with different bath temperature and material sets. The plots can be seen in figure 4.6. In (a) we consider three different temperatures for a material parameter set in which we did not observe any negative dissipation in [99], while in (b) the material parameter set led to phase boundaries with negative dissipation in [99]. Note that no matter what material parameter set we use higher bath temperatures result in faster phase boundary speeds at the same driving force, in agreement with [98]. To compare results across different material sets we use a normalized phase boundary velocity $\dot{s}/c_1$ and normalized driving force given by:

$$f_{normalized} = \frac{[|W|] - \langle T\rangle[|\lambda|] - \langle M\rangle[|\kappa|]}{\frac{2}{l_0}\sqrt{SC+g^2}}. \tag{4.24}$$

Here $\frac{2}{l_0}\sqrt{SC+g^2}$ is the normalizing factor for the driving force, $l_0 = \frac{\lambda_H^0-\lambda_L^0}{\kappa_H^0-\kappa_L^0}$.

The function used to fit the driving force is [98, 99]

$$f_{driving} = q_1(\Theta) + \frac{q_2(\Theta)}{1-\frac{\dot{s}^2}{c_1^2}}. \tag{4.25}$$

The parameters q_1 and q_2 are functions of bath temperature and material set. From our fits we have empirically deduced that $q_2 = a_1 + a_2 \log\Theta$ where a_1 and a_2 are two constants, Θ is bath temperature. Similarly, $q_1 = a_3 + a_4 \log\Theta$ where a_3 and a_4 are two constants. The form (4.25) works for all material sets and bath temperatures in our simulations. We list the constants from our fits in table 4.1.

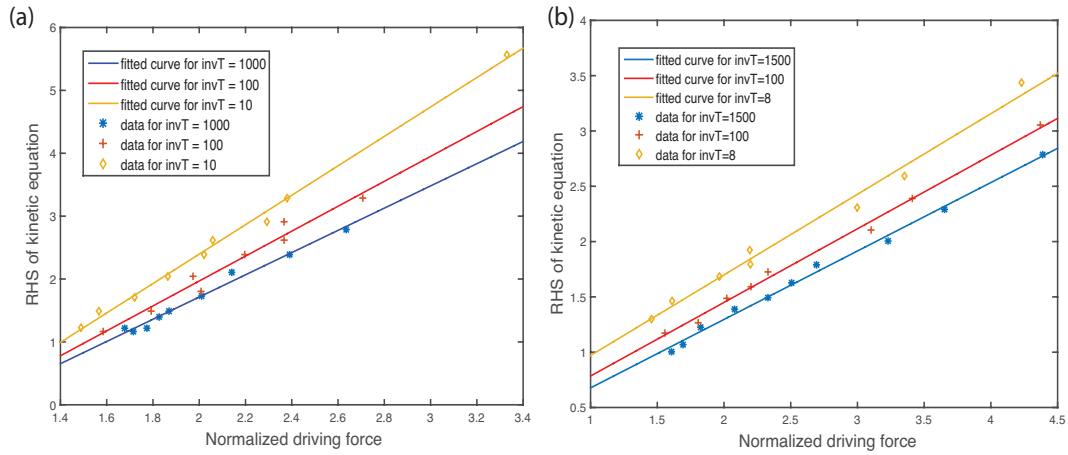

Figure 4.6: (a) Kinetic relation from Riemann problems. The data for this plot was obtained for material set $B_1 = 10$, $B_2 = 7.6$, $B_3 = 10$. The viscosity we use is $\nu_1 = \nu_2 = 0.0002$. We have plotted results with different inverse temperatures. Phase boundary velocity $\dot{s}$ is normalized against c_1 and we plot $\frac{1}{1-\dot{s}^2/c_1^2}$ on the y-axis. Driving force $f_{driving}$ is normalized according to equation 4.24 and plotted on the x-axis. By fitting a straight line to the data we get constants q_1 and q_2 for each bath temperature. (b) The data for this plot was obtained for material set $B_1 = 10$, $B_2 = 3$, $B_3 = 10$. Again, $\nu_1 = \nu_2 = 0.0002$, and we have plotted results with different inverse temperatures.

4.3 Conclusions

In this chapter we have studied the dynamics of a mass-spring chain with extensional and rotational degrees of freedom at each mass at finite temperature. This is accomplished by simulating the dynamics of a mass-spring chain immersed in a heat bath. The energy landscape of the springs has multiple wells in the stretch-twist plane, as would be the case for a rod capable of phase transitions. Similar to [98], we implemented Langevin's dynamics calculation both in extensional and rotational degrees of freedom. We have employed a quasi-sympletic algorithm to integrate our equations as described in [52]. We have shown that the kinetic relation in this circumstance still has the same form as in [98], but the constants appearing in it are temperature dependent. When bath temperature is large enough, we no long observe cases of negative dissipation that we had observed in an adiabatic environment as in [99].

Chapter 5

Phase boundaries with discontinuous stretch and twist in DNA

Single molecule mechanics experiments have given us insight into the behavior of DNA for at least the last two decades [78]. Early experiments applied only tensile forces [76] on the molecule but in the late 1990s magnetic tweezers were developed that allowed for the application of both tension and torque on DNA [11]. These experiments revealed that unlike most polymers DNA is capable of storing twist due to its double stranded nature [53]. Now, the twist applied on a DNA molecule can be positive or negative – positive, when it is in the same sense as the right handed double helix, and negative, when it is in the opposite sense. When twist (positive or negative) is applied on DNA at low tensions it forms plectonemes or super-coils [34, 40, 65]. These have been studied quite thoroughly using elastic rod theories coupled with electrostatic and entropic effects [12, 25]. But, if torsion is applied at high tensions (so that plectonemes are avoided) then DNA exhibits a rich variety of phase change phenomena [22]. In different regions of the tension-torque plane different phases of DNA are most stable. The transitions between these phases are first order phase transitions [12, 22]. Our focus in this paper is on three of those phases – B-DNA which is a right-handed helix that is stable at tensions below 65pN, S-DNA which is almost ladder-like (with little helicity) and stable at tensions above 65pN, and L-DNA which is a left-handed helix that is stable at

negative torques. Single molecule equilibrium experiments at constant tension have revealed that the transition from B-DNA to L-DNA occurs at a constant torque which is a function of the applied tension and temperature [59, 74]. Similarly, at zero torque the transition from B-DNA to S-DNA occurs at a constant tension of 65pN at room temperature [77]. If the DNA is torsionally constrained the B-DNA to S-DNA transition occurs at higher tensions [69]. It has been demonstrated by fluorescence experiments that there are one or two phase boundaries propagating through the DNA during the B-DNA to S-DNA transition [90]. It is possible that other phase transitions in DNA also proceed in a similar way. If we view a long DNA molecule as one-dimensional continuum capable of storing elastic energy then we can model the propagation of these phase boundaries using well-established techniques in mechanics. Indeed, we have shown that such an approach can account for the force-extension behavior of a wide variety of molecules [67]. Several other authors have also applied similar theories of phase transitions to biological macromolecules. Fischer *et al.* proposed a model similar to [67] to address the time-dependent behaviors of the whelk egg capsule bio-polymer [33]. Benichou *et al.* have used a chain of bi-stable springs to gain some key insights into the mechanical behavior of muscle protein titin [17, 18]. Mechanically induced folding and unfolding of passive cross-linkers has been modeled by bi-stable units in Caruela *et al.* [23, 24] who obtained good agreement with experimentally observed behavior of skeletal muscles. In all these models only the force-extension behavior is studied. The same approach has not yet been applied to torque-rotation curves.

In this paper we model DNA as a one-dimensional continuum whose stored energy function is a function of both extension and twist, or more precisely, the stretch λ and twisting curvature κ_3. Since we want to allow for the existence of multiple phases of the

DNA the stored energy function is non-convex. There are wells in the energy landscape in the $\lambda - \kappa_3$ plane that represent different phases of the DNA. Propagating boundaries between these phases are discontinuities across which both λ and κ_3 can jump. To the best of our knowledge, such phase boundaries have not been deeply studied in mechanics. Propagating discontinuities across which the uni-axial and shear strains can jump have been studied in the context of elasto-plastic impact of bars [26, 49]. A similar framework can be applied to our propagating phase boundaries with discontinuities in λ and κ_3, but unlike plasticity our deformations are fully recoverable. Also unlike impact of bars, inertia forces are negligible in the DNA single molecule experiments that we aim to study. They are overwhelmed by the drag forces imposed by the surrounding fluid [67]. As a result our partial differential equations are parabolic, not hyperbolic as in elasto-plastic impact of bars.

This paper is organized as follows. First, we develop a continuum mechanical framework for a one-dimensional continuum which can have propagating discontinuities with jumps in stretch and twisting curvature. The main goal of this analysis is to identify the driving force across the discontinuity. Second, we plot phase diagrams for DNA using piece-wise quadratic energy densities. Such an energy excludes the effects of thermal fluctuations (in bending and torsion) and is a good approximation to the stored energy function of DNA at high tensile forces. Third, we give details of the finite difference computational method in which phase boundaries are represented by moving nodes. Our method builds upon previously published work [67] in which only one strain variable suffered a jump across the phase boundary (here two variables jump across the phase boundary). Fourth and fifth, we use our computational method to interpret equilibrium and non-equilibrium experiments on DNA.

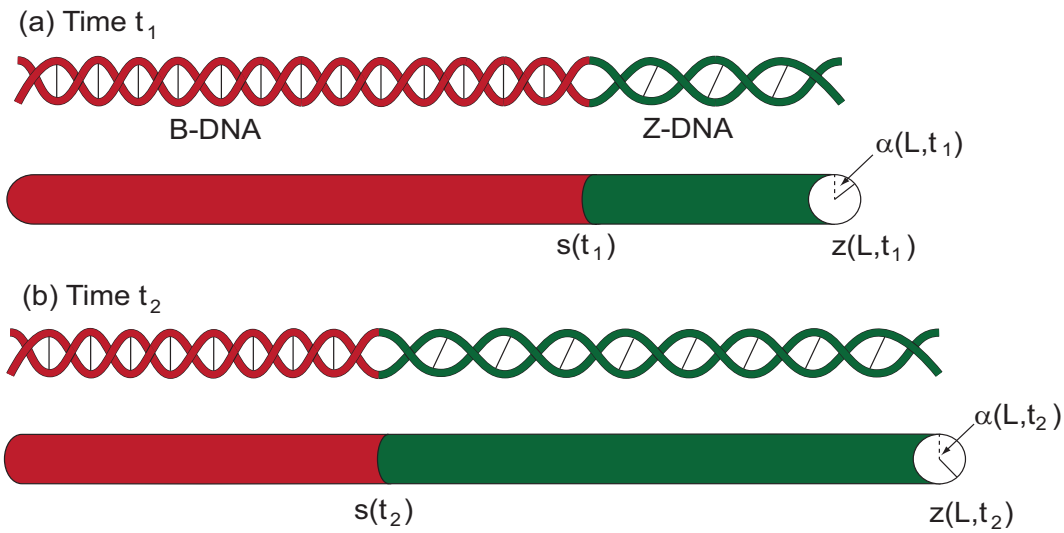

Figure 5.1: Schematic of DNA undergoing a phase transition in which stretch and twisting curvature jump across a phase boundary. Snapshots at two different times are shown. There is a single interface located in both snapshots at different positions. To the left of this interface the DNA is a right handed double helix (like B-DNA), while to the right it is a left handed double helix with a different pitch (like L-DNA or Z-DNA). At the right end the DNA is pulled at some velocity v_p or a tension T_1 is applied. It is also rotated at angular velocity ω. The bottom panels show the DNA represented by a 1D continuum, or a rod. At each reference position x there are two variables – $z(x,t)$ is the linear position and $\alpha(x,t)$ is the angular deflection in the deformed configuration. If the right end is rotated at constant angular velocity ω then we expect $\alpha(L,t_2) - \alpha(L,t_1) = \omega(t_2 - t_1)$. The position of the phase boundary in the reference configuration is $s(t)$.

5.1 Thermomechanics of 1-D rod

In this paper we consider phase boundaries propagating in a one-dimensional continuum in the interval $0 \leq x \leq L$. Here x is the reference coordinate along the continuum (or the center line of an elastic rod) of reference length L which represents a DNA molecule subjected to tension and twist (see figure 5.1). We confine ourselves to large tensile forces so that the bending deformations of the DNA can be neglected in comparison to the stretching and twisting deformations. Hence, at each reference point we have two variables – the deformed position $z(x,t)$ of the rod cross-section located at x at time t, and $\alpha(x,t)$ the angle through which that cross-section has rotated at time t. We require that $z(x,t)$ and $\alpha(x,t)$ be continuous at all x and t so that the rod does not break. The stretch of the rod is $\lambda(x,t) = \frac{\partial z}{\partial x}$ and the twist is $\kappa_3(x,t) = \frac{\partial \alpha}{\partial x}$. These quantities are allowed to jump at a finite number of points in our continuum. If one such jump is located at $x = s(t)$ then let us denote $x > s(t)$ as the + side, $x < s(t)$ as the - side. For any quantity $y(x,t)$ we denote $y(x_+,t) - y(x_-,t)$ by $[|y|]$ and $\frac{y(x_+,t)+y(x-,t)}{2}$ by $\langle y \rangle$. From continuity of the deformed material we have $[|z|] = 0$ and $[|\alpha|] = 0$. Differentiating these two equations with respect to time we get the kinematic jump conditions

$$\dot{s}[|\lambda|] + [|\dot{z}|] = 0, \tag{5.1}$$

$$\dot{s}[|\kappa_3|] + [|\dot{\alpha}|] = 0. \tag{5.2}$$

The equation for balance of linear momentum for a portion of the rod in the interval (x_1, x_2) is

$$\frac{d}{dt}\int_{x_1}^{x_2} \rho \dot{z}\, dx = T|_{x_1}^{x_2} + \int_{x_1}^{x_2} b dx, \tag{5.3}$$

where $\rho(x,t)$ is the mass per unit length, $b(x,t)$ is the distributed load and $T(x,t)$ is the tension in the bar[65, 67]. If we localize this equation to a discontinuity $s(t)$ (with $x_1 \leq s(t) \leq x_2$) then we get the linear momentum jump condition

$$[|T|] + \dot{s}[|\rho v|] = 0. \tag{5.4}$$

If we assume the rod is immersed in fluid such that the drag coefficient is d_w then we can take $b = -d_w(\frac{\partial z}{\partial t}(s,t) - v)$ where v is the velocity of the surrounding fluid. If we localize this away from discontinuity we get $\rho\ddot{z} = \frac{\partial T}{\partial x} + b$. If we neglect the effect of inertia so that $\rho = 0$, this will lead to

$$\frac{\partial T}{\partial x} = d_w(\frac{\partial z}{\partial t} - v). \tag{5.5}$$

The equation for the balance of angular momentum for a portion of the rod in the interval (x_1, x_2) is

$$\frac{d}{dt}\int_{x_1}^{x_2} \rho I\dot{\alpha}dx = \int_{x_1}^{x_2} -d_r\dot{\alpha}dx + M|_{x_1}^{x_2}, \tag{5.6}$$

where I is the polar moment of inertia of the cross-section, d_r is an angular drag coefficient and $M(x,t)$ is the torque in the rod. If we localize this equation to a discontinuity $s(t)$ (with $x_1 \leq s(t) \leq x_2$) then we have

$$[|M|] + \dot{s}[|\rho I\dot{\alpha}|] = 0. \tag{5.7}$$

If we localize this equation away from the discontinuity at $x = s(t)$ then we get $\rho I\ddot{\alpha} =$

$-d_r\dot{\alpha} + \frac{\partial M}{\partial x}$. Once again, we will neglect inertia and set $\rho I = 0$ to get

$$\frac{\partial M}{\partial x} = d_r\dot{\alpha}. \tag{5.8}$$

Note that if inertia is neglected then the linear and angular momentum jump conditions boil down to

$$[|T|] = 0, \qquad [|M|] = 0, \tag{5.9}$$

which shows that there can be no jumps in force and moment at a discontinuity. Let us multiply (5.5) by $\dot{z}$ and (5.8) by $\dot{\alpha}$ and add them to arrive at the balance of mechanical power for the rod in the domain (x_1, x_2) as

$$\int_{x_1}^{x_2} (\frac{\partial T}{\partial x}\dot{z} + \frac{\partial M}{\partial x}\dot{\alpha})dx = \int_{x_1}^{x_2} [d_w(\dot{z} - v)\dot{z} + d_r\dot{\alpha}^2]dx. \tag{5.10}$$

After accounting for the presence of the jump at $x = s(t)$ this leads to

$$T\dot{z}|_{x_1}^{x_2} - [|T\dot{z}|] - \int_{x_1}^{x_2} T\frac{\partial \dot{z}}{\partial x}dx + M\dot{\alpha}|_{x_1}^{x_2} - [|M\dot{\alpha}|] - \int_{x_1}^{x_2} M\frac{\partial \dot{\alpha}}{dx}\,dx = \int_{x_1}^{x_2} [d_w(\dot{z} - v)\dot{z} + d_r\dot{\alpha}^2]dx. \tag{5.11}$$

Remembering that $[|T|] = 0$ and $[|M|] = 0$ this can be simplified to

$$T\dot{z}|_{x_1}^{x_2} + T\dot{s}[|\lambda|] - \int_{x_1}^{x_2} T\dot{\lambda}dx + M\dot{\alpha}|_{x_1}^{x_2} + M\dot{s}[|\kappa_3|] - \int_{x_1}^{x_2} M\dot{\kappa_3}dx =$$

$$\int_{x_1}^{x_2} [d_w\dot{z}^2 - d_w v\dot{z} + d_r|\dot{\alpha}|^2]dx, \tag{5.12}$$

From the balance of energy of the rod in the domain (x_1, x_2) we have

$$\frac{d}{dt}\int_{x_1}^{x_2} w\,dx = -q|_{x_1}^{x_2} + T\dot{z}|_{x_1}^{x_2} + M\dot{\alpha}|_{x_1}^{x_2} - \int_{x_1}^{x_2} d_w(\dot{z}-v)\dot{z}dx - \int_{x_1}^{x_2} d_r\dot{\alpha}^2\,dx, \tag{5.13}$$

where $w(x,t)$ is the internal energy per unit length and q is heat (heat flux through a cross-section times area of cross-section). Substituting this into eqn. (5.12) we get

$$\frac{d}{dt}\int_{x_1}^{x_2} wdx = -q|_{x_1}^{x_2} + T\dot{s}[|\lambda|] + \int_{x_1}^{x_2} T\dot{\lambda}dx - M\dot{s}[|\kappa_3|] + \int_{x_1}^{x_2} M\dot{\kappa_3}dx. \tag{5.14}$$

Assuming a discontinuity at $x = s(t)$ leads to

$$\int_{x_1}^{x_2} (\dot{w} - T\dot{\lambda} + \frac{\partial q}{\partial x} - M\dot{\kappa_3})dx = \dot{s}([|w|] - T[|\lambda|] - M[|\kappa_3|]) - [|q|]. \tag{5.15}$$

Away from the discontinuity we localize this balance of energy to get

$$\dot{w} = T\dot{\lambda} + M\dot{\kappa_3} - \frac{\partial q}{\partial x}, \tag{5.16}$$

while at a discontinuity $x = s(t)$ we get

$$\dot{s}([|w|] - \langle T\rangle[|\lambda|] - \langle M\rangle[|\kappa_3|]) = [|q|]. \tag{5.17}$$

From the entropy inequality we have

$$\frac{d}{dt}\int_{x_1}^{x_2} \eta dx \geq -\frac{q}{\Theta}|_{x_1}^{x_2}, \tag{5.18}$$

where $\Theta(x,t)$ is the local temperature and $\eta(x,t)$ is the entropy per unit length in the

reference configuration. Since we are dealing with a molecule immersed in a fluid at constant temperature Θ we will assume that $\Theta(x,t)$ is constant and equal to the fluid (or bath) temperature. Localizing this equation away from the discontinuity we get

$$\dot{\eta} + \frac{1}{\Theta}\frac{\partial q}{\partial x} \geq 0. \tag{5.19}$$

Now, let $W = w - \Theta\eta$ be the Helmholtz free energy per unit reference length of the rod, then from equation (5.16), $\dot{W} = T\dot{\lambda} + M\dot{\kappa_3} - \frac{\partial q}{\partial x} - \Theta\dot{\eta}$. So, $\dot{\eta} = \frac{1}{\Theta}T\dot{\lambda} + \frac{1}{\Theta}M\dot{\kappa_3} - \frac{\dot{W}}{\Theta} - \frac{1}{\Theta}\frac{\partial q}{\partial x}$. Substituting this into eqn. (5.19) we get

$$\frac{1}{\Theta}T\dot{\lambda} + \frac{1}{\Theta}M\dot{\kappa_3} - \frac{\dot{W}}{\Theta} \geq 0, \tag{5.20}$$

which can be localized to a discontinuity to get

$$\dot{s}([|W|] - \langle T\rangle[|\lambda|] - \langle M\rangle[|\kappa_3|]) \geq 0. \tag{5.21}$$

If we define driving force as $f_{driving} = [|W|] - \langle T\rangle[|\lambda|] - \langle M\rangle[|\kappa_3|]$ then the above equation says that the rate of dissipation $f_{driving}\dot{s}$ at a moving discontinuity must be non-negative. Thus, our description of moving discontinuities in a rod with jumps in both stretch and twist is consistent with numerous other works [1, 2, 4–7, 65, 67, 85].

5.2 Phase diagram

Our focus in this paper is on studying DNA phase transitions under combined tension and torsion. We will confine ourselves to the high tension regime in which bending fluctuations

	B-DNA	S-DNA	L-DNA	Z-DNA
A	$205pNnm^2$	$28.7pNnm^2$	$36.9pNnm^2$	$820pNnm^2$
C	$369pNnm^2$	$41pNnm^2$	$82pNnm^2$	$94.3pNnm^2$
S	1220 pN	270 pN	610 pN	3030 pN
g	-84 pNnm	-122 pNnm	-100 pNnm	-81 pNnm
λ_j^0	1	1.706	1.353	1.0898
κ_j^0	$0nm^{-1}$	$-0.699nm^{-1}$	$-0.3437nm^{-1}$	$-0.3437nm^{-1}$

Table 5.1: Properties of different DNA phases from previous works. The B-DNA phase is stable at room temperature, and zero tension and torque. Unstretched B-DNA along the x-axis is our reference configuration with 0.34nm per base-pair.

can be safely neglected and the Helmholtz free energy function in each phase of the DNA can be approximated as [12, 55]

$$W_j = \frac{S_j}{2}(\lambda - \lambda_j^0)^2 + g_j(\lambda - \lambda_j^0)(\kappa_3 - \kappa_j^0) + \frac{C_j}{2}(\kappa_3 - \kappa_j^0)^2, \tag{5.22}$$

where j denotes a phase of the DNA molecule, S_j is the stretching modulus of phase j, C_j is the twisting modulus and g_j is the twist-stretch coupling modulus. The constants λ_j^0 and κ_j^0 have to do with the intrinsic stretch and twist of phase j with respect to the B-DNA phase. Hence, for B-DNA $\lambda_B^0 = 1$ and $\kappa_B^0 = 0$. Following the treatment by Marko and Neukirch(2013) and Argudo and Purohit (2014), we can extract the properties of the phases of DNA we consider in this paper as summarized in table 1.

For each phase of DNA we can now write the constitutive relation using stretch and twist as the independent variables by differentiating the expression for the stored energy density given by equation (5.22).

$$T = \frac{\partial W_j}{\partial \lambda} = S_j(\lambda - \lambda_j^0) + g_j(\kappa_3 - \kappa_j^0), \tag{5.23}$$

$$M = \frac{\partial W_j}{\partial \kappa_3} = C_j(\kappa_3 - \kappa_j^0) + g_j(\lambda - \lambda_j^0). \tag{5.24}$$

These can be rewritten with T and M as independent variables by solving for λ and κ_3 in each phase. The resulting equations are given below.

$$\lambda = \frac{g_j M - C_j T}{g_j^2 - S_j C_j} + \lambda_j^0, \tag{5.25}$$

$$\kappa_3 = \frac{g_j T - S_j M}{g_j^2 - S_j C_j} + \kappa_j^0. \tag{5.26}$$

It is clear that for any pair of force and moment values (T, M) the stretch λ and twist κ_3 will be different depending on the phase of the DNA. We have implied here that there are combinations (T, M) in which multiple phases of DNA can co-exist. Since it is well known that the transitions between the phases of DNA are first order phase transitions [16, 50] we can compute the co-existence lines on the $T - M$ plane using the Clapeyron equation [45]. For example, the curve for the co-existence between B-DNA and S-DNA can be computed by solving the following differential equation.

$$\frac{\partial M}{\partial T} = \frac{\lambda_B - \lambda_S}{\kappa_{3S} - \kappa_{3B}} = \frac{\frac{g_B M - C_B T}{g_B^2 - S_B C_B} + \lambda_B^0 - \frac{g_S M - C_S T}{g_S^2 - S_S C_S} - \lambda_S^0}{\frac{g_S T - S_S M}{g_S^2 - S_S C_S} + \kappa_S^0 - \frac{g_B T - S_B M}{g_B^2 - S_B C_B} - \kappa_B^0}, \tag{5.27}$$

where $g_B, g_S, C_B, C_S, S_B, S_S, \lambda_B^0, \lambda_S^0, \kappa_B^0$ and κ_S^0 are the constitutive parameters for B-DNA and S-DNA. Since this is a first order ordinary differential equation we need one constraint to uniquely determine the co-existence curve. From experiments it is known that the B- and S- phase coexist at $T = 54pN$, $M = -5pNnm$ [50, 96], so our co-existence curve must pass through this point on the $T - M$ plane. We can perform a similar exercise to get the co-existence curves for B-DNA and L-DNA as well as S-DNA and L-DNA. The resulting phase diagram is plotted in figure 5.2.

We have plotted a second phase diagram in figure 5.2 with L-DNA replaced by Z-DNA.

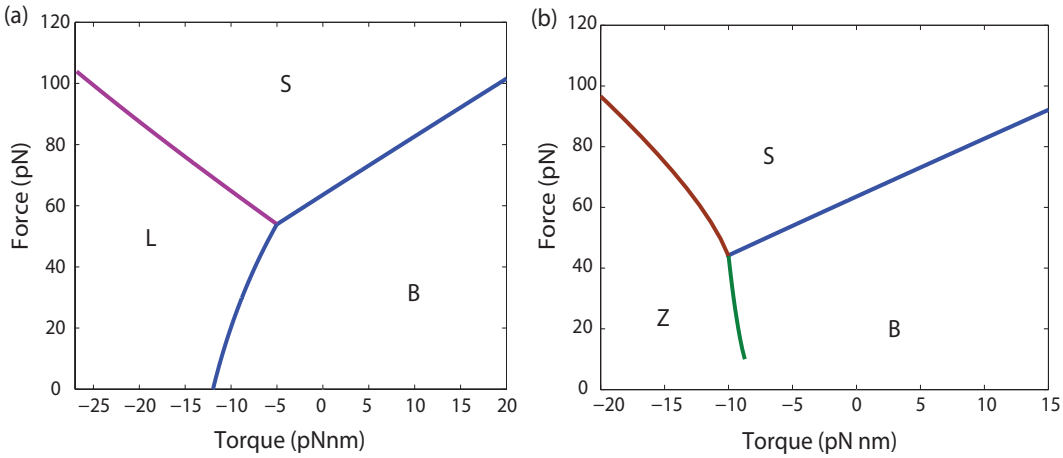

Figure 5.2: Phase diagram of DNA. (a) The three phases B-DNA, L-DNA and S-DNA are stable in different regions of the $T - M$ plane. These regions are separated by co-existence lines which are computed using the Clapeyron equation. (b) Phase diagram with Z-DNA instead of L-DNA. Z-DNA is also a left handed phase of DNA, like L-DNA.

Z-DNA is a left handed phase of DNA that has been known since the 1970s [35]. It has been suggested in the literature that L-DNA is not a separate phase of DNA, rather it is a mixture of Z-DNA and another phase, perhaps S-DNA [12, 59]. We will test this possibility in the following, so it is useful to know the co-existence curves for Z-DNA with the other phases.

5.3 Propagating interfaces between different phases of DNA

It is now known that the B-DNA to S-DNA transition in DNA can occur in displacement controlled experiments (with no torsional constraints) by the motion of one or two interfaces through the length of the DNA [40]. These interfaces, or phase boundaries, are often nucleated at the boundaries or at defects in the DNA strands and propagate as the two ends of the DNA are pulled away from each other. For the following analysis we admit the possibility of propagating interfaces even in DNA stretched with torsional constraints. We will integrate the equations of motion allowing for the presence of these propagating phase

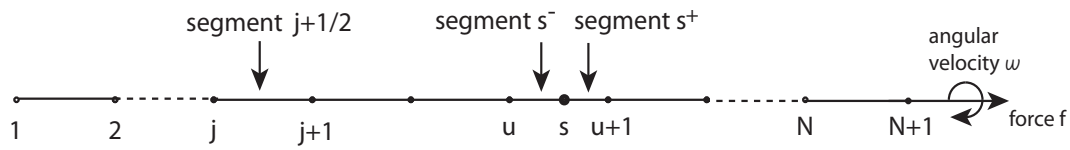

Figure 5.3: A schematic representation of the discrezation of our continuum. The big dot between node u and $u+1$ represents a moving phase boundary. The continuum is fixed at the left end at node $j=1$. It is held at constant force T_1 and rotated at angular velocity ω at the right end.

boundaries by following the ideas in Raj and Purohit [66, 67] who use a finite difference method. We first discrete our DNA represented by a 1D continuum into N segments of length Δ, so that $L = N\Delta$ where L is the reference length of the DNA sample. At the jth node there are two degrees of freedom, the deformed position z_j and the deformed angle α_j. These nodes are static in the reference configuration.

Away from discontinuity, the motion of a node is governed by equations $\frac{\partial M}{\partial x} = d_r\dot{\alpha}$ and $\frac{\partial T}{\partial x} = d_w\dot{z}$ as inertia effects are neglected and the surrounding fluid is assumed static. We discretize these equations for our numerical calculation as $\frac{T^i_{j+\frac{1}{2}} - T^i_{j-\frac{1}{2}}}{\Delta} = \frac{d_w(z^{i+1}_j - z^i_j)}{\delta t}$ and $\frac{M^i_{j+\frac{1}{2}} - M^i_{j-\frac{1}{2}}}{\Delta} = \frac{d_r(\alpha^{i+1}_j - \alpha^i_j)}{\delta t}$. Here the superscript i denotes the time instant and the subscript j refers to the node. For example, $T^i_{j+\frac{1}{2}}$ denotes the force in the region between node j and node $j+1$ at time instant i. These equations result in the following updating scheme for the degrees of freedom z_j and α_j at the nodes:

$$z^{i+1}_j = z^i_j + \frac{T^i_{j+\frac{1}{2}} - T^i_{j-\frac{1}{2}}}{d_w}\frac{\delta t}{\Delta}, \tag{5.28}$$

$$\alpha^{i+1}_j = \alpha^i_j + \frac{M^i_{j+\frac{1}{2}} - M^i_{j-\frac{1}{2}}}{d_r}\frac{\delta t}{\Delta}, \tag{5.29}$$

where δt is the length of the time-step. We assume that the linear and angular positions z^i_j and α^i_j at time instant i are known for $j = 1, 2, ..., N+1$. Then for each node the linear and

angular positions at time instant $i+1$ can be computed using the above updating scheme. This scheme does not work when a phase boundary is present between two nodes. We deal with this case next.

To represent propagating phase boundaries we use another kind of node that moves through the reference configuration. Across these moving nodes the stretch λ and twist κ_3 can be discontinuous. The motion of these nodes is governed by the kinematic jump conditions and linear/angular momentum jump conditions. Let us assume that there is at most one phase boundary in the sample. The node representing this phase boundary is labeled by s. Suppose this phase boundary is between node u and node $u+1$. We need equations to update the positions of these nodes and an equation to update the position of the phase boundary. From equation (5.4) and (5.7) we must have $[|T|] = 0$ and $[|M|] = 0$ across this phase boundary. This gives us two equations. Now, for convenience, let us assume that on one side of this phase boundary we have B-DNA, and on the other side we have S-DNA. The reference length of the segment between nodes u and $u+1$ in the B-DNA phase is Δ_B and that in the S-DNA phase is $\Delta_S = \Delta - \Delta_B$. Then, continuity of z and α gives us two more equations. If the phase transition occurs at equilibrium then a fifth equation can be obtained by observing that the B-DNA and S-DNA phases can co-exist only on a curve in the $T-M$ plane given by (5.27). We linearize this curve at the force prevailing between node u and $u+1$ at time instant i to obtain the fifth equation. If the phase transition occurs away from equilibrium then the fifth equation comes from a *kinetic relation* which shows how the phase boundary velocity $\dot{s}$ depends on the driving force $f_{driving}$. To sum it up, for an equilibrium calculation in which phase boundary motion can be described by the coexistence curve, the five conditions we enforce at each time instant

are

$$S_B(\lambda_B - \lambda_B^0) + g_B(\kappa_{3B} - \kappa_B^0) = S_S(\lambda_S - \lambda_S^0) + g_S(\kappa_{3S} - \kappa_S^0), \tag{5.30}$$

$$C_B(\kappa_{3B} - \kappa_B^0) + g_B(\lambda_B - \lambda_B^0) = C_S(\kappa_{3S} - \kappa_B^0) + g_S(\lambda_S - \lambda_S^0), \tag{5.31}$$

$$\lambda_B \Delta_B + \lambda_S \Delta_S = z_{u+1} - z_u, \tag{5.32}$$

$$\kappa_{3B} \Delta_B + \kappa_{3S} \Delta_S = \alpha_{u+1} - \alpha_u, \tag{5.33}$$

$$A_1 \lambda_S + A_2 \kappa_{3S} = A_3, \tag{5.34}$$

where λ_B and κ_{3B} are the stretch and twist in the B-DNA side, λ_S and κ_{3S} those on the S-DNA side, and A_1, A_2 and A_3 are three constants that are obtained by linearizing the co-existence curve. An example for how this linearization is performed for a transition from B-DNA to S-DNA is described in the appendix. A similar procedure can be followed for a B-DNA to L-DNA transition or S-DNA to L-DNA transition. To implement this numerically, we assume that at time instant i we know the linear and angular positions of all nodes including the phase boundary. Then we get the new positions at time instant $i+1$ as follows:

$$z_u^{i+1} = z_u^i + \frac{T_{s^-}^i - T_{u-\frac{1}{2}}^i}{d_w} \frac{\delta t}{\frac{1}{2}(\Delta + \Delta_B^i)}, \tag{5.35}$$

$$\alpha_u^{i+1} = \alpha_u^i + \frac{M_{s^-}^i - M_{u-\frac{1}{2}}^i}{d_r} \frac{\delta t}{\frac{1}{2}(\Delta + \Delta_B^i)}, \tag{5.36}$$

$$z_{u+1}^{i+1} = z_{u+1}^i + \frac{T_{u+\frac{3}{2}}^i - T_{s^+}^i}{d_w} \frac{\delta t}{\frac{1}{2}(\Delta + \Delta_S^i)}, \tag{5.37}$$

$$\alpha_{u+1}^{i+1} = \alpha_{u+1}^i + \frac{M_{u+\frac{3}{2}}^i - M_{s^+}^i}{d_r} \frac{\delta t}{\frac{1}{2}(\Delta + \Delta_S^i)}. \tag{5.38}$$

Here, $M_{s^+}^i$ denotes the moment in the segment between nodes s and $u+1$ at time instant i

and similarly for other quantities. The forces and moments $T^i_{s^+}$, $M^i_{u-\frac{1}{2}}$, etc., are obtained from the stretches and curvatures at time instant i. Now the stretches and curvatures at time instant $i+1$ are obtained by enforcing (5.30)-(5.34) as follows. We first solve the matrix equation

$$\begin{pmatrix} S_B & -S_S & g_B & -g_S \\ g_B & -g_S & C_B & -C_S \\ \Delta^i_B & \Delta^i_S & 0 & 0 \\ 0 & A^i_1 & 0 & A^i_2 \end{pmatrix} \begin{pmatrix} \lambda^{i+1}_B \\ \lambda^{i+1}_S \\ \kappa^{i+1}_{3B} \\ \kappa^{i+1}_{3S} \end{pmatrix} = \begin{pmatrix} S_B\lambda^0_B + g_B\kappa^0_B - S_S\lambda^0_S - g_S\kappa^0_S \\ g_B\lambda^0_B + C_B\kappa^0_B - g_S\lambda^0_S - C_S\kappa^0_B \\ z^{i+1}_{u+1} - z^{i+1}_u \\ A^i_3 \end{pmatrix}. \tag{5.39}$$

for the unknowns λ^{i+1}_B, λ^{i+1}_S, κ^{i+1}_{3B} and κ^{i+1}_{3S}. Then, we compute Δ^{i+1}_B and Δ^{i+1}_S using

$$\kappa^{i+1}_{3B}\Delta^{i+1}_B + \kappa^{i+1}_{3S}\Delta^{i+1}_S = \alpha^{i+1}_{u+1} - \alpha^{i+1}_u. \tag{5.40}$$

5.3.1 Simulation of equilibrium phase transition

We have employed the method described above to simulate the experiment in Sheinin *et al.* [74]. In this experiment a constant force T_1 is applied to a piece of DNA which is known to be in the B- phase initially. A constant twist rate $\frac{\partial\alpha}{\partial t}|_L = -\omega$ is applied to one end while the other end is held fixed. This causes the right handed B-DNA to 'melt' and form left handed L-DNA. Hence the boundary conditions applied to the DNA in this experiment are

$$\alpha(0,t) = 0, \qquad \alpha(L,t) = -\omega t, \qquad z(0,t) = 0, \qquad T(L,t) = T_1. \tag{5.41}$$

Sheinin *et al.* [74] do not give the value of L in their paper, but it is easy to compute it using the data provided in their paper for $\omega = 0$. We fit the force-extension data for $T < 65$pN

and zero twist using the worm-like-chain formula

$$\frac{\langle x \rangle}{L} = 1 - \frac{k_B \Theta}{\sqrt{4Af}} + \frac{T}{S}, \tag{5.42}$$

where A is the bending modulus in the B-DNA phase, S is the stretching modulus and $k_B\Theta = 4.1$pNnm at $\Theta = 300$K. From the experiment we know $\langle x \rangle$ as a function of T, so L is the only fitting parameter. We find that $L \approx 700$nm. With the reference length of the DNA known, we integrated our equations of motion assuming that a single phase boundary between B-DNA and L-DNA is nucleated at $x = L$ and moves left toward $x = 0$. The resulting extension-twist curve is plotted in figure 5.4 for three different values of the force T_1. The corresponding experimental data is also plotted. We clearly capture the general profile of the force-extension curve using our computational method. The curves for $M(L,t)$ as a function of $\alpha(L,t) = -\omega t$ for each of these forces is also shown in figure 5.5 although this was not measured in the experiment.

Even though Sheinin *et al.* [74] regard the 'melted' phase as L-DNA it is possible that B-DNA transitions into Z-DNA in their experiments. We can use our computational method to simulate the experiment assuming that the 'melted' phase is Z-DNA and not L-DNA. The corresponding extension-twist curves are plotted in figure 5.4 together with the experimental data. For each force T_1 we can compute an error as the square of the difference between the experimental and theoretical curves integrated over the full range of applied twist. We find that the error is three times smaller if we assume that the melted phase is Z-DNA. This shows that in the experiments of Sheinin *et al.* [74] Z-DNA could indeed be present, as has been suggested earlier [12]. Now, because of the constant thermal bombardment from the surrounding fluid Z-DNA can convert to S-DNA and vice-versa if

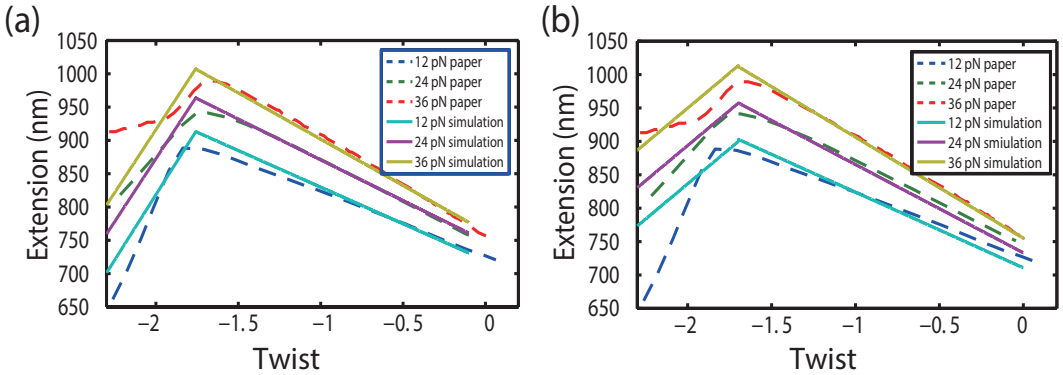

Figure 5.4: Simulation of the DNA-melting experiment of Sheinin *et al.* [74] with (a) Z-DNA, and (b) L-DNA. Initially, the DNA is in the B- phase in these experiments. It is held at a constant tension T_1 and rotated at angular velocity $-\omega$ to cause the phase transition. Although the general form of experimental curves is captured in both cases the difference between the experimental data and our computation is smaller if we assume that B-DNA transitions into Z-DNA.

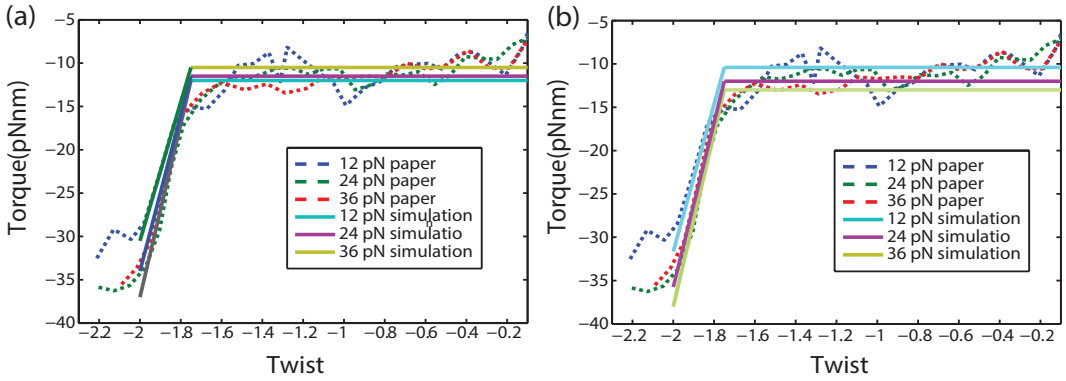

Figure 5.5: Prediction of torque vs. twist curves from our simulation of the experiment in Sheinin *et al.* [74]. The results are shown for both (a) Z-DNA, and (b) L-DNA. Recall that initially all the DNA is in the B- phase. The general form of the curves is captured correctly by our computation and there is quantitative agreement with experiments.

the free energy difference between these phases is on the order of k_BT or lower. This will result in a mixture of Z-DNA and S-DNA behind the phase boundary. We can compute the free energy per unit length of DNA under tension and torsion using a formula given by Argudo and Purohit (1998)[12]:

$$G_j = -\frac{1}{2\tilde{C}}(\frac{g_jT}{S_j} - M)^2 - \frac{T^2}{2S_j} + \kappa_j^0 M + G_{0j}, \tag{5.43}$$

where $\tilde{C} = C_j - \frac{{g_j}^2}{S_j}$, T is force, M is torque, g_j, S_j and C_j are coupling, stretching and twisting modulus in phase j and G_{0j} is the free energy per unit length at a reference state $T = 0, M = 0$ for phase j. The material properties appearing in the equation above will be different depending on the phase of the DNA. Some of these properties are summarized in table 1. G_{0z} for Z-DNA is 1.5 $k_B\Theta$ and G_{0s} for S-DNA is 5 $k_B\Theta$ per base-pair. With this free energy density we can easily calculate the probability that one base pair (which is $l = 0.34$nm long in the reference configuration) will be in the Z-DNA phase over the probability that it will be in the S-DNA phase at a given force and torque using[45]

$$\frac{P(Z)}{P(S)} = \exp\left(-\frac{l(G_z(T,M) - G_s(T,M)}{k_B\Theta})\right). \tag{5.44}$$

We have plotted this probability as a function of force and torque seen in the experiments in figure 5.6. We see that the probability for Z-DNA is higher than for S-DNA. However, since the ratio $\frac{P(Z)}{P(S)}$ is not much larger than 1, the phase resulting after the phase transition is indeed a mixture of Z-DNA and S-DNA as has been suggested earlier [12].

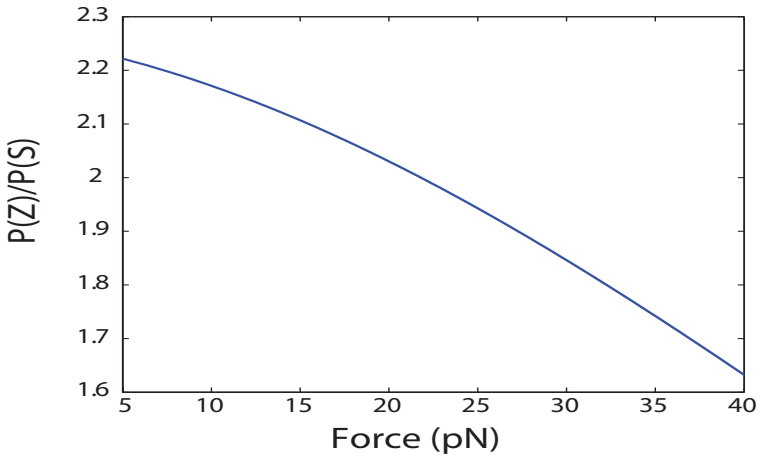

Figure 5.6: Ratio of probabilities that a single base pair of DNA is in the Z-DNA phase vs. S-DNA phase on phase co-existence line between B-DNA and Z-DNA. At higher tensions the probability of converting Z-DNA to S-DNA increases, consistent with the phase diagram in figure 5.2.

5.3.2 Simulation of non-equilibrium phase transition

When the phase transition occurs away from equilibrium we can no longer rely on the equation for the co-existence line to compute the position of the phase boundary. Recall that the co-existence line is a result of integrating the Clapeyron equation which was derived from equilibrium considerations[45]. Instead of the co-existence line, we now use a kinetic relation to compute the position of the phase boundary. If the transition occurs not far from equilibrium we can use a linear kinetic law, such as

$$\dot{s} = c f_{driving} = c([|W|] - \langle T \rangle [|\lambda|] - \langle M \rangle [|\kappa_3|]), \tag{5.45}$$

with $c > 0$ so that the dissipation inequality is satisfied.

We have used this idea to simulate the B-DNA to Z-DNA transition in another torque spectroscopy experiment [59]. In this experiment, a constant force is applied to the DNA chains using a magnetic bead type assay so that it is initially stretched. There is a transducer

segment which connects between the magnetic bead (bead A) and the 'sequence of interest'. At the junction between the transducer segment and the sequence of interest another bead (bead B) is attached to report the rotations there. The paper [59] mentions that the torque in the transducer segment is given as $M_t = k_{TD}\theta_{AB}$ where θ_{AB} is the difference in rotation between bead A and bead B and k_{TD} is estimated from the fluctuations of θ_{AB} measured in the experiments. Bead A is rotated at constant angular velocity ω and its angle is denoted as θ_A while the angle of rotation of bead B is $\theta_B(L,t)$ where L is the length of the sequence of interest. Hence, the boundary conditions are

$$\alpha(0,t) = 0, \qquad z(0,t) = 0, \qquad T(L,t) = T_1, \qquad \theta_A(t) = \omega t. \tag{5.46}$$

In Florian *et al* [59] $T_1 = 4$pN. Initially, the sequence of interest is in the B-DNA phase.

From figure 1 of Florian *et al* [59] we see that in the beginning of the experiment the torque increases linearly, then an abrupt jump in the torque occurs signaling the start of the phase transition. Subsequently, the torque is not fluctuating about a constant value but is increasing in magnitude. This is not expected in an equilibrium phase transition at constant tension in which the torque should be also constant. Hence, there is the possibility that the phase transition occurs out of equilibrium.

We start our simulation at a torque just below the maximum torque before the abrupt jump occurs. A phase boundary is nucleated at $x = L$ when a critical torque is reached. This phase boundary propagates through the sequence of interest until it reaches $x = 0$. If the phase boundary is between nodes u and $u + 1$ at time instant i, then the stretches and

twisting curvatures at time instant $i+1$ near the phase boundary are computed using

$$\begin{pmatrix} S_B & -S_Z & g_B & -g_Z \\ g_B & -g_Z & C_B & -C_Z \\ \Delta_B^i & \Delta_Z^i & 0 & 0 \\ 0 & 0 & \Delta_B^i & \Delta_Z^i \end{pmatrix} \begin{pmatrix} \lambda_B^{i+1} \\ \lambda_Z^{i+1} \\ \kappa_{3B}^{i+1} \\ \kappa_{3Z}^{i+1} \end{pmatrix} = \begin{pmatrix} S_B\lambda_B^0 + g_B\kappa_B^0 - S_Z\lambda_Z^0 - g_Z\kappa_Z^0 \\ g_B\lambda_B^0 + C_B\kappa_B^0 - g_Z\lambda_Z^0 - C_S\kappa_B^0 \\ z_{u+1}^{i+1} - z_u^{i+1} \\ \alpha_{u+1}^{i+1} - \alpha_u^{i+1} \end{pmatrix}. \tag{5.47}$$

Then, we compute $\Delta_Z^{i+1} = \Delta - \Delta_B^{i+1}$ using

$$\Delta_Z^{i+1} = \Delta_Z^i + \dot{s}^i \delta t, \tag{5.48}$$

where $\dot{s}^i$ is the phase boundary velocity at time instant i which is determined using (5.45). The value of c is not known to us, so we fit it by trial and error until our plots for the torque vs. twist matches the experimental data in Florian *et al* [59]. $c = 0.137 pN^{-1}nm^{-1}\mu s^{-1}$ gives a good fit to the experimental data as shown in figure 5.7. In performing our numerical simulations we also ensure that our results are independent of δt. We have plotted the extension of the DNA molecule from our calculation. This has not been measured in the experiments of Florian *et al* [59], but is easily done. From the result we see that due to linear kinetics the extension is no longer a linear function of the twist. We have also calculated the energy dissipated by the phase boundary as $W_d = \int f_{driving} \cdot \dot{s}\, dt$ and found that it is 56 percent of the external work done on the system. This suggests that in our calculation the system is indeed away from equilibrium.

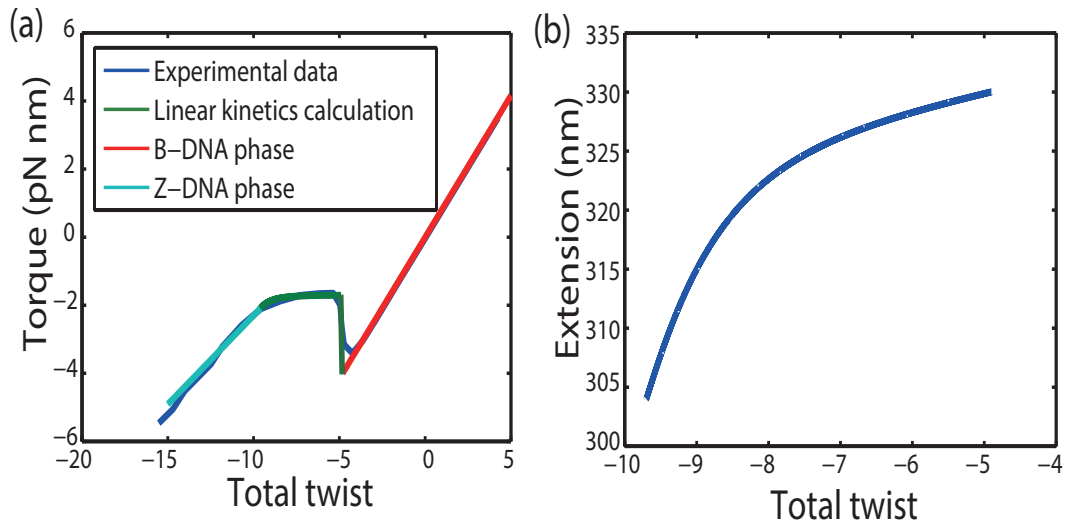

Figure 5.7: (a) Simulation of the experiment in Florian *et al.* [59]. The experiment is performed using a magnetic bead assay. Initially, B-DNA is stretched to 4pN and then the bead is rotated. We have employed a linear kinetic relation (5.45) for our simulation of the phase transition between B-DNA and Z-DNA. By trial and error we find that $c = 0.137$ $\mathrm{pN}^{-1}\mathrm{nm}^{-1}\mathrm{s}^{-1}$ gives a good fit to the experimental data. (b) The extension vs twist relation predicted from our calculation during the phase transition process.

5.4 Conclusions

In this chapter we have studied phase boundaries in one-dimensional continua across which both the stretch and twisting curvature can suffer jumps. Discontinuities of this type had been used to model impact of elasto-plastic bars, but we are not aware of an attempt to use them in the study of phase transitions. The introduction of a second strain variable (the twisting curvature) means that we have to account for the balance of angular momentum in our one-dimensional continuum in addition to the balance of linear momentum and energy. The free energy is now a function of two variables (stretch and twisting curvature) and this opens up the possibility of an 'egg carton' type landscape with multiple wells corresponding to different phases on the stretch-curvature plane. The expression for the thermodynamic driving force for phase boundaries between any two phases now has contributions from both the stretch and twist. The speed of the propagation of the phase boundaries is determined

as a function of the driving force by a kinetic relation. We use this kinetic relation in a finite difference computational method for integrating the equations of motion of our one-dimensional continuum.

We have shown in this paper that experimental results for combined tension and torsion in which DNA undergoes phase transitions from B-DNA to L-DNA can be accurately explained by the propagation of this type of phase boundaries. We have considered phase transitions both at equilibrium and out of equilibrium. We have confirmed the plausibility of the idea that in some of the experiments B-DNA is actually converting to another left handed phase called Z-DNA, rather than L-DNA. Even though we have confined our attention only to DNA in this paper our framework is general enough to be extended to other rod-like macromolecules that are capable of undergoing phase transitions, such as, coiled-coil proteins.

Chapter 6

Conclusion

In this thesis we have mainly studied phase transition phenomena in mass-spring chains. In each of the problems where we integrated Newton's second law for the mass-spring chains we have shown analogies with problems in phase transforming continua. We have exploited these analogies to extract kinetic relations for moving phase boundaries. Recall that in the continuum theory of phase transitions these kinetic relations would have been supplied as constitutive information. We have also extended the continuum theory of phase transitions to study the phase behavior of DNA in single molecule experiments. In the following we briefly summarize the work in this thesis and provide some pointers to future directions.

In chapter 2 we have shown how to obtain kinetic relations for moving phase boundaries in mass-spring chains. We demonstrated that the kinetic relations can be used to solve continuum Riemann problems to give results that are consistent with the mass-spring chain. We also integrated Langevin's equation of motion for the masses to simulate an isothermal bar immersed in a heat bath. We showed rigorously that our implementation of the numerical integrator for Langevin's equation passes important statistical mechanical

tests. We demonstrated that the kinetic relation is a function of the bath temperature. We studied a relatively simple problem, but we laid the foundation on which a majority of this thesis is built.

In chapter 3 we have studied the dynamics of a mass-spring chain with extensional and rotational degrees of freedom at each mass. The energy landscape of the springs has multiple wells, as would be the case for a rod capable of phase transitions. We have shown that the solutions of continuum Riemann and impact problems in rods capable of twist-stretch phase transitions are analogous to the those in the numerical solutions of our chains. In particular, we have observed discontinuities across which the twist and stretch can jump. Discontinuities of this type had been used to model impact of elasto-plastic bars and nano tubes [26, 56, 79], but we are not aware of an attempt to use them in the study of phase transitions, except [9]. Our mass-spring chain has furnished a kinetic relation for phase boundaries across which the twist and stretch can jump. Although, we obtained a kinetic relation whose form is familiar from earlier work we found that it gave unphysical negative dissipation for some combinations of parameters. The problem at the root of this anomaly is that we cannot neglect the energy stored in the oscillations of the masses in the interpretation of the dynamics of mass-spring chains. In particular, we must incorporate temperature into the numerical solutions of these chains. We have made an attempt to do so by defining a temperature that is proportional to the energy in the vibrations of the masses and springs that a purely mechanical continuum theory neglects. A temperature defined in this way jumps only across a phase boundary and not a sonic wave. This is exactly what happens in a Mie-Gruneisen type material when it undergoes adiabatic phase transitions. We have used this insight to extract a new kinetic relation that does not suffer

from the problem of giving negative dissipation rates.

In chapter 4 we have studied the dynamics of a mass-spring chain with extensional and rotational degrees of freedom at each mass at finite temperature. This is accomplished by simulating the dynamics of a mass-spring chain immersed in a heat bath. The energy landscape of the springs has multiple wells as in chapter 3. Similar to [98], we implemented a Langevin dynamics calculation both in extensional and rotational degrees of freedom. We employed a quasi-sympletic algorithm to integrate our equations as described in [52]. We have shown that the kinetic relation in this circumstance still has the same form as in [98], but the constants appearing in it are temperature dependent. When bath temperature is large enough, we no longer observe cases of negative dissipation that we had observed in an adiabatic environment as in [99].

In chapter 5 we have studied phase boundaries in one-dimensional continua across which both the stretch and twisting curvature can suffer jumps. While in chapters 3 and 4 this type of continuum problems were solved assuming that the inertia forces are large, in chapter 5 inertia forces are assumed negligible. Just as in chapters 3 and 4 the free energy is now a function of two variables (stretch and twisting curvature) and this opens up the possibility of an 'egg carton' type landscape with multiple wells corresponding to different phases on the stretch-curvature plane. Hence, the expression for the thermodynamic driving force for phase boundaries between any two phases now has contributions from both the stretch and twist. The speed of the propagation of the phase boundaries is determined as a function of the driving force by a kinetic relation. We use this kinetic relation in a finite difference computational method for integrating the equations of motion of our one-dimensional continuum. We have shown in this chapter that experimental results for

combined tension and torsion in which DNA undergoes structural transitions from B-DNA to L-DNA can be accurately explained by the propagation of this type of phase boundaries. We have considered structural transitions both at equilibrium and out of equilibrium. We have confirmed the plausibility of the idea that in some of the experiments B-DNA is actually converting to another left handed phase called Z-DNA, rather than L-DNA. Even though we have confined our attention only to DNA in this chapter our framework is general enough to be extended to other rod-like macromolecules that are capable of undergoing phase transitions, such as, coiled-coil proteins [21, 72].

Even though we have extended the Abeyaratne-Knowles theory of phase transitions in one-dimensional continua by introducing twist as a new variable in this thesis there are several new directions that could be explored in future work. One new direction is to bring fluctuation theorems [28, 39] of non-equilibrium statistical mechanics to bear on continuum problems involving phase transitions. For example, it is known that hysteresis in loading/unloading experiments performed in a constant temperature bath is connected to information theoretic ideas of entropy. On the other hand, we know from the continuum theory of phase transitions that hysteresis is connected to phase boundary kinetics [7]. So, a possible idea to explore is, "Can kinetic relations for phase boundaries in mass-spring chains immersed in a heat bath be derived using information theoretic ideas of entropy?" To answer this question we will have to build on the simulations of chapter 4. Another new direction is to build on the methods of chapter 5 to study transitions of B- and S-DNA to P-DNA [22]. P-DNA is right-handed helical form of DNA that has not been as deeply studied as the left-handed Z- and L-DNA phases. Lastly, an important aspect of the analysis that was ignored in chapter 5 is to see how our numerical method must be modified to deal with

a triple point in the DNA phase diagram. Future work should address this lacuna.

Appendix A

Appendix - Chapter 2

We assume there exists a discontinuity at reference location $x = s(t)$ and denote $x \geq s(t)$ as the + side, $x \leq s(t)$ as the - side. For any quantity $f(x,t)$ we denote $f(x_+,t) - f(x_-,t)$ by $[|f|]$ and $\frac{f(x_+,t)+f(x-,t)}{2}$ by $\langle f \rangle$. From continuity of the deformed material we have $[|u|]$ = 0. Differentiating this equation with respect to time we get

$$\dot{s}[|\epsilon|] + [|v|] = 0 \tag{A.1}$$

where $v(x,t) = \dot{u} = \frac{\partial u}{\partial t}$ is the particle velocity. We refer the reader to Purohit and Bhattacharya (JMPS) [65] for details of the derivations given here. The equation for balance of linear momentum for a portion of the bar in the interval (x_1, x_2) is:

$$\frac{\partial}{\partial t} \int_{x_1}^{x_2} \rho \dot{u} \, dx = T|_{x_1}^{x_2}, \tag{A.2}$$

where $\rho(x,t)$ is the mass per unit length and $T(x,t)$ is the tension in the bar. If we localize this equation to a discontinuity $s(t)$ (with $x_1 \leq s(t) \leq x_2$) then we get the linear momentum

the jump condition

$$[|T|] + \dot{s}[|\rho v|] = 0. \tag{A.3}$$

From the balance of mechanical power of the bar in the domain (x_1, x_2) we have

$$\frac{\partial}{\partial t}\frac{1}{2}\int_{x_1}^{x_2} \rho v^2 \, dx = Tv|_{x_1}^{x_2} - \int_{x_1}^{x_2} T\dot{\epsilon} dx \tag{A.4}$$

The term on the LHS is the rate of change of kinetic energy, the first term on the RHS is the rate of work done at the boundaries, the second term on the RHS is the rate of change of the stored elastic energy. When this is localized to a discontinuity $s(t)$ we get the following jump condition after using (A.1) and (A.3)

$$[|\frac{1}{2}\rho v^2|] + \langle T \rangle [|\epsilon|] = 0. \tag{A.5}$$

If we denote $\theta(x,t)$ as the temperature, $G(\theta)$ as the rate of heat loss per unit length from the bar to the environment, $\varepsilon(x,t)$ as the internal energy per unit mass and $q(x,t)$ as the heat flow across cross section at x and time t then the balance of energy can be written as

$$\frac{\partial}{\partial t}\int_{x_1}^{x_2} \rho\varepsilon + \frac{1}{2}\rho v^2 \, dx = -q|_{x_1}^{x_2} + Tv|_{x_1}^{x_2} - \int_{x_1}^{x_2} G(\theta) dx$$

By localizing this equation to the discontinuity at $s(t)$ we get the jump condition

$$\dot{s}(\rho[|\varepsilon|] - \langle T \rangle [|\epsilon|]) = [|q|]. \tag{A.6}$$

The entropy inequality (or the second law of thermodynamics) for the portion of the bar between x_1 and x_2 can be written as:

$$\frac{\partial}{\partial t}\int_{x_1}^{x_2} \rho\eta \, dx \geq -\frac{q}{\theta}|_{x_1}^{x_2} - \int_{x_1}^{x_2} \frac{G(\theta)}{\theta} \, dx \tag{A.7}$$

where $\eta(x,t)$ is the entropy per unit length of the bar. By localizing this to the discontinuity at $x = s(t)$ we get the jump condition:

$$\rho\dot{s}[|\eta|] \leq [|\frac{q}{\theta}|]. \tag{A.8}$$

If we now introduce $\psi = \varepsilon - \theta\eta$ as the Helmholtz free energy density then (A.6) and (A.8) can be combined to give

$$\dot{s}(\rho[|\psi|] - \langle T\rangle[|\epsilon|] + \langle\rho\eta - \frac{q}{\theta}\rangle[|\theta|]) \geq 0 \tag{A.9}$$

This is of the form $f\dot{s} \geq 0$ where $f = \rho[|\psi|] - \langle T\rangle[|\epsilon|] + \langle\rho\eta - \frac{q}{\theta}\rangle[|\theta|]$. We call this f as the driving force [**?**]. If we assume perfect heat conduction within the continuum, then θ is continuous and driving force f is reduced to $f = \rho[|\psi|] - \langle T\rangle[|\epsilon|]$. This expression for the driving force is used in the purely mechanical version of the theory. More detailed derivations can be found in reference [66]. Specific expressions for f for a trilinear material will be given in the following and can also be found in [66].

Appendix B

Appendix - Chapter 3

In this appendix we show how the coefficient A_1, A_2, A_3 in (5.34) for an equilibrium phase transition can be calculated. We will take the example of the phase transition between B-DNA and S-DNA. When the phase transition happens in equilibrium, the force and torque must observe the phase coexistence curve which is given by (5.27). By solving this differential equation we get a relation between force and torque as follows:

$$M = 0.4375f + 5.696 - 0.6615\sqrt{0.0768f^2 + 15.31f + 1047.17}, \tag{B.1}$$

where force f is in units of pN and torque M is in units pNnm. We can take the derivative of the equation above to get

$$\frac{\partial M}{\partial f} = 0.4375 - \frac{0.0508f + 5.064}{\sqrt{0.0768f^2 + 15.31f + 1047.17}}. \tag{B.2}$$

At f=65pN, $\frac{\partial M}{\partial f} = 0.2655$ nm so the linearized relation becomes $M = 0.2655f - 15.26$. We can express force and torque in terms of stretch λ and twisting curvature κ_3 using equation

(5.23) (5.24) to get

$$(g_S - 0.2655S_S)\lambda_S + (C_S - 0.2655g_S)\kappa_{3S} = C_S\kappa_S^0 + g_S\lambda_S^0 - 0.266S_S\lambda_S^0 - 0.2655g_S\kappa_S^0 - 15.26. \tag{B.3}$$

So, A_1 is the coefficient of λ_S, A_2 is the coefficient of κ_{3S} and A_3 is the constant on the right hand side. At $f = 65$pN, $A_1 = -289.4$, $A_2 = 116.6nm$ and $A_3 = -436.1$.

Appendix C

Appendix - Chapter 4

Here we give a short summary of Mie-Gruneisen type thermoelastic material with only a translational degree of freedom. A detailed description of phase transitions in this type of material can be found in [7]. The constitutive relations for the stress and entropy of a two-phase Mie-Grueisen material in one dimension are given by:

$$T = \begin{cases} S\lambda - \rho c\beta(\theta - \theta_T), & \text{for the 'L' phase,} \\ S(\lambda + \gamma_T) - \rho c\beta(\theta - \theta_T), & \text{for the 'H' phase,} \end{cases} \tag{C.1}$$

$$\eta = \begin{cases} \beta c\lambda + c(1 + \log(\theta/\theta_T)), & \text{for the 'L' phase,} \\ \beta c(\lambda + \gamma_T) + c(1 + \log(\theta/\theta_T)) - \lambda_T/\theta_T, & \text{for the 'H' phase,} \end{cases} \tag{C.2}$$

where S is the stretching modulus, λ is stretch, ρ is density, θ is temperature, c is specific heat, β is Gruneisen parameter and γ_T, λ_T and θ_T are constants. For a propagating discontinuity in a bar made of such a material the following jump conditions must be

satisfied under adiabatic conditions:

$$
\begin{aligned}
[|v|] + \dot{s}[|\lambda|] &= 0, \\
[|T|] + \rho\dot{s}[|v|] &= 0, \\
(\rho[|c\theta|] - \langle T\rangle[|\lambda|])\dot{s} &= 0,
\end{aligned}
\tag{C.3}
$$

where v is the particle velocity. The driving force at such a discontinuity is given by:

$$
f_{driving} = -\rho\langle\theta\rangle[|\eta|]. \tag{C.4}
$$

We can specialize this to a phase boundary by substituting the appropriate constitutive relations for η. If we assume $\beta = 0$ we get for a phase boundary

$$
f_{driving} = (\lambda_T/\theta_T + c\log(\theta^+/\theta^-)). \tag{C.5}
$$

If λ_T (the latent heat) is also zero (since the bottom of the two wells are at the same height) then we are left with $f_{driving} = c\log(\theta^+/\theta^-)$ which is what we have used as the driving force in the text.

References

1. Rohan Abeyaratne and James K Knowles. On the driving traction acting on a surface of strain discontinuity in a continuum. *Journal of the Mechanics and Physics of Solids*, 38(3):345–360, 1990.

2. Rohan Abeyaratne and James K Knowles. Kinetic relations and the propagation of phase boundaries in solids. *Archive for rational mechanics and analysis*, 114(2):119–154, 1991.

3. Rohan Abeyaratne and James K Knowles. Wave propagation in linear, bilinear and trilinear elastic bars. *Wave motion*, 15(1):77–92, 1992.

4. Rohan Abeyaratne and James K Knowles. A continuum model of a thermoelastic solid capable of undergoing phase transitions. *Journal of the Mechanics and Physics of Solids*, 41(3):541–571, 1993.

5. Rohan Abeyaratne and James K Knowles. Dynamics of propagating phase boundaries: thermoelastic solids with heat conduction. *Archive for rational mechanics and analysis*, 126(3):203–230, 1994.

6. Rohan Abeyaratne and James K Knowles. Impact–induced phase transitions in ther-

moelastic solids. *Philosophical Transactions of the Royal Society of London A: Mathematical, Physical and Engineering Sciences*, 355(1726):843–867, 1997.

7. Rohan Abeyaratne and James K Knowles. *Evolution of phase transitions: a continuum theory*. Cambridge University Press, 2006.

8. Rohan Abeyaratne and Srikanth Vedantam. A lattice-based model of the kinetics of twin boundary motion. *Journal of the Mechanics and Physics of Solids*, 51(9):1675–1700, 2003.

9. Rohan C Abeyaratne. Discontinuous deformation gradients in the finite twisting of an incompressible elastic tube. *Journal of Elasticity*, 11(1):43–80, 1981.

10. Vaibhav Agrawal and Kaushik Dayal. A dynamic phase-field model for structural transformations and twinning: Regularized interfaces with transparent prescription of complex kinetics and nucleation. part i: Formulation and one-dimensional characterization. *Journal of the Mechanics and Physics of Solids*, 85:270–290, 2015.

11. JF Allemand, D Bensimon, R Lavery, and V Croquette. Stretched and overwound dna forms a pauling-like structure with exposed bases. *Proceedings of the National Academy of Sciences*, 95(24):14152–14157, 1998.

12. David Argudo and Prashant K Purohit. Torsion of dna modeled as a heterogeneous fluctuating rod. *Journal of the Mechanics and Physics of Solids*, 62:228–256, 2014.

13. Alexander M Balk, Andrej V Cherkaev, and Leonid I Slepyan. Dynamics of chains with non-monotone stress–strain relations. i. model and numerical experiments. *Journal of the Mechanics and Physics of Solids*, 49(1):131–148, 2001.

14. Alexander M Balk, Andrej V Cherkaev, and Leonid I Slepyan. Dynamics of chains with non-monotone stress–strain relations. ii. nonlinear waves and waves of phase transition. *Journal of the Mechanics and Physics of Solids*, 49(1):149–171, 2001.

15. John M Ball and Richard D James. Proposed experimental tests of a theory of fine microstructure and the two-well problem. *Philosophical Transactions of the Royal Society of London A: Mathematical, Physical and Engineering Sciences*, 338(1650):389–450, 1992.

16. Christoph G Baumann, Steven B Smith, Victor A Bloomfield, and Carlos Bustamante. Ionic effects on the elasticity of single dna molecules. *Proceedings of the National Academy of Sciences*, 94(12):6185–6190, 1997.

17. Itamar Benichou and Sefi Givli. The hidden ingenuity in titin structure. *Applied Physics Letters*, 98(9):091904, 2011.

18. Itamar Benichou and Sefi Givli. Structures undergoing discrete phase transformation. *Journal of the Mechanics and Physics of Solids*, 61(1):94–113, 2013.

19. Kaushik Bhattacharya. *Microstructure of martensite: why it forms and how it gives rise to the shape-memory effect*, volume 2. Oxford University Press, 2003.

20. Kaushik Bhattacharya and Richard D James. A theory of thin films of martensitic materials withapplications to microactuators. *Journal of the Mechanics and Physics of Solids*, 47(3):531–576, 1999.

21. Carl Ivar Branden et al. *Introduction to protein structure*. Garland Science, 1999.

22. Zev Bryant, Michael D Stone, Jeff Gore, Steven B Smith, Nicholas R Cozzarelli, and

Carlos Bustamante. Structural transitions and elasticity from torque measurements on dna. *Nature*, 424(6946):338–341, 2003.

23. Matthieu Caruel, J-M Allain, and Lev Truskinovsky. Mechanics of collective unfolding. *Journal of the Mechanics and Physics of Solids*, 76:237–259, 2015.

24. Matthieu Caruel, Jean-Marc Allain, and Lev Truskinovsky. Cooperative folding of muscle myosins: I. mechanical model. *arXiv preprint arXiv:1312.0384*, 2013.

25. Nicolas Clauvelin, Basile Audoly, and S Neukirch. Elasticity and electrostatics of plectonemic dna. *Biophysical Journal*, 96(9):3716–3723, 2009.

26. RJ Clifton. An analysis of combined longitudinal and torsional plastic waves in a thin-walled tube. Technical report, DTIC Document, 1966.

27. T Cohen and S Givli. Dynamics of a discrete chain of bi-stable elements: A biomimetic shock absorbing mechanism. *Journal of the Mechanics and Physics of Solids*, 64:426–439, 2014.

28. Gavin Earl Crooks. Excursions in statistical dynamics. *Phd thesis*, 1999.

29. Kaushik Dayal and Kaushik Bhattacharya. Kinetics of phase transformations in the peridynamic formulation of continuum mechanics. *Journal of the Mechanics and Physics of Solids*, 54(9):1811–1842, 2006.

30. Kaushik Dayal and Kaushik Bhattacharya. A real-space non-local phase-field model of ferroelectric domain patterns in complex geometries. *Acta materialia*, 55(6):1907–1917, 2007.

31. Yalchin R Efendiev and Lev Truskinovsky. Thermalization of a driven bi-stable fpu chain. *Continuum mechanics and thermodynamics*, 22(6-8):679–698, 2010.

32. Wayne Falk and Richard D James. Elasticity theory for self-assembled protein lattices with application to the martensitic phase transition in bacteriophage t4 tail sheath. *Physical Review E*, 73(1):011917, 2006.

33. FD Fischer, MJ Harrington, and P Fratzl. Thermodynamic modeling of a phase transformation in protein filaments with mechanical function. *New Journal of Physics*, 15(6):065004, 2013.

34. Scott Forth, Maxim Y Sheinin, James Inman, and Michelle D Wang. Torque measurement at the single-molecule level. *Annual review of biophysics*, 42:583–604, 2013.

35. F Brock Fuller. The writhing number of a space curve. *Proceedings of the National Academy of Sciences*, 68(4):815–819, 1971.

36. David L Goodstein. *States of matter*. Courier Corporation, 2014.

37. Mica Grujicic, GB Olson, and WS Owen. Mobility of martensitic interfaces. *Metallurgical Transactions A*, 16(10):1713–1722, 1985.

38. RICHARD D James and Manfred Wuttig. Magnetostriction of martensite. *Philosophical Magazine A*, 77(5):1273–1299, 1998.

39. Christopher Jarzynski. Equalities and inequalities: irreversibility and the second law of thermodynamics at the nanoscale. *Annu. Rev. Condens. Matter Phys.*, 2(1):329–351, 2011.

40. Graeme A King, Peter Gross, Ulrich Bockelmann, Mauro Modesti, Gijs JL Wuite, and Erwin JG Peterman. Revealing the competition between peeled ssdna, melting bubbles, and s-dna during dna overstretching using fluorescence microscopy. *Proceedings of the National Academy of Sciences*, 110(10):3859–3864, 2013.

41. Charles Kittel. *Introduction to solid state physics.* Wiley, 2005.

42. TR Koehler, AR Bishop, JA Krumhansl, and JR Schrieffer. Molecular dynamics simulation of a model for (one-dimensional) structural phase transitions. *Solid State Communications*, 17(12):1515–1519, 1975.

43. JA Krumhansl and JR Schrieffer. Dynamics and statistical mechanics of a one-dimensional model hamiltonian for structural phase transitions. *Physical Review B*, 11(9):3535, 1975.

44. Tony Ladd. Numerical methods for molecular and continuum dynamics. *Lectures at the 3rd Warsaw School of Statistical Physics (Kazimierz, Poland)[http://www. che. ufl. edu/ladd/publications/kmz-09. pdf]*, 2009.

45. LD Landau and EM Lifshitz. *Statistical physics, vol. 5*, volume 30. 1980.

46. James S Langer and Takeshi Egami. Glass dynamics at high strain rates. *Physical Review E*, 86(1):011502, 2012.

47. Richard Law, George Liao, Sandy Harper, Guoliang Yang, David W Speicher, and Dennis E Discher. Pathway shifts and thermal softening in temperature-coupled forced unfolding of spectrin domains. *Biophysical journal*, 85(5):3286–3293, 2003.

48. Márcio D Lima, Na Li, Monica Jung De Andrade, Shaoli Fang, Jiyoung Oh, Geoffrey M

Spinks, Mikhail E Kozlov, Carter S Haines, Dongseok Suh, Javad Foroughi, et al. Electrically, chemically, and photonically powered torsional and tensile actuation of hybrid carbon nanotube yarn muscles. *Science*, 338(6109):928–932, 2012.

49. X Lin and J Ballmann. A riemann solver and a second-order godunov method for elastic-plastic wave propagation in solids. *International journal of impact engineering*, 13(3):463–478, 1993.

50. John F Marko and Sébastien Neukirch. Global force-torque phase diagram for the dna double helix: Structural transitions, triple points, and collapsed plectonemes. *Physical Review E*, 88(6):062722, 2013.

51. John F Marko and Eric D Siggia. Stretching dna. *Macromolecules*, 28(26):8759–8770, 1995.

52. GN Milstein, Yu M Repin, and Michael V Tretyakov. Symplectic integration of hamiltonian systems with additive noise. *SIAM Journal on Numerical Analysis*, 39(6):2066–2088, 2002.

53. J David Moroz and Philip Nelson. Torsional directed walks, entropic elasticity, and dna twist stiffness. *Proceedings of the National Academy of Sciences*, 94(26):14418–14422, 1997.

54. Neel Nadkarni, Chiara Daraio, and Dennis M Kochmann. Dynamics of periodic mechanical structures containing bistable elastic elements: From elastic to solitary wave propagation. *Physical Review E*, 90(2):023204, 2014.

55. Philip Nelson. *Biological physics*. WH Freeman New York, 2004.

56. KL Ng and QP Sun. Stress-induced phase transformation and detwinning in niti polycrystalline shape memory alloy tubes. *Mechanics of Materials*, 38(1):41–56, 2006.

57. S-C Ngan and L Truskinovsky. Thermo-elastic aspects of dynamic nucleation. *Journal of the Mechanics and Physics of Solids*, 50(6):1193–1229, 2002.

58. Shing-Chung Ngan and Lev Truskinovsky. Thermal trapping and kinetics of martensitic phase boundaries. *Journal of the Mechanics and Physics of Solids*, 47(1):141–172, 1998.

59. Florian C Oberstrass, Louis E Fernandes, Paul Lebel, and Zev Bryant. Torque spectroscopy of dna: base-pair stability, boundary effects, backbending, and breathing dynamics. *Physical review letters*, 110(17):178103, 2013.

60. David A Porter, Kenneth E Easterling, and Mohamed Sherif. *Phase Transformations in Metals and Alloys, (Revised Reprint)*. CRC press, 2009.

61. Mason A Porter, Norman J Zabusky, Bambi Hu, and David K Campbell. Fermi, pasta, ulam and the birth of experimental mathematics a numerical experiment that enrico fermi, john pasta, and stanislaw ulam reported 54 years ago continues to inspire discovery. *American Scientist*, 97(3):214–221, 2009.

62. G Puglisi and L Truskinovsky. Mechanics of a discrete chain with bi-stable elements. *Journal of the Mechanics and Physics of Solids*, 48(1):1–27, 2000.

63. Prashant K Purohit. *Dynamics of phase transitions in strings, beams and atomic chains*. PhD thesis, California Institute of Technology, 2001.

64. Prashant K Purohit and Kaushik Bhattacharya. On beams made of a phase-

transforming material. *International journal of solids and structures*, 39(13):3907–3929, 2002.

65. Prashant K Purohit and Kaushik Bhattacharya. Dynamics of strings made of phase-transforming materials. *Journal of the Mechanics and Physics of Solids*, 51(3):393–424, 2003.

66. Ritwik Raj and Prashant K Purohit. Moving interfaces in rod-like macromolecules. *EPL (Europhysics Letters)*, 91(2):28003, 2010.

67. Ritwik Raj and Prashant K Purohit. Phase boundaries as agents of structural change in macromolecules. *Journal of the Mechanics and Physics of Solids*, 59(10):2044–2069, 2011.

68. Matthias Rief, Hauke Clausen-Schaumann, and Hermann E Gaub. Sequence-dependent mechanics of single dna molecules. *Nature Structural & Molecular Biology*, 6(4):346–349, 1999.

69. Matthias Rief, Mathias Gautel, Filipp Oesterhelt, Julio M Fernandez, and Hermann E Gaub. Reversible unfolding of individual titin immunoglobulin domains by afm. *science*, 276(5315):1109–1112, 1997.

70. Phoebus Rosakis and James K Knowles. Unstable kinetic relations and the dynamics of solid-solid phase transitions. *Journal of the Mechanics and Physics of Solids*, 45(11):2055–2081, 1997.

71. Michael Schlierf and Matthias Rief. Temperature softening of a protein in single-molecule experiments. *Journal of molecular biology*, 354(2):497–503, 2005.

72. Ingo Schwaiger, Clara Sattler, Daniel R Hostetter, and Matthias Rief. The myosin coiled-coil is a truly elastic protein structure. *Nature materials*, 1(4):232–235, 2002.

73. Hartmut Schwetlick and Johannes Zimmer. Kinetic relations for a lattice model of phase transitions. *Archive for Rational Mechanics and Analysis*, 206(2):707–724, 2012.

74. Maxim Y Sheinin, Scott Forth, John F Marko, and Michelle D Wang. Underwound dna under tension: structure, elasticity, and sequence-dependent behaviors. *Physical review letters*, 107(10):108102, 2011.

75. LI Slepyan and LV Troyankina. Fracture wave in a chain structure. *Journal of Applied Mechanics and Technical Physics*, 25(6):921–927, 1984.

76. Craig A Smith, Terry Farrah, and Raymond G Goodwin. The tnf receptor superfamily of cellular and viral proteins: activation, costimulation, and death. *Cell*, 76(6):959–962, 1994.

77. Steven B Smith, Yujia Cui, and Carlos Bustamante. Overstretching b-dna: the elastic response of individual double-stranded and single-stranded dna molecules. *Science*, 271(5250):795–799, 1996.

78. TR Strick, J-F Allemand, D Bensimon, and V Croquette. Behavior of supercoiled dna. *Biophysical journal*, 74(4):2016–2028, 1998.

79. Qing-Ping Sun and Zhi-Qi Li. Phase transformation in superelastic niti polycrystalline micro-tubes under tension and torsion—-from localization to homogeneous deformation. *International Journal of Solids and Structures*, 39(13):3797–3809, 2002.

80. Narasipur Venkataram Suryanarayana. *Engineering heat transfer*. West Publishing, 1995.

81. Barney K Tam, Jennifer H Shin, Emily Pfeiffer, P Matsudaira, and L Mahadevan. Calcium regulation of an actin spring. *Biophysical journal*, 97(4):1125–1129, 2009.

82. Likun Tan, Amit Acharya, and Kaushik Dayal. Coarse variables of autonomous ode systems and their evolution. *Computer Methods in Applied Mechanics and Engineering*, 253:199–218, 2013.

83. Likun Tan, Amit Acharya, and Kaushik Dayal. Modeling of slow time-scale behavior of fast molecular dynamic systems. *Journal of the Mechanics and Physics of Solids*, 64:24–43, 2014.

84. R Tickle and RD James. Magnetic and magnetomechanical properties of ni 2 mnga. *Journal of Magnetism and Magnetic Materials*, 195(3):627–638, 1999.

85. Lev Truskinovsky and Anna Vainchtein. Kinetics of martensitic phase transitions: lattice model. *SIAM Journal on Applied Mathematics*, 66(2):533–553, 2005.

86. Lev Truskinovsky and Anna Vainchtein. Dynamics of martensitic phase boundaries: discreteness, dissipation and inertia. *Continuum Mechanics and Thermodynamics*, 20(2):97–122, 2008.

87. Job Ubbink and Theo Odijk. Polymer-and salt-induced toroids of hexagonal dna. *Biophysical journal*, 68(1):54, 1995.

88. Anna Vainchtein. The role of spinodal region in the kinetics of lattice phase transitions. *Journal of the Mechanics and Physics of Solids*, 58(2):227–240, 2010.

89. Anna Vainchtein and Panayotis G Kevrekidis. Dynamics of phase transitions in a piecewise linear diatomic chain. *Journal of nonlinear science*, 22(1):107–134, 2012.

90. Joost van Mameren, Peter Gross, Geraldine Farge, Pleuni Hooijman, Mauro Modesti, Maria Falkenberg, Gijs JL Wuite, and Erwin JG Peterman. Unraveling the structure of dna during overstretching by using multicolor, single-molecule fluorescence imaging. *Proceedings of the National Academy of Sciences*, 106(43):18231–18236, 2009.

91. Nikki Vercauteren and Carsten Hartmann. *Numerical investigation of solutions of Langevin equations*. PhD thesis, Masters thesis, Ecole Polytechnique Federale de Lausanne, Lausanne, Switzerland, 2005.

92. Robert J Webster and Bryan A Jones. Design and kinematic modeling of constant curvature continuum robots: A review. *The International Journal of Robotics Research*, 2010.

93. Gerald Beresford Whitham. *Linear and nonlinear waves*, volume 42. John Wiley & Sons, 2011.

94. Mark C Williams and Ioulia Rouzina. Force spectroscopy of single dna and rna molecules. *Current opinion in structural biology*, 12(3):330–336, 2002.

95. Mark C Williams, Ioulia Rouzina, and Victor A Bloomfield. Thermodynamics of dna interactions from single molecule stretching experiments. *Accounts of chemical research*, 35(3):159–166, 2002.

96. Xinghua Zhang, Hu Chen, Shimin Le, Ioulia Rouzina, Patrick S Doyle, and Jie Yan. Revealing the competition between peeled ssdna, melting bubbles, and s-dna dur-

ing dna overstretching by single-molecule calorimetry. *Proceedings of the National Academy of Sciences*, 110(10):3865–3870, 2013.

97. Yanqiu Zhang, Shuyong Jiang, Li Hu, and Yulong Liang. Deformation mechanism of niti shape memory alloy subjected to severe plastic deformation at low temperature. *Materials Science and Engineering: A*, 559:607–614, 2013.

98. Qingze Zhao and Prashant K Purohit. Extracting a kinetic relation from the dynamics of a bistable chain. *Modelling and Simulation in Materials Science and Engineering*, 22(4):045004, 2014.

99. Qingze Zhao and Prashant K Purohit. (adiabatic) phase boundaries in a bistable chain with twist and stretch. *Journal of the Mechanics and Physics of Solids*, 2016.

100. Qingze Zhao and Prashant K Purohit. Phase boundaries with discontinuous stretch and twist in dna. *International Journal of Solids and Structures*, 2016.